Departamento de Tecnología y Química Farmacéuticas

Facultad de Farmacia y Nutrición

UNIVERSIDAD DE NAVARRA

Pharmacometrics to facilitate decision-making in pain research and perioperative management

Nicolás Marco Ariño

Pamplona, 2022

Departamento de Tecnología y Química Farmacéuticas

Facultad de Farmacia y Nutrición

UNIVERSIDAD DE NAVARRA

TESIS DOCTORAL

Pharmacometrics to facilitate decision-making in pain research and perioperative management

Trabajo presentado por Nicolás Marco Ariño para obtener el grado de Doctor por la Universidad de Navarra

Fdo. Nicolás Marco Ariño

Pamplona, 2022

UNIVERSIDAD DE NAVARRA

FACULTAD DE FARMACIA Y NUTRICIÓN

Departamento de Tecnología y Química Farmacéuticas

D. JOSÉ IGNACIO FERNÁNDEZ DE TROCÓNIZ FERNÁNDEZ, Doctor en Farmacia y Catedrático del Departamento de Tecnología y Química Farmacéuticas, certifica:

> Que el presente trabajo, titulado "Pharmacometrics to facilitate decision-making in pain research and perioperative management", presentado por DON. NICOLÁS MARCO ARIÑO, para optar al grado de Doctor en Farmacia, ha sido realizado bajo su dirección en el Departamento de Tecnología y Química Farmacéuticas. Considerando finalizado el trabajo autoriza su presentación a fin de que pueda ser juzgado y calificado por el Tribunal correspondiente.

Y para que así conste, firma la presente:

Fdo: Dr. José Ignacio Fernández de Trocóniz Fernández

Pamplona, 2022

"How often have I said to you that when you have eliminated the impossible, whatever remains, however improbable, must be the truth?"

— Arthur Conan Doyle, The Sign of Four

Agradecimientos/Acknowledgements

En primer lugar, quisiera agradecer al personal de la Universidad de Navarra y al Departamento de Tecnología y Química Farmacéuticas su apoyo durante la realización de esta tesis doctoral.

En particular, a mi director, el profesor Iñaki Trocóniz por ser el gran artífice detrás de este trabajo. Gracias por darme la oportunidad de formar parte de este grupo y poder aprender de vosotros todos los días. Gracias a su vez a las doctoras María Jesús Garrido y Sara Zalba.

A los *senior modellers* del grupo, Zinnia y Edu, tantas gracias como el número de preguntas que me habéis respondido en este tiempo. Asimismo, gracias a Itziar, Leire, Belén y Violeta que hicisteis que los inicios de esta tesis fueran más fáciles. A todos los MIDIS (Javi, Fran, Tania, Jaime y Carmen) y estancias internacionales (Fernando, Bibiana, Alejandra y Natalia) que pusisteis vuestro granito de arena durante esta etapa. Especialmente a Fernando por los días de pinchos, ensaladas, videollamadas y risas. A los nuevos, Sara, Alejandro y Maite —porque siempre seréis los nuevos—, mucho ánimo con el resto del camino. Ya sabéis que la senda pica hacia arriba, pero al final las vistas merecen la pena.

A mis dos principales compañeros de viaje. Gracias Diego, por tus conocimientos informáticos, tu sentido del humor y siempre estar ahí para echar un cable. Aymara, gracias por no parar quieta y ser el motor escalador, crosfitero, lúdico-festivo, cafetero y anímico que cualquier persona quisiera tener.

My gratitude to the PK/PD scientists Sonya Tate, Kimberley Jackson and Feras Khalil, with whom I had the pleasure to collaborate during this time, for their support and advice during my development.

To my *Swedish* friends Simas, David, Lovisa and Markus for all the virtual gatherings that made the distance between us very small. Special thanks also to Alex and Olivia for the endless talks and support during these years.

A los amigos de Barbastro, que siempre están ahí independientemente de la distancia, y a los oscenses en el exilio Marina y Santiago, por traer la esencia aragonesa a tierras navarras.

Finalmente, a mi familia, mis abuelas, mis tíos y mi prima. A mi padre por los innumerables viajes y todo el apoyo recibido durante este tiempo. A mi madre, sufridora nata, pero sustento inquebrantable, no hubiera llegado a ser lo que soy sin ti. A mi hermano, ejemplo de constancia para alcanzar lo que uno desea.

Y a Ana, por haber estado a mi lado durante todo este camino. Hay historias que merecen un final feliz.

Muchas gracias

Table of content

Abbreviations

-2LL	-2 x log-likelihood
ADME	Absorption, distribution, metabolism and excretion
AIC	Akaike information criteria
AUC	Area under the concentration-time curve
BIS	Bispectral Index
BMI	Body mass index
CL	Elimination clearance
CL_D	Distribution clearance
C_{max}	Maximum drug concentration
CWRES	Conditional weighted residuals
FFM	Fat-free mass
GOF	Goodness of fit
Hb	Haemoglobin concentrations
ICSH	International council for standardization in hematology
IIV	Inter-individual variability
IMI	Innovative medicines initiative
IOV	Inter-occasion variability
ISV	Inter-study variability
IWRES	Individual weighted residuals
LRT	Log-likelihood ratio test
MBDD	Model-based drug development
MID3	Model-informed drug discovery and development
MIPD	Model-informed precision dosing
NCA	Non-compartmental analysis
NLME	Nonlinear mixed-effects

NMB	Neuromuscular blockade
OFV	Objective function
PBPK	Physiologically-based pharmacokinetics
PD	Pharmacodynamics
PDiam	Pupil diameter
PRD	Pupillary reflex dilation
PE	Prediction error
PK	Pharmacokinetics
popPK/PD	Population pharmacokinetics/pharmacodynamics
PsN	Perl-speaks-NONMEM
PTC	Post-tetanic count
Q	Intercompartmental clearance
QSP	Quantitative system pharmacology
RBC	Red blood cells
RSE	Relative standard error
RV	Residual variability
SCM	Stepwise covariate model
SD	Standard deviation
SM	Supplementary material
SS	Steady-state
TBW	Total body weight
TCI	Target-controlled infusion
TDM	Therapeutic drug monitoring
TOF	Train-of-four
T_{max}	Time to maximum plasma concentration

V	Apparent volume of distribution
VPCs	Visual predictive checks

Preface

Pharmacometrics is a quantitative discipline with multiple applications in drug development and therapeutic drug monitoring. By combining elements from disciplines such as pharmacology and statistics, pharmacometrics allows to quantitatively characterise the variability associated with drug exposure and effect to provide a temporal description of the pharmacological response. As a consequence, the contribution of the individual characteristics to the response can be differentiated from confounding factors that would otherwise limit data interpretation, thus allowing the individualization of drug administration. This feature represents the main application of pharmacometrics and an opportunity for implementing model-informed precision dosing (MIPD) as part of personalised medicine.

This thesis is about the use of pharmacometrics in two areas, pain management and perioperative medicine. Throughout the different sections, several examples of the application of MDPI in these clinical settings are presented. The thesis is organized as follows:

The *Introduction* provides an overview of the evolution of pharmacometrics, its main components and the current state of the field to contextualise the methodologies that will be developed in the following sections. At the end of the introduction, the *Objectives* condense the concrete aims of this work.

The *Methods* detail the clinical studies, measured variables and the different pharmacometric techniques that were used in this thesis. The *Results* provide a comprehensive description of the evaluation, validation and clinical applicability of the developed population pharmacokinetics/pharmacodynamics (popPK/PD) models, which constitute the main findings of this work.

The *Discussion* provides an overview of the highlights, the applicability, as well as the limitations of this work taking into consideration the present and future of the field. Finally, the *Conclusions* summarise the most relevant findings of this thesis in both English and Spanish.

Preface

The *Appendix* contains two pieces of work not directly linked with the primary objective of this thesis. In the first one, an overview of PAINCARE, a public-private collaboration aiming to improve the clinical success rate of novel analgesics, is provided. The second one proposes a population PK model for piperacillin in critically ill children with or without continuous kidney replacement therapy, an area with high medical need due to the vulnerability of this population.

Partial results of the presented work have also been included in the following publications:

Marco-Ariño N, Vide S, Agustí M, et al. Semimechanistic models to relate noxious stimulation, movement, and pupillary dilation responses in the presence of opioids. *CPT Pharmacometrics Syst Pharmacol.* Novemeber 2021. doi:10.1002/psp4.12729[1]

Couto M, Vide S, Marco-Ariño N, et al. Comparison of two pharmacokinetic-pharmacodynamic models of rocuronium bromide during profound neuromuscular block: analysis of estimated and measured post-tetanic count effect. *Br J Anaesth*. February 2022. doi:10.1016/j.bja.2021.12.010[2]

Jaramillo S, Marco-Ariño N, Montane-Muntane M, et al. A semi-mechanistic model for predicting perioperative haemoglobin concentration in non-cardiac surgical patients. Submitted.

Bloms-Funke P, Marco-Ariño N, Birch J, et al. Perspectives on Public-Private-Partnership in Pain Research: Concepts, Methods and Findings of the IMI-PainCare Consortium. Manuscript in preparation.

Butragueño-Laiseca, L., Marco-Ariño, N., Troconiz IF, et al. Population Pharmacokinetics of Piperacillin in critically ill children including those undergoing continuous kidney replacement therapy. Submitted.

Introduction

Since ancient times, humans have used medicinal products to fight disease and its symptoms[3]. During most of this period, the discovery of pharmacologically active substances was accidental or based on trial and error testing of natural products. In the 19th century, the development of chemistry and pharmacology led to the production of the first synthetic drugs[4], opening the possibility to custom-made molecules. However, it is not until the 20th century that a systematic process for the discovery and evaluation of new medicines, a process known today as drug development, is established.

Drug development is a long and complex process and, despite the technological advances that occurred in the last decades, it is still associated with considerable attrition rates[5]. The failure of development programs, particularly in clinical stages, entails a significant burden for pharmaceutical companies[6,7] and ultimately limits the number of new medicines available to patients. In an effort to improve success rates, pharmaceutical companies and regulatory authorities have implemented a series of guidelines[8] and frameworks[9] promoting the use of quantitative approaches across the drug development cycle. Among these, one discipline that has received significant attention for its capability to integrate information and support data-driven decision-making is pharmacometrics.

Pharmacometrics

Pharmacometrics can be defined as "the science of developing and applying mathematical and statistical methods to characterize, understand, and predict a drug's pharmacokinetic, pharmacodynamic, and biomarker–outcomes behaviour"[10]. Pharmacometrics is the result of the pioneering work carried out in 1970-2000 applying nonlinear mixed-effects (NLME) models for the analysis of pharmacokinetic/pharmacodynamics data (PK/PD)[11–13]. In approximately 50 years, pharmacometrics has expanded from being a niche discipline to becoming a multidisciplinary field[14] with influence in high-level decisions such as trial design, drug labelling and approval[15]. This expansion has been accompanied by the development of specific

methodologies and software tools, which untimely has led to the creation of sub-areas of expertise. Among these, quantitative system pharmacology (QSP)[16,17], physiologically-based pharmacokinetic (PBPK)[18] and particularly, population PK/PD (popPK/PD) modelling, constitute the core of pharmacometrics. PopPK/PD has been the subject of this thesis and an overview of its main features is provided in the following sections.

Pharmacokinetics

Commonly known as "what the body does to the drug", pharmacokinetics (PK) is the science that studies the absorption, distribution, metabolism and excretion (ADME) of a drug in the organism. Traditionally, two approaches have been used to characterise pharmacokinetic data: non-compartmental and compartmental analysis.

In non-compartmental analysis (NCA) the concentration vs time profile for an individual is summarised in a series of metrics, such as maximum drug concentration (C_{max}), time at which C_{max} is achieved (T_{max}) or area under the drug concentration vs time curve (AUC), to provide an indicator of drug exposure. NCA is a model-independent method ideal to obtain a simple and robust overview of the PK characteristics of the drug. However, because NCA does not take into account the properties of drug or physiology[19], limited information about different experimental setups or undelaying biological processes is obtained. For this reason, NCA is mainly used at the initial stages of drug characterization or bioequivalence studies.

In compartmental analysis, the body is divided into a series of interconnected compartments where mass balance is guided by specified input, transfer and output processes[20]. Compartments are kinetically homogenous entities that could be semi-empirical (when portions of the system with similar distribution kinetics are lumped together) or physiological (where each compartment represents an actual organ). These models are in general parameterized in terms of apparent volumes of distribution (V) and distribution (CL_D) and/or elimination clearances (CL)–corresponding to primary pharmacokinetic parameters, which by definition, are

influenced solely by the physio-pathological conditions of the patients. This possibility, particularly when combined with population analysis, represents a significant advantage of compartmental vs NCA.

Pharmacodynamics

Echoing PK, pharmacodynamics (PD) can be described as "what the drug does to the body". Although it is usually associated with therapeutic response, PD is a broad term that englobes any response elicited by the drug, including beneficial and side effects[21]. In practical terms, the aim of PD is to describe drug response as a function of drug concentration in the site of action. However, PD measurements are rarely performed at steady-state (SS) concentration in the site of action and often a PK/PD model is needed to link concentration with drug effect. Figure 1 shows the integration of PK and PD data into a PK/PD model to provide a description of the pharmacological response over time.

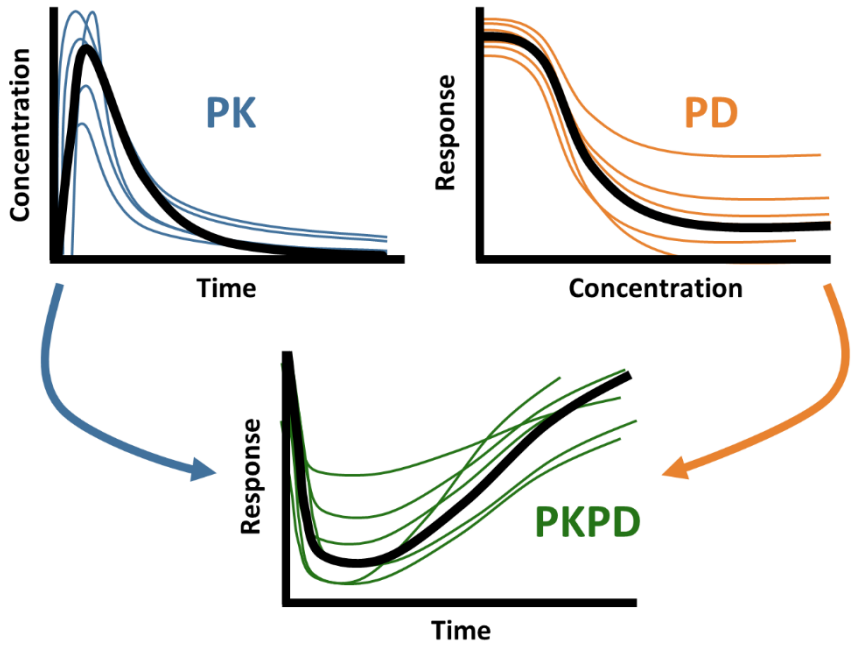

Figure 1. Overview of the main components of population PK/PD. Colour lines represent the individual data and black lines the typical population profile. PK: Pharmacokinetics, PD: Pharmacodynamics.

The most common PK/PD approach is to link measured concentrations (usually in plasma) with response through a direct model[22]. On some occasions, PD effects are delayed compared to measured drug concentrations, a process known as hysteresis. Hysteresis could be the result of delayed equilibration between the site of action and the site of measurement, irreversible drug effects or signal maturation and transduction. A wide range of pharmacodynamic models has been proposed to account for these processes[13,23,24].

Another temporal aspect to take into account when modelling PD data is the self-progression of the disease in absence of pharmacological intervention. For many diseases, it is unethical not to administer available treatments, and drug effects have to be disentangled from the natural course of the disease and placebo/nocebo effects[25]. Of note that while PK data is mainly continuous (the exception being modelling data below the limit of quantification), discrete PD is not uncommon. Figure 2 provides a graphical example of continuous and discrete variables used in popPK/PD analysis. Specific modelling alternatives have been developed to span the different types of discrete data such as categorical[26], count[27] and time-to-event[28] among others.

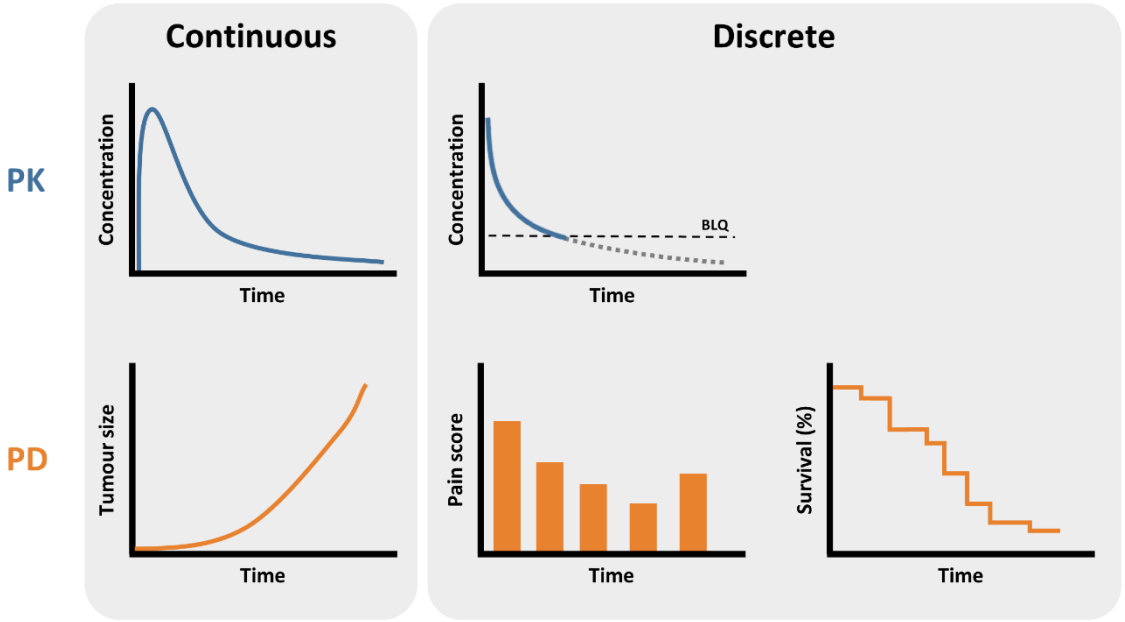

Figure 2. Examples of continuous and discrete variables in population PK/PD. PK: Pharmacokinetics, PD: Pharmacodynamics.

Similarly to PK, PD models range from empirical to semi-mechanistic and ultimately to mechanistic depending on the granularity of the physiological processes described. The more mechanistic the model is, the more detailed description of the biological system is provided but the higher the complexity and computational cost of the model. As a consequence, PD models tend to be "fit for purpose", being the granularity of the model dependent on the objective of the model and data availability.

Population Approach

The goal of PK/PD analysis is to describe the behaviour of a variable, usually dug concentration or PD response, in a set of individuals. Due to biological and environmental factors, study variables do not behave homogenously in all individuals and PK/PD analysis intrinsically implies understanding how individuals from a population differ from each other and other populations. Prior to the use of NLME, the individual metrics and parameters derived from PK and PD analysis were gathered to provide summary statistics for the study population. For example, the mean and the standard deviation of the individual CL was computed to evaluate the elimination of the drug in the study population in a process known as the two-stage approach[29]. However, this method entails a series of limitations: (i) rich data for all individuals is necessary to characterise with precision the individual parameters, (ii) data has to be balanced, (iii) variability is overestimated and (iv) evaluation of covariate effects is limited[30,31].

In NLME modelling, data from all individuals is pooled and analysed simultaneously to identify the population (hence the name population approach) parameters describing the typical tendency of the population and random effects which account for differences in parameters between individuals. Mathematically, NLME models can be represented by the following expression:

$$y_{ij} = f(\psi_i, x_{ij}) + \varepsilon_{ij} \ ; \ i = 1, \dots, N'; j = 1, \dots, n_i$$

$$\varepsilon_{ij} \sim_{i.i.d} N(0, \sigma^2)$$

Where y_{ij} is the j^{th} observation for the i^{th} individual, f is a non-linear function relating the vector of individual parameters (ψ_i) and the vector of independent variables (x_{ij}), N' the number of individuals and n_i the number of observations for the individual i^{th}, and ε_{ij} accounts for the discrepancies between the observations and the model predictions (residual error), which are assumed to be independent identically distributed (i.i.d) random variables following a normal distribution with a mean of 0 and a variance of σ^2.

At a second level of hierarchy (interindividual variation level), the model characterises the individual parameters as a function (g) of fixed population effects (ψ_{pop}), subject-specific covariates (Z_i) and the variance-covariance matrix of random effects (Ω).

$$\psi_i \sim \left(g\left(\psi_{pop}, \mathrm{Z}_i\right), \Omega\right)$$

Assuming for simplicity that the set of regression parameters $g(\psi_{pop},Z_i)$ is represented by ψ_{pop} and that the individual parameters (ψ_i) are independent and follow a log-normal distribution, the individual value for the k parameter can be decomposed into a fixed (ψ_{pop}) and a random effect (η_{ik}).

$$\psi_{ik} = \psi_{pop} \,.\, e^{\eta_{ik}}$$

$$\eta_{ik} \sim N\left(0,\ \omega_k^2\right)$$

Where ψ_{pop} represents the typical population parameter (equal for all individuals in the absence of significant covariates) and η_{ik}, the discrepancy between ψ_{ik} *and* ψ_{pop}. The set of ω^2s forms the diagonal elements of the variance-covariance matrix Ω. The off-diagonal elements are reserved for the covariances across ω^2s.

The fixed-effect parameters accounting for the population and covariate models (ψ_{pop} and Z_i, respectively*)* are commonly known as the structural part of the model. Covariate models evaluate and quantify the influence of patient and study factors in the population parameters. The inclusion of covariates in a PK/PD model is associated with a reduction of the variability and

often facilitates the clinical interpretation of the model[32], setting the basis for dose individualization.

Random effects represent the statistical part of the model and account for the variability in the model not explained by the covariates. In a typical popPK/PD analysis, there are two main sources of variability, inter-individual variability (IIV) and residual variability (RV)[33]. While IIV represents the variability in model parameters across individuals, RV quantifies the differences between the individual predictions and observations (See Figure 3 for a graphical representation of these variabilities in relation to the observations and population and individual predictions). In certain models, a third level of variability -such as inter-occasion variability (IOV)[34] or inter-study variability (ISV)- may be included to account for the differences across studies or research centres.

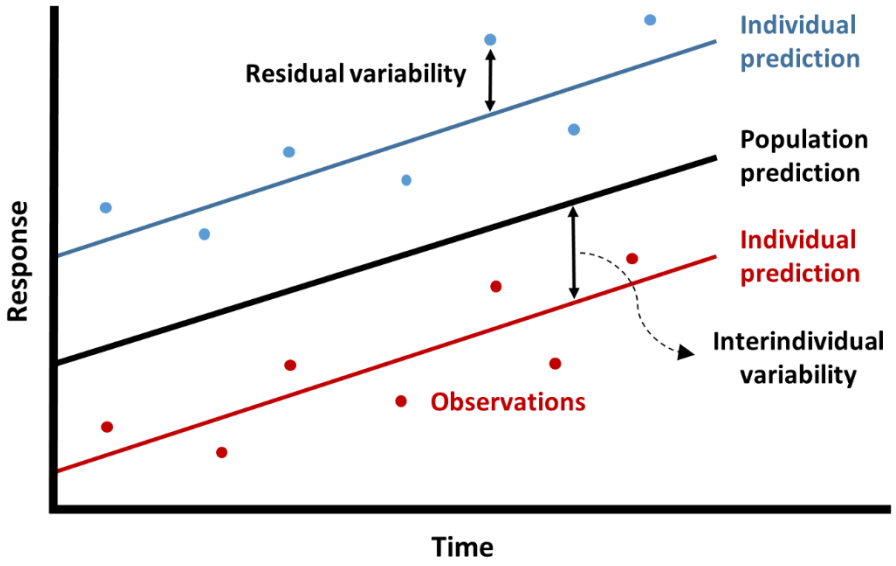

Figure 3. Graphical representation of the variabilities in nonlinear mixed-effects models.

Modelling each of the elements briefly described above represents a challenge as different alternatives are possible to characterise the structure of the model, the influence of covariates, the distribution of the individual parameters and the residual error. As a consequence,

developing a population model represents an endeavour requiring large amounts of resources, particularly in terms of time and specialized personnel.

Pharmacometrics in drug development

The pharmaceutical industry is the sector where pharmacometrics has received more recognition. By combining information from multiple disciplines and development stages, pharmacometrics provides quantitative evidence to overcome frequent challenges in drug development such as dose selection, efficacy evaluation and extrapolation to different populations[14]. As proposed by Sheiner in his "learn and confirm" paradigm[35], the sequence of preclinical and clinical phases necessary to develop a new medicine provides a unique framework to use the information generated in previous stages to facilitate decision making for the next development steps. With the expansion of pharmacometrics, the concept of "learn and confirm" led to model-based drug development (MBDD)[36], where modelling and simulation tools provide quantitative decision criteria across all the drug development process. More recently, a general framework called model-informed drug discovery and development (MID3) has been proposed to promote the use and standardization of MBDD in the pharmaceutical industry[37,38].

As pharmaceutical companies, regulatory authorities have progressively embraced the use of pharmacometrics to support drug approval and labelling decisions[39]. Several authors have reviewed the impact and contributions of pharmacometrics to regulatory purposes[40,41], which could be classified into four categories: dose optimization, supportive evidence for efficacy, clinical trial design and informing policy[42]. The interaction between industry[43] and regulators[44] is constantly evolving and has pushed the focus of MID3 into areas beyond their traditional scope such as work standards, effective communication and management of expertise and innovation.

Pharmacometrics in clinical settings

Unlike in the pharmaceutical industry, the use of pharmacometrics in clinical practice is scarce[45]. With the exception of the areas of anaesthesia[46], where the need to understand the induction and duration of drug effects is more evident, and therapeutic drug monitoring (TDM)[47], few clinical specialities have implemented popPK/PD modelling in everyday practice. The reasons are multiple. One of them is the shortage of expertise in the field due to the lack of specific pharmacometrics training in clinical programs and funding opportunities[14]. Another potential reason is the failure of phamacometricians to effectively communicate their work to other disciples, which may result in the perception of pharmacometric analysis as "complex" and "of little use"[48]. In this regard, several authors have reviewed the basic principles of pharmacometrics for a clinical audience[32,49,50].

Data organisation, standardization and quality control are tedious aspects that may also hamper the application of pharmacometrics in clinical settings. While data in drug development is subjected to a thorough process of evaluation, validation and processing before analysis, routine clinical data does not undergo quality controls and is often not suitable for quantitative evaluation[51]. In this sense, automatic learning tools could provide an opportunity to organise and standardise clinical data[51], although quality control and patient privacy would still be a challenge.

Ultimately, the main limitation for the application of pharmacometrics in clinical practice is the lack of direct evidence supporting that model-informed precision dosing (MIPD) improves patient outcomes (i.e. efficacy or toxicity) vs standard care[45]. The few randomised clinical studies that have addressed this question have shown an improvement in the safety of chemotherapy[52,53] and antibiotics[54] when administered following a MIPD approach. Despite this fact, no confirmatory studies have been undertaken and currently, MIPD remains an opportunity.

Pain and perioperative management

In this work, we aimed to mitigate the lack of quantitative tools for the clinical management of pain and perioperative care, two areas where decision-making often relies on indirect signs or clinicians' criteria. Particularly, we focused on developing popPK/PD methods to improve the intraperioperative administration of opioids and neuromuscular blockade (NMB) agents and assist in the selection of patients requiring red blood cells (RBC) transfusions, which lack an optimal solution.

Opioids are the main drugs used to archive analgesia in surgical procedures, although careful titration is required to attain the right balance between therapeutic and side effects. Theoretically, movement, which is the most direct and clinically observed response to painful stimulation, could be used to guide opioid administration, but in practice, its applicability is limited due to the effect of the anaesthesia and NMB agents. Previous research has shown that Pupillary Reflex Dilation (PRD) —a supra-spinal parasympathetic reflex[55,56]— is diminished by opioid administration[57,58] and predicts movement after noxious stimuli[59], suggesting it could be used for the assessment of analgesia in patients under general anaesthesia. In this work, we used pharmacometric techniques to quantify the influence of remifentanil on PRD, and its relationship with the reflex movement response to a standardized noxious stimulus.

In a similar manner, the administration of NMB agents is not fully optimised. During profound NMB, train-of-four (TOF), the usual monitor of NMB, is overcome (TOF=0) and Post-Tetanic Count (PTC) stimuli are often used to assess the remaining neuromuscular function[60]. PTC is a non-invasive technique that applies a tetanic pulse of 50 Hz for 5 seconds, followed by a rest of 3 seconds and then 10-20 single twitches of 1 Hz[61]. Afterwards, the number of positive twitches (those causing mechanical contraction) before an absence of response is added to provide the final PTC count. Most of the PK/PD studies for rocuronium —one of the most used NMB agents— have been performed in non-profound NMB using TOF response[62–67]. In this thesis, we

investigated the PK/PD relationship of rocuronium and PTC in deep levels of NMB using two pharmacokinetic models from the literature.

Transfusion medicine is another clinical area where quantitative methods play a residual role. Decisions on red blood cell transfusions are taken predominantly based on haemoglobin concentrations (Hb)[68–70], which are known to fluctuate significantly and unpredictably during the early perioperative period. Although some of the factors contributing to these variations have been indentified[71–74], perioperative Hb remains unpredictable. As a result, clinicians often face the decision of whether or not to transfuse a patient (both perioperative anaemia and RBC transfusions are associated with adverse clinical outcomes[75–79]) without reliable criteria to support their choice. In this work, we developed a semi-mechanistic model using physiological and surgery-related variables to characterize the time course of Hb, thus supporting decision-making for red blood cell transfusion.

Concluding remarks

Pharmacometrics is an integrative field comprising elements from multiple disciplines such as pharmacology, medicine and statistics. Given the quantitative nature of pharmacometrics and the uncertainty surrounding drug development, pharmacometrics has become a central tool to support decision making in the pharmaceutical industry. On the contrary, the expansion of pharmacometrics in clinical practice has been very limited and there is a clear opportunity to incorporate the use of pharmacometrics techniques in this scenario, thus contributing towards MIPD and personalised medicine.

Objectives

Pharmacometrics is a discipline tightly associated with drug development. Nevertheless, the use of pharmacometrics is not limited to the process of developing a drug per se and could also be applied to support other aspects such as the characterization of biomarkers in areas with low success rates. In this thesis, we explored the use of pharmacometrics to improve the development of quantitative models in clinical practice.

In the latter, the use of pharmacometrics is in its infancy. We acknowledge that the application of pharmacometrics in clinical settings is challenging but there is a need to move towards the generation of real-world evidence in broader populations outside clinical trials. This thesis aims to constitute a step towards MIPD, providing clinicians with quantitative tools to guide decision-making in perioperative management. This is a complicated scenario where decisions are often taken based on indirect signs and/or individual experience, and quantitative techniques could represent a powerful instrument to optimise drug administration. In this sense, we believe that the rise of personalised medicine represents a unique opportunity to consolidate the use of modelling and simulation techniques in clinical practice.

These general aims can be summarised in the following objectives and sub-objectives:

1. To evaluate Pupillary Reflex Dilation (PRD) as a prospective biomarker of analgesia depth to individualise the dose of analgesics during surgery.
    - To develop population PD models to characterise PRD and movement response to tetanic stimulation in the absence of opioids.
    - To link the developed PD models with patients' predicted plasma drug concentrations to explore the effects of propofol and remifentanil on pupillary and movement reflexes over the time course of the surgical procedure.
    - To explore the dynamics of PRD and movement models taking into consideration the potential applicability of PRD as a biomarker for pain.

Objectives

2. To investigate the PK/PD relationship between rocuronium and post-tetanic counts (PTC), a marker of profound neuromuscular blockade, thus enabling anaesthesiologists to optimise dosing during surgery.
    - To evaluate the performance of two published PK models for rocuronium.
    - To explore the suitability of different modelling approaches [i.e., continuous vs non-continuous (ordered categorical and count data) response analysis] to characterize the PTC response.

3. To characterise the changes in haemoglobin concentrations after surgery, hence supporting decision-making in red blood cell transfusion and perioperative care.
    - To develop a population PK/PD model to describe the changes in haemoglobin mass and the balance between fluid administration and elimination in perioperative patients using variables routinely collected in surgical procedures.
    - To investigate the clinical applications of the model by exploring the probability of requiring a blood transfusion based on patient and surgical characteristics, aiming to provide a simple and cost-effective framework for decision-making in blood transfusion.

Methods

Clinical Studies

Data from three different clinical studies in surgical patients was used to develop the popPK/PD models. An overview of the patient characteristics, the study protocols and the measured variables from each study is provided in the following sections.

Clinical study 1: PRD and movement models

Patient population and characteristics

Under Institutional Review Board and Ethics Committee approval (Hospital CLINIC de Barcelona nº HCB/2016/0318) and following written informed consent, 78 female patients scheduled for gynaecologic surgery under general anaesthesia in the Ambulatory Surgery facility at Hospital CLINIC de Barcelona, Spain, were included in the current study. Exclusion criteria were prior eye surgery, any ophthalmologic diseases besides refraction errors, prescription of drugs affecting the size or reflex of the pupil and morbid obesity (BMI>35).

Study protocol

Upon arrival in the operating room, routine monitors were placed. General anaesthesia was achieved and maintained with propofol and remifentanil administered using a Target-Controlled Infusion (TCI) system (Base Primea, Fresenius Kabi AG, Bad Homburg, Germany).

Loss of consciousness was induced setting the predicted effect-site concentration of propofol ($C_{e,Prop}$) between 5 and 11 $\mu g \cdot mL^{-1}$ (based on Schnider model[80,81]).

Two minutes after reaching the predicted pseudo-steady state for propofol, the PRD was elicited using the videopupilometer Algiscan® (IDMed, Marseille, France) connected to two electrodes placed on the volar surface of the right arm. The stimulus consisted of a 60 mA tetanus for a period of 5 seconds. Pupil diameter (PDiam) was measured and recorded at 67 Hz for 13 seconds: 2 seconds before the stimulation, during the 5 seconds stimulation and until 6 seconds after the stimulation ended. A rubber cup covered the measured eye, and the contralateral eye was taped closed.

Methods

The investigational procedure was video recorded. Retrospectively, two clinicians examined the video recordings to evaluate the intensity and duration of the movement response. Movement intensity was classified into a four-level categorical scale: 0 - absence of movement, 1 - movement of only one limb, 2 - movement of two or three limbs and 3 - movement of the whole body.

Within approximately 5 min after the first stimulation, while maintaining the same propofol effect-site concentration, remifentanil administration was started achieving predicted effect-site concentrations ($C_{e,remi}$)[82] varying between 0.5 and 6 ng·mL^{-1}. Two minutes after reaching the predicted pseudo-steady state equilibration, a second and a third PRDs were elicited as described above and PDiam and movement response were recorded.

Then, the airway was secured either by placing a laryngeal mask or by endotracheal intubation. When intubation was required, 30 mg of rocuronium bromide were administered, two minutes before laryngoscopy. The hypnotic effect was titrated to maintain a Bispectral Index (BIS, BIS Vista, Medtronic, Ireland) value between 45 and 60. The analgesic effect was titrated at the discretion of the attending anaesthesiologist.

At the end of surgery $C_{e,prop}$ and $C_{e,remi}$ were set to 1 µg·mL^{-1} and 0 ng·mL^{-1} respectively. When propofol Ce target was reached, one or two additional stimulations separated by at least three minutes were carried out before the patient spontaneously awakened or moved.

General description of the data

Demographic characteristics of the patients included in the study are shown in Table 1.

Table 1. Patient characteristics

Subjects (n)	78
Female (n)	78
Age (years)	45 (27 - 85)
Height (cm)	160 (140 - 173)
Weight (Kg)	64 (38 - 93)
Lean Body Mass (Kg)	44 (31 - 58)
Body surface area (m^2)	1.65 (1.26 - 2.04)

Expressed as median (range)

Figure 4 shows the raw data profiles for pupillary size, movement response and predicted drug concentrations used for the model development. Of all pupil measurements, 1082 were recorded in the presence of propofol (first stimulus) and 2775 were recorded with a combination of propofol and remifentanil (stimuli 2-4). For the movement analysis, 1092 observations correspond to the first stimulus and 2816 to stimuli 2-4. In both endpoints, the number of observations after surgery was lower than for those performed before surgery started as subjects were recovering consciousness after the surgical procedure, and measures were interrupted when a patient showed signs of arousal. Data corresponding to the 5^{th} stimulus (the second after surgery) was not used for model development but as an internal validation dataset.

Predicted propofol and remifentanil concentrations were recorded every second during the experimental procedure. Figure 5 shows the distribution of the different combinations of propofol and remifentanil targeted during the study.

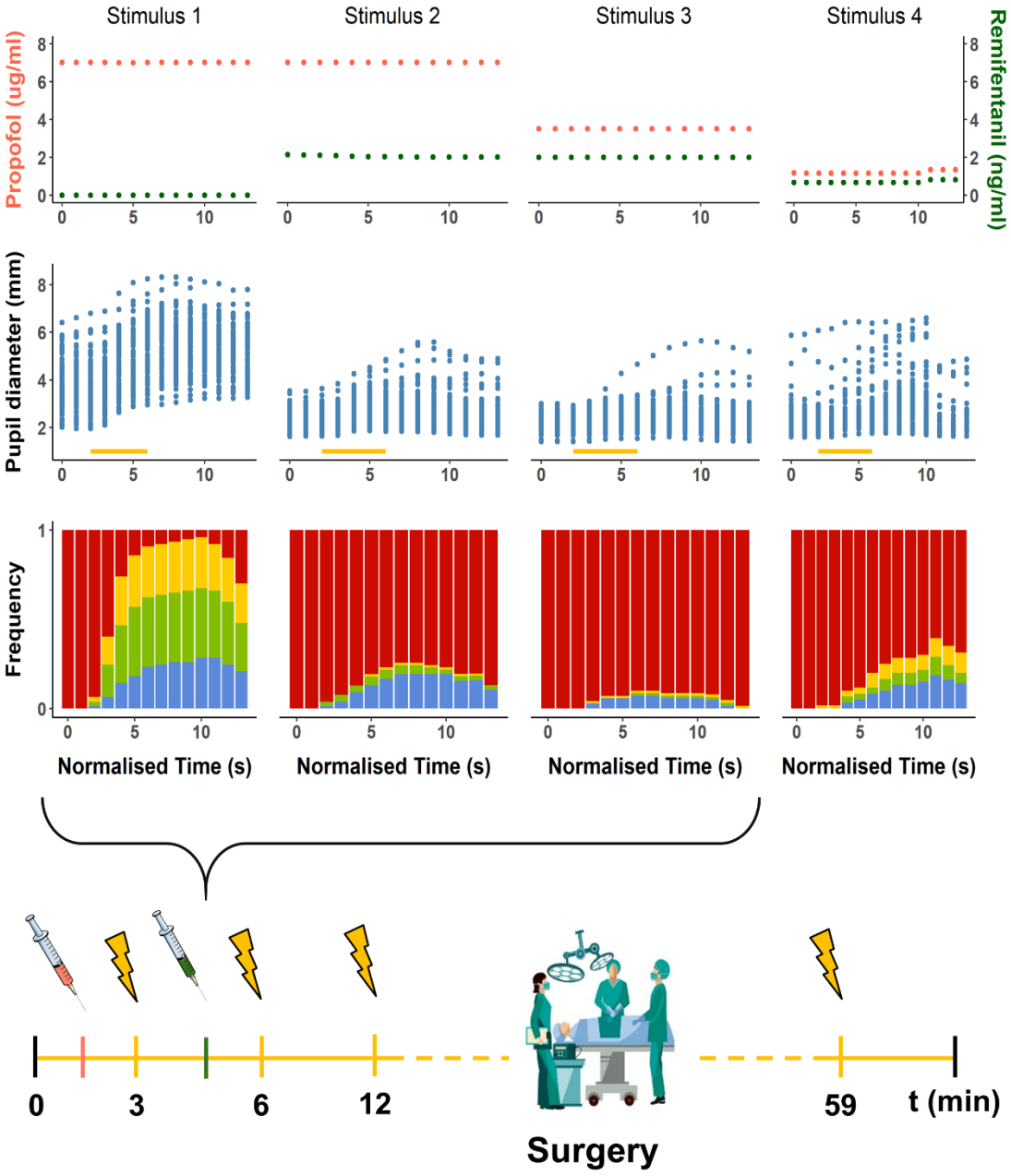

Figure 4. Overview of the experimental set-up and data generated during the experimental procedure. Upper panels show the median concentrations of propofol (red) and remifentanil (green) over the four cycles of stimulation. Middle panels depict the raw pupil profiles for each stimulus. The orange line highlights the period of 5 seconds when electric stimulation is delivered. Lower panels represent the distribution of the movement scores per stimulus (Grade 0: red, grade1: blue, grade 2: green, grade 3: yellow). The bottom figure represents the timeline of the experimental procedure with the administration of propofol (red syringe), electric stimuli (yellow lightning), administration of remifentanil (green syringe) and surgical procedure. Times represent the mean starting time for each stimulus among all the individuals. Images were modified from Servier Medical Art[83] and Freepik[84].

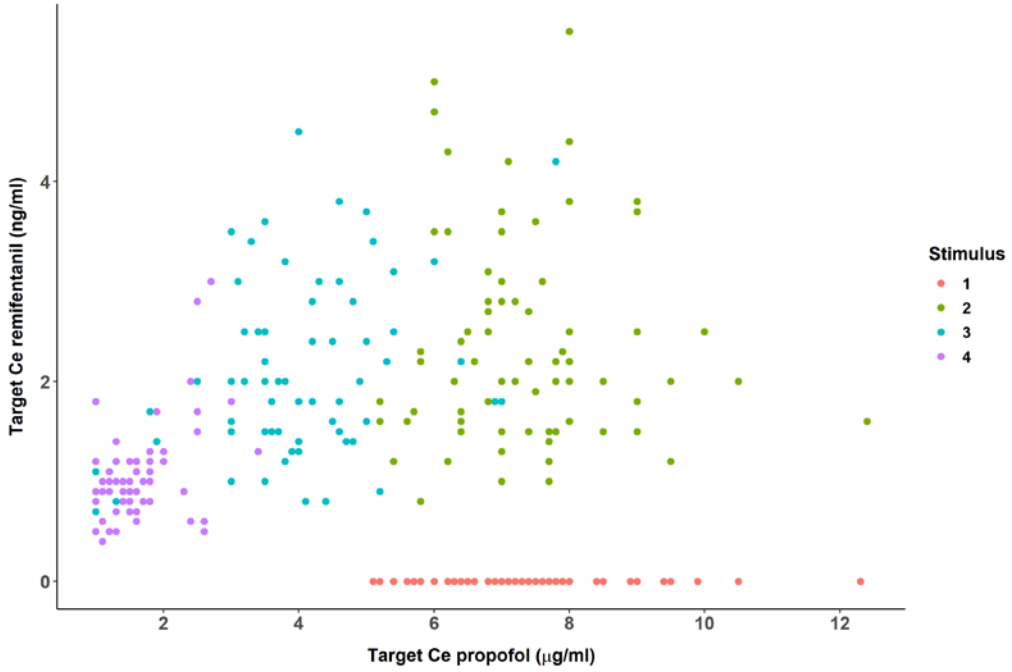

Figure 5. Drug combinations. Combinations of propofol and remifentanil predicted concentrations in the effect site (Ce) targeted across the different stimuli.

Clinical study 2: PTC model

Patient population and characteristics

This prospective, non-randomised, observational study was carried out at the Centro Hospitalar e Universitario do Porto (CHUP, Porto, Portugal) and performed according to Good Clinical Practice guidelines and pharmacovigilance directives[85]. Approval of the protocol was obtained from the Research Coordinating Office and the Ethics Committee at CHUP (reference 2018-209 (184-DEFI/183-CES)). Accordingly, agreement and written informed consent were obtained from all patients enrolled in the study.

The study was conducted on adult patients (18-80 years old), classified as ASA I-IV (American Society of Anesthesiologists Physical Status Classification System), scheduled for routine laparoscopic or neurosurgical procedures, performing general anaesthesia with a minimum duration of 90 minutes that allowed continuous infusion of rocuronium for profound NMB. Patients were excluded from the study if presented any neuromuscular diseases, severe

cardiovascular, hepatic or renal pathologies, contra-indications for any of the drugs used, a BMI>35kg m^{-2}, or were pregnant/nursing.

Study protocol

The protocol did not significantly change routine clinical practice. All monitoring was based on standard ASA guidelines, including electrocardiogram, pulse oximeter, non-invasive blood pressure, BIS, central temperature and neuromuscular monitoring. General anaesthesia consisted of propofol and remifentanil administered using a TCI (Fresenius Orchestra Base Primea, Homburg, Germany), with effect-site target concentrations titrated to achieve and maintain a BIS value between 40-60 (BIS, Medtronic, Ireland). Mean arterial pressure was maintained between [-30% +30%] of the patient's baseline value. For the NMB, rocuronium was administered using an Alaris TIVA infusion pump (BD, Becton, Dickinson and Company, Franklin Lakes, USA) and the infusion data was recorded to a laptop. NMB monitoring was performed using TOF-Watch® SX, measuring the response at the adductor pollicis muscle. After the skin was degreased, two electrodes were placed over the ulnar nerve and contractions were measured by an accelerometer sensor at the thumb. Calibration was carried out according to manufacture specifications (CAL 2)[85]. Data acquisition throughout the case was performed via TOF-Watch® SX Monitor software (version 2.5INT, Organon, 2007).

After the loss of consciousness, all patients received 1mg kg^{-1} of Fat-Free Mass (FFM)[86] of rocuronium, specifying the induction dose for each individual. Initially, using TOF-Watch® SX, the assessment of the NMB function was performed by continuous TOF stimuli every 15 seconds, primarily to confirm the onset (TOF=0) and appropriate conditions for intubation and, secondly, to ensure the absence of moderate NMB during the procedure. After tracheal intubation was complete, PTC measurements were performed every 3 minutes. Besides ensuring good intubation conditions, the initial dose was selected with the objective of promptly achieving complete NMB (PTC=0). Next, after measuring at least two consecutive PTC

measurements above zero, a constant infusion of rocuronium was started and titrated to maintain the NMB target of 1-2 PTC. At the end of the surgery, after surgical dressing, propofol and rocuronium infusions were stopped, and reversal of NMB was performed with 4 mg kg^{-1} sugammadex. For all subjects, extubation was carried out when the TOF-ratio was consistently over 0.9. Normothermia was ensured during NMB monitoring and, although the hand was secured and supervised, any disturbances during measurements were recorded for future exclusion from data analysis.

General description of the data

Thirty patients undergoing elective abdominal and neurosurgical procedures were enrolled in this study. The baseline characteristics of the study population are presented in Table 2. Surgical procedures had a mean duration of 219 (76.4 standard deviation (SD)) min. A total of 1955 post-tetanic count stimuli were included in the analysis.

The induction bolus provided appropriate intubation conditions and abolished the initial PTC measurements in all subjects, taking approximately 26.3 min (10.4 SD) (considering PTC monitoring performed every 3 minutes) to recover a positive PTC response. Next, the infusion was started and manually adjusted along the procedure to maintain 1-2 PTC. The length of the infusion was approximately 190 min (78.3 SD), during which, a mean of 58.2 PTC stimuli (25.7 SD) were applied. For this population, 65.9% (13.9 SD) of the observed measurements were within the NMB target, 12.6% (11.0 SD) were below (PTC=0), and 21.5% (9.5 SD) were above the target (PTC>2). The rocuronium used via continuous infusion for the maintenance of the NMB degree showed a demand of 0.56 mg kg^{-1} h^{-1} (reference of total body weight (TBW)). At the end of the surgical procedure, all patients were successfully extubated at TOF-ratio>0.9 within 3-6 min.

Table 2. Patient characteristics (mean (SD or range) or n).

Patient sample		30
Age		62.1 (23-79)
Sex	Male	15
	Female	15
ASA class	I	0
	II	25
	III	4
	IV	1
Total body weight (kg)		72.4 (13.4)
Height (m)		1.64 (0.09)
BMI (kg m^{-2})		27.1 (4.6)
FFM (kg)		48.7 (9.9)

Abbreviations: ASA - American Society of Anesthesiologists Physical Status Classification System; BMI - Body mass index; FFM – Fat-free mass

Clinical study 3: Haemoglobin and fluid models

Patient population and characteristics

This prospective observational study was conducted at Hospital Clinic de Barcelona (Spain). The study was approved by the institutional review board (HCB/2016/0906/2) and registered in Clinicaltrials.gov (NCT03740438). Adult patients electively scheduled for laparoscopic urologic and gynecologic surgery were included consecutively after signed written consent was obtained. The study design considered two cohorts of patients in two consecutive enrolment periods, the first for model development (development group) and the second for model validation (validation group).

Study protocol

The study protocol for both cohorts consisted of serial measurements of Hb along with recordings of blood loss, fluid infusions, urine volume and laboratory assessments.

Exclusion criteria were: history of bleeding disorders, preoperative thrombocytopenia (<150 $x10^3$/mL), prolonged prothrombin time (>15 seconds) or prolonged activated partial thromboplastin time (>35 seconds), intraoperative blood volume loss <500 mL, requirement for surgical gauzes during surgery including conversion to open surgical techniques, blood transfusion or use of blood recovery systems during the perioperative period, significant postoperative bleeding (>100 mL/24h in surgical drains, gross haematuria, or any other type of significant blood loss), major postoperative complications during hospitalization, including postoperative haemodynamic instability (defined in this study as the need of vasoactive drugs infusions after surgery), infectious complications (presence of fever, SIRS, sepsis or septic shock), respiratory complications (extubation failure, ventilation support, respiratory failure), and surgical reintervention.

Medical, anthropometric and procedure data were collected prospectively. Standard preoperative care included the proper interruption of antihypertensive, antiplatelet, anticoagulant and other medications according to the ESA and ESC/ESA guidelines[87,88], and an 8-hour period of fasting before surgery. No fluid infusion was administered prior to surgery.

General anaesthesia was administered in all cases. A urinary catheter was placed in all patients prior to surgery. During surgery, fluid infusions, urine volume and surgical time were recorded by an automatic electronic system (Centricity Anesthesia, GE Healthcare, Barrington, IL). Intraoperative fluid infusion therapy consisted of a crystalloid solution (Plasmalyte 148, Baxter Healthcare, Norfolk, UK) in volumes according to the anaesthesiologist's criteria. Intraoperative blood loss was measured at the end of the surgery using a previously described method based

on the assessment of blood volume loss[89] and haemoglobin mass loss[90], with measurement precisions of ±50 mL and ±4 g, respectively.

Postoperative fluid infusion therapy consisted of glucose solution (10% glucose, 0.8-1 mL/kg/h) and a crystalloid solution (Plasmalyte 148) in rates determined by the anaesthesiologist's criteria. Fluid infusions and urine were registered as cumulative volumes every 24 hours on a 50 mL scale. Intraperitoneal surgical drains were placed in all patients before the end of the surgery and withdrawn after 48 to 72 hours, which allowed detecting any significant postoperative bleeding. All clinical variables were recorded in an automatic electronic system.

Laboratory assessments were performed prior to surgery, immediately after surgery and every 24 hours until: (1) the patient regained complete tolerance to oral fluid intake or, (2) urinary catheter was removed. Blood measurements included: Hb (g/L), white blood cells complete and differential count (counts/mm^3) and C reactive protein (mg/dL). Blood samples were analyzed using Advia 2120i automated hematology analyzer (Siemens Healthcare, Erlangen, Germany), which has a reported precision (SD) of ±1.4 g/L for the measurement of Hb. All samples were obtained from the arms' large veins using a standard protocol (in a supine position, between 07.00 and 09.00 hours).

General description of the data

Table 3 summarizes patient characteristics and data available for analysis. Between November 2018 and May 2021, a total of 154 patients were considered eligible for the study. Of those, 118 subjects were enrolled in the development group, while 36 patients were enrolled in the second period of recruitment for the validation group. Hb values of both groups (792 observations) were measured up to a maximum of 96 hours after surgery. Hb values, fluid infusions and urine volumes for each perioperative time point are summarized in Figure 6.

Table 3. Patient characteristics.

	Development group	**Validation group**
Subjects (n)	118	36
Gender (M/F) (n)	62/56	17/19
Age (years)*	57 (28 - 88)	52 (34 - 76)
Height (cm)*	167 (131 - 195)	166 (135 - 194)
Weight (kg)*	77 (56 - 107)	74 (57 - 98)
Body Mass Index (kg/m^2)*	27.7 (17.0 - 39.6)	27.0 (16.6 - 39.5)
Blood volume loss (L)*	0.88 (0.53 - 2.78)	0.90 (0.53 - 2.89)
Haemoglobin mass loss (g)*	110 (53 - 322)	107 (55 - 311)
Calculated intravascular volume (L)*	5.5 (4.0 - 7.8)	5.6 (4.0 - 7.3)
Surgical procedure (n)		
Robotic Prostatectomy	39	10
Partial Nephrectomy	26	10
Radical Nephrectomy	7	2
Nephroureterectomy	6	1
Hysterectomy with adnexectomy	7	2
Hysterectomy	19	6
Myomectomy	7	2
Endometriosis	7	3

*Expressed as median (range).

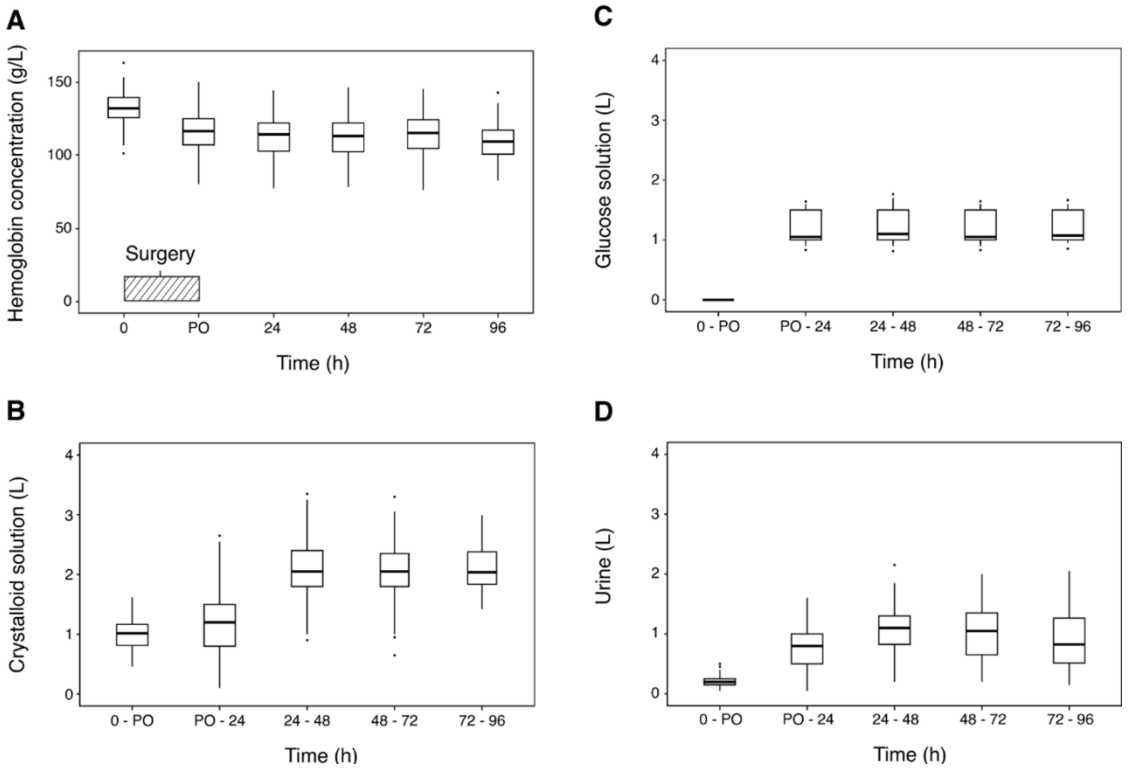

Figure 6: Overview of the data collected. Hb data are shown for each time point (A), while fluid infusions (crystalloid and glucose solutions) and urine are shown in the intervals between each time point (B, C and D, respectively). Note that due to the different lengths of the surgical procedures, the first postoperative time points are gathered into a single time point (PO) comprising 2 to 6 hours.

Data analysis

Data was analysed using the population approach with NLME modelling and the software NONMEM 7.4[91]. The First Order Conditional Estimation (FOCE) method with interaction was used for the analysis of continuous data, while discrete variables were analysed using the Laplacian estimation method.

Continuous variables were natural-logarithm transformed and the residual error was initially modelled additively in the logarithmic scale —residual variability does not apply in the case of the analysis of non-continuous response. In the case of variables measured very frequently, a model for autocorrelated errors[92] was also explored in the analysis.

IIV in model parameters was modelled exponentially. Only for the case of IIV associated with the Logit (L) transformation of categorical scores, an additive model was used, since regardless of the magnitude of the individual random effect, probabilities were kept between 0 and 1.

Model selection

The minimum value of the objective function (OFV), approximately equal to -2 x log-likelihood (-2LL), was used to discriminate between competing models through the log-likelihood ratio test (LRT). A decrease of 3.84 or 6.61 in the -2LL –corresponding to a 5 or 1 % level of significance respectively– was considered statistically significant for nested models differing in one parameter. For comparison across non-nested models, the Akaike Information Criteria (AIC) was used[93]. In addition to LRT or AIC, parameter precision expressed as the percentage of relative standard error (RSE) –calculated as the ratio between the standard error and the estimate of the parameter– and goodness of fit (GOFs) plots were used as criteria to accept or reject a model. Models with RSE values ≥ 0.5 were not accepted.

Covariate evaluation

Correlations between covariates and between covariates and individual parameters were first evaluated visually. For covariates showing a high level of correlation, only the covariate with the lowest level of missing data was included in the statistical analysis. Additionally, for random effects with η-shrinkage values<30%, if no tendencies were detected between individual estimates of model parameters and patient characteristics, no further investigation of potential covariate effects was undertaken.

Statistical evaluation of covariates was performed with the stepwise covariate model (SCM)[94] method with p-values of 0.05 for the stepwise forward inclusion and 0.01 for the backward elimination. Categorical covariates were tested for significance as follows:

$$TVP = \theta_{Ref} \times \left(1 + \theta_{Cat_i}\right) \quad (eq. 1)$$

Where *TVP* is the typical value of the parameter for a certain i[th] category of a unique categorical covariate (*Cat*), θ_{Cat_i} is the fractional change for the i[th] category with respect to the typical estimate for the reference category (θ_{Ref}). θ_{Cat_i} is equal to zero for the reference category.

Continuous covariates were evaluated as follows:

$$TVP = \theta_m \times (1 + \theta_{Cov} \times (Cov - Cov_{median})) \quad (eq. 2)$$

Where *TVP* is the typical value of the parameter for a certain covariate value (*Cov*), Cov_{median} the median value of the covariate, and θ_{Cov} the fractional change per unit of covariate regarding the typical estimate for the median value of the covariate (θ_m).

The impact of selected covariates was further evaluated in forest plots where the relative change in the parameter estimate driven by the covariate was compared with the reference category (categorical covariates) or the 2.5[th] and 97.5[th] percentiles versus the median (continuous covariates). The 95% symmetric confidence interval for covariate relationships were calculated using NONMEM standard errors, and an absolute change higher than 20% from the reference value was considered significant.

Model evaluation

Visual predictive checks (VPCs)[95], corresponding to a simulation-based diagnostics, were used to evaluate the performance of the selected models. One thousand datasets (five hundred for the PTC model) of the same characteristics as the original one were simulated using the structure and parameter estimates from the selected models. For each of the simulated datasets and each measurement time, either the 2.5[th], 50[th] and 97.5[th] percentiles (continuous variables) or the probability of a certain score (categorical data) were calculated. Then, the areas covering the 95% prediction intervals for each of the simulated percentiles or each score were generated and plotted together with the corresponding raw data. Agreement between predictions and

observations was made visually. Additionally, the frequency of each score in the observed and simulated datasets was calculated for categorical data in the PTC models.

Parameter precision of the selected models was further evaluated by analysing one thousand (five hundred for the PTC models) non-parametric bootstrap datasets and computing the 95% (90% for PTC models) confidence interval for each of the parameter estimates.

Model validation

Data not used for model development (5th stimulus in the case of Study 1 and validation group in Study 3) was used to validate the developed models.

In the case of Study 1, the model developed for stimuli 1-4 was used to simulate the pupil diameter and movement grades during the 5th stimulus, and this simulation was compared with the observations. Additionally, in the case of pupil response, individual model parameters were used to predict the pupil diameter during the 5th stimulus. For Study 3, the developed model was used to obtain the empirical Bayes estimates (EBE) and individual predictions of Hb in the validation group.

Prediction errors (PE) –calculated as *Observation - Prediction*–, normalised PE (NPE) –calculated with equation 3– and absolute NPE (ANPE) –calculated with equation 4– were computed to quantify the precision of the individual predictions.

$$NPE_i = \sum_{j=1}^{n} \frac{Pred_j - Obs_j}{Obs_j} \quad (eq.3)$$

$$ANPE_i = \sum_{j=1}^{n} \frac{|\, Pred_j - Obs_j \,|}{Obs_j} \quad (eq.4)$$

Where $Pred_j$ and Obs_j, refer to the individual model prediction and observation for the ith subject obtained at time jth, respectively.

Software and tools

R (versions 3.6.1 and 3.6.3) with RStudio[96] interface (version 1.2.5001) were used for data curation and generating the graphical output (Xpose[97] and ggplot2[98] packages). VPCs, covariate evaluation and bootstrap simulations were performed with Perl-Speaks-NONMEM (PsN)[99,100]

Results

Clinical study 1: PRD and movement models

Pharmacodynamic models

The raw data profiles presented in Figure 4 show two features that are relevant from a modelling point of view: (i) there is a delay between the beginning of the nociceptive electric impulse and the onset of the pupil and movement responses, and (ii) remifentanil reduces both the PDiam and the probability of movement. Consequently, models based on the concept of the indirect response[23], and drug inhibitory effects either on the perception and/or transduction of the nociceptive signal, were fit to the data.

Pupillary Reflex Dilation response

A model considering that PRD is influenced by the time course of unobserved levels of nociceptors (N_{act}) provided better fits compared to just one turn-over compartment (Δ-2LL=-890; $p<0.01$). In absence of either electric stimulation or remifentanil, N_{act} was arbitrarily set to a baseline value of 1 ($N_{act,0}$), maintained by the balance between the zero and first-order rate constants of turn-over, K_S and K_D respectively, as shown by equation 5. At baseline, the rate of change of N_{act} (dN_{act}/dt) is null, and K_S equal K_D as $N_{act,0} = 1$.

$$\frac{dN_{act}}{dt} = K_S - K_D \times N_{act,0} \quad (eq.5)$$

A turnover model was used to transduce the N_{act} dynamics to pupil response as shown in equation 6, where $K_{P,S}$ and $K_{P,D}$ represent the zero-order and first-order rate turnover constants respectively, being $K_{P,S} = K_{P,D} \times PDiam_0$, and $PDiam_0$, the value of PDiam at baseline.

$$\frac{dPDiam}{dt} = K_{P,S} \times N_{act} - K_{P,D} \times PDiam \quad (eq.6)$$

Results

Electric stimulation increases N_{act} as indicated in equation 7, where θ_{ES} is the parameter accounting for its nociceptive effects, and ES is a variable with a value of 1 during the application of the electrical stimulus and 0 otherwise.

Remifentanil showed significant ($p < 0.01$) effects in (i) reducing of the nociception activation triggered by the application of the electric stimulus (that is modulating θ_{ES}), and (ii) increasing the first-order rate constant K_D, which are expressed in equation 7 by $f(C_{e,remi})$, and $g(C_{e,remi})$, respectively.

$$\frac{dN_{act}}{dt} = K_S \times \left[1 + \theta_{ES} \times ES \times f\left(C_{e,remi}\right)\right] - K_D \times g\left(C_{e,remi}\right) \times N_{act} \quad (eq.7)$$

During model development, different structures for f() and g() considering the predicted remifentanil concentration in plasma ($C_{p,remi}$) and effect site ($C_{e,remi}$) were explored, leading to the final model for N_{act} represented in equation 8.

$$\frac{dN_{act}}{dt} = K_S \times \left(1 + \theta_{ES} \times ES \times \frac{1}{1 + \frac{C_{P,Remi}}{C_{50}}}\right) - K_D \times \left(1 + \theta_{Remi} \times C_{e,Remi}\right) \times N_{act} \quad (eq.8)$$

Where C_{50} is the concentration of remifentanil ($C_{p,remi}$) reducing the impact of θ_{ES} to half its maximum value. The terms θ_{ES} and C_{50} account for the induction of the PRD response by the electrical stimulation and the attenuation by remifentanil, respectively. The term θ_{Remi} refers to the slope at which the concentrations of remifentanil in the effect site increases K_D and is related to the decrease of pupil diameter over time after administration of remifentanil. As this effect is linear, remifentanil could decrease PDiam below physiological constraints. In order to prevent this from happening, a feedback mechanism limiting the effect of remifentanil (PDiam-θ_{Limit}/PDiam) was incorporated into the model.

Predicted values of $C_{e,remi}$ were obtained using equation 9, which represents the effect compartment model[13].

$$\frac{dC_{e,remi}}{dt} = k_{e0} \times \left(C_{p,remi} - C_{e,remi}\right) \quad (eq.9)$$

Where k_{e0}, is the first-order rate constant governing the drug distribution equilibrium between the central and effect site compartments.

Additional effects of remifentanil as well as the contribution of propofol to the activation of nociceptors and pupil turnover were also investigated. Neither of these processes resulted in a significant improvement in model fit ($p>0.05$), and therefore, were not incorporated in the model. Figure 7A shows both the schematic and the full mathematical representation of the structural part of the population model for PRD response.

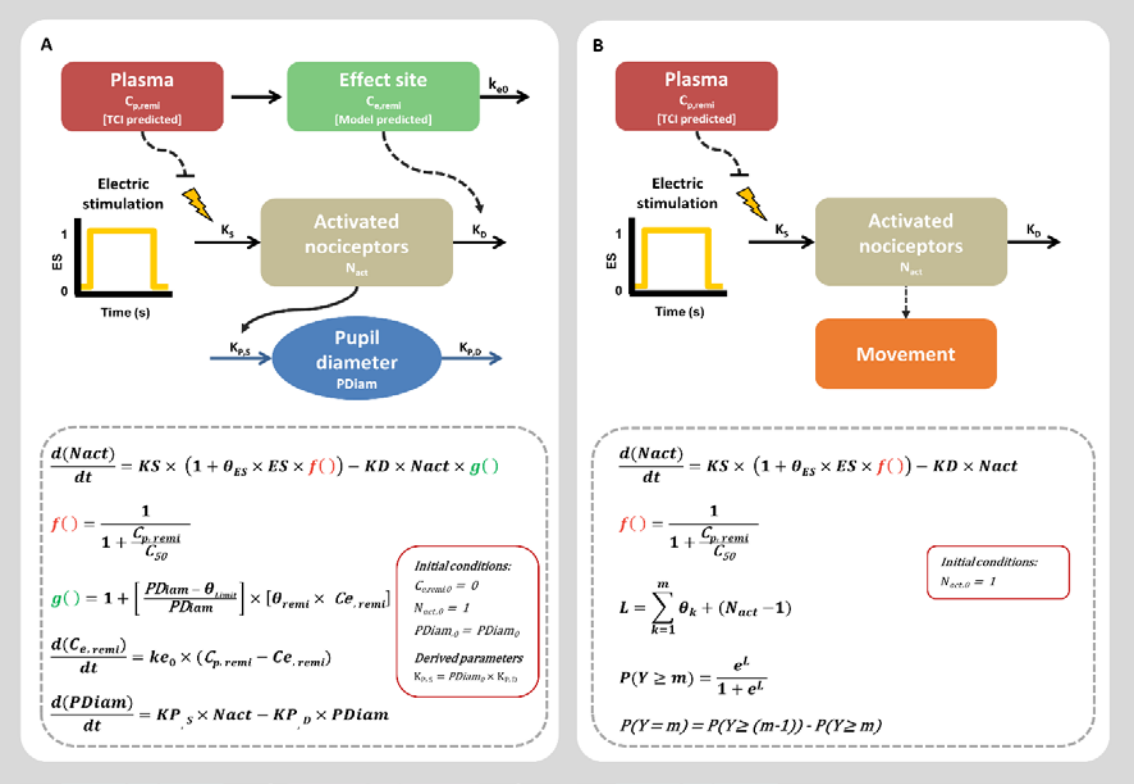

Figure 7. Schematic and mathematical representation of the PKPD models developed for pupil diameter (A) and movement response (B). All parameters are described in the text. Note that in our model K_S and K_D are the same parameter.

Results

The model parameters, shown in table 4, were estimated with good precision. The estimated PDiam at baseline was 3.8 mm. The estimates of the first-order rate constants K_D, $K_{P,D}$, and k_{e0} corresponds to half-lives of 9.5 s, 1.3 s and 3.56 min respectively, indicating faster turn-overs of N_{act} and PDiam than the distribution of remifentanil from plasma to the effect site. The steady-state concentration of remifentanil to reduce by half the impact of θ_{ES} and double K_D are 1.15 and 0.67 ng/mL respectively.

Data supported the estimation of moderate IIV on $PDiam_0$, θ_{ES}, $K_{P,D}$ and θ_{remi} ranging from 24 to 56% coefficient of variation. A correlation of -0.51 was found between random effects associated with $PDiam_0$ and θ_{ES}. As no tendencies were detected between individual estimates of model parameters and patient characteristics, no further investigation of potential covariate effects was undertaken. Although including autocorrelation in the residual model decreased the −2LL, the model performed worse as reflected by the individual predictions and VPCs, and therefore autocorrelation was not included in the selected model.

Figure 8 shows the goodness of fit plots corresponding to all data used for model development (A) and the results of the simulation-based diagnostics (B), both indicating adequate model performance and absence of model misspecifications. Similar results, model accuracy and lack of bias (NPE below 10% except for outliers and centred around 0), were found for the internal model validation using the data corresponding to the 5^{th} stimulus (Figure 9). Supplementary material (SM) 1 shows the NMTRAN code corresponding to the selected model.

Table 4. Models parameter estimates

Parameter	Estimate	RSE (%)	2.5th – 97.5th	Shrinkage (%)
Pupillary Reflex Dilation Response				
K_S (s^{-1})	0.0726	19.6	0.0203 – 0.152	-
$PDiam_0$ (mm)	3.80	3.3	3.57 – 4.02	-
IIV $PDiam_0$ (%)	24.6	7.7	20.9 – 28.4	1
$K_{P,D}$ (s^{-1})	0.531	13.9	0.294 – 1.07	-
IIV $K_{P,D}$ (%)	54.4	22.0	31.5 – 107	26
θ_{ES}	1.54	11.0	1.10 – 4.33	-
IIV θ_{ES} (%)	49.6	11.5	36.9 – 63.7	9
Cov (ω^2_{PDiam0}, $\omega^2_{\theta ES}$)	-0.0574	18.7	-0.0978 – -0.0236	-
C_{50} (ng/ml)	1.15	14.0	0.868 – 1.52	-
θ_{remi} (ml/ng)	1.50	12.9	1.10 – 2.39	-
IIV θ_{remi} (%)	55.6	8.7	44.1 – 73.9	2
k_{e0} (s^{-1})	0.00324	8.0	(2.67 – 3.82) x 10^{-3}	-
θ_{Limit} (mm)	1.41	6.1	1.18 – 1.61	-
Residual error (%)	9.90	6.6	8.50 – 11.0	3
Movement Response				
K_S (s^{-1})	0.437	13.9	0.336 – 0.617	-
θ_{ES}	6.63	8.2	5.67 – 7.98	-
θ_1	-4.90	4.0	-5.38 – -4.58	-
θ_2	-0.754	11.2	-0.916 – -0.584	-
θ_3	-0.978	17.1	-1.32 – -0.697	-
$\theta_{1,1}$	1.76	13.1	1.30 – 2.17	-
$\theta_{2,2}$	1.93	16.2	1.31 – 2.63	-
$\theta_{3,3}$	2.43	16.7	1.58 – 3.50	-
C_{50} (ng/ml)	0.617	23.3	0.360 – 1.02	-

Cov, covariance. IIV is expressed as percentage coefficient of variation calculated as $\sqrt{e^{\omega^2} - 1} \times 100$, where ω^2 corresponds to the variance of the random effects. $\theta_{1\text{-}3}$ define the baseline probabilities of movement as described in eq. 10. $\theta_{m,m}$ is the parameter defining the probability of maintaining an m movement grade once it is reached. The rest of the terms are defined in the main text.

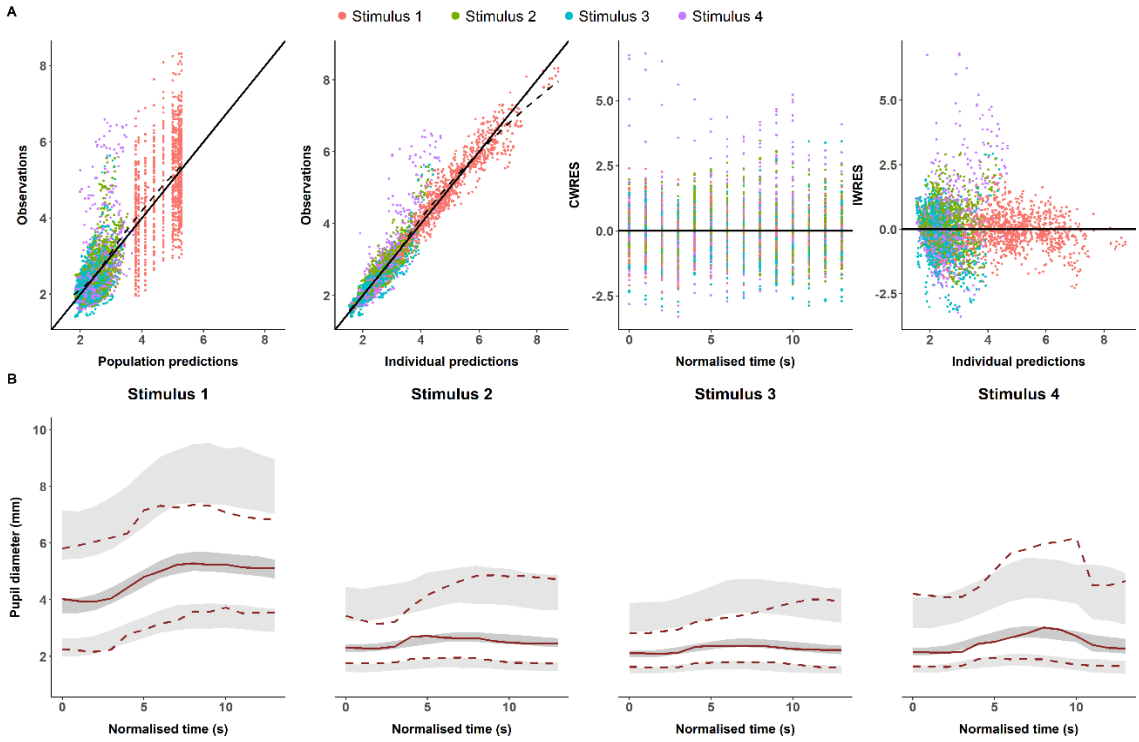

Figure 8. Pupil Diameter model evaluation. A. Goodness of fit plots. Data are coloured according to the stimulus: **1**, *red*; **2**, *green*; **3**, *blue*; **4**, *purple*. The dashed line represents the loess smoothing curve. CWRES, conditional weighted residuals; IWRES, individual weighted residuals. **B.** Visual Predictive Checks for stimulus 1 to 4**.** Median (solid line), 2.5th and 97.5th percentiles (dashed lines) of observed data compared to 95% prediction intervals (shaded area) for the median, 2.5th and 97.5th percentiles based on 1000 simulations.

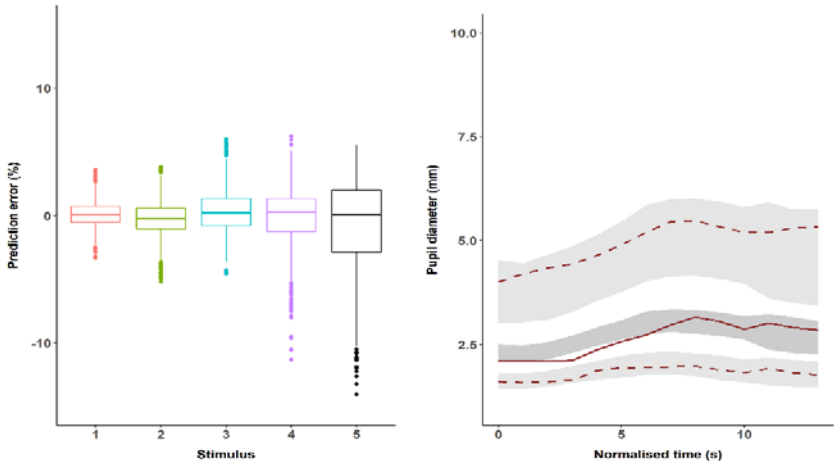

Figure 9. Pupil model validation. Prediction errors (PE) for each stimulus (**left**). Note that data from stimulus 5 was not used for model building and is part of the internal model validation. Visual Predictive Check for the stimulus 5 (**right**). Median (solid line), 2.5th and 97.5th percentiles (dashed lines) of observed data compared to 95% prediction intervals (shaded area) for the median, 2.5th and 97.5th percentiles computed from 1000 simulations.

Reflex movement response

Movement response was recorded as an ordered categorical variable and was modelled using the proportional odds logistic regression approach. To account for the observed similarities between PDdiam and movement responses, the dynamics of N_{act} (equation 7) were assumed to also drive the probability of movement. L, the logit, brings together the parameters defining the baseline probabilities of movement and the contribution of N_{act}, represented in equation 10 as θ_k and $h(N_{act})$, respectively.

$$L = \sum_{k=1}^{m} \theta_k + h(N_{act}) + \eta_i \quad (eq. 10)$$

The cumulative conditional probability of observing a score ≥ than a certain m category in the i^{th} subject at the j^{th} observation time is denoted $P(Y_{ij} \geq m | \eta_i)$ and is described by equation 11, where η_i is the individual random effect that belongs to a distribution of mean 0 and variance ω^2.

$$P(Y_{i,j} \geq m | \eta_i) = \frac{e^L}{1 + e^L} \quad (eq. 11)$$

Finally, the probability of observing a m score $P(Y_{ij} = m | \eta_i)$ is given by equation 12:

$$P(Y_{ij} = m | \eta_i) = P(Y_{ij} \geq (m-1) | \eta_i) - P(Y_{ij} \geq m | \eta_i) \quad (eq. 12)$$

In the movement response, the addition of a second turn-over compartment as in the case of PDiam did not improve the fit significantly ($p > 0.05$). Remifentanil elicited a significant effect ($p < 0.01$) reducing the nociceptive effects triggered by electric stimulation as it was previously described for PDiam. Figure 7B shows the schematic and mathematical representation of the model for movement reflex. Regarding the structure of the logit, the function h() (see equation 6) has as argument $N_{act} - 1$, which gives the value of zero in unperturbed conditions. The addition of a random effect on the L was not significant ($p > 0.05$), and as in the case of the PDiam, propofol was not shown to significantly contribute to antinociception.

Results

The possibility that the probability of each score at a certain time is influenced at least in part on the score achieved in the previous time (first-order Markov process) was also investigated. The addition of the parameters accounting for all transitions resulted in a significant ($p < 0.01$) improvement in the predictions, particularly for movement grades 1 and 3 (Figure 10 Panel C). On the contrary, a non-proportional odds model was not statistically significant ($p > 0.05$).

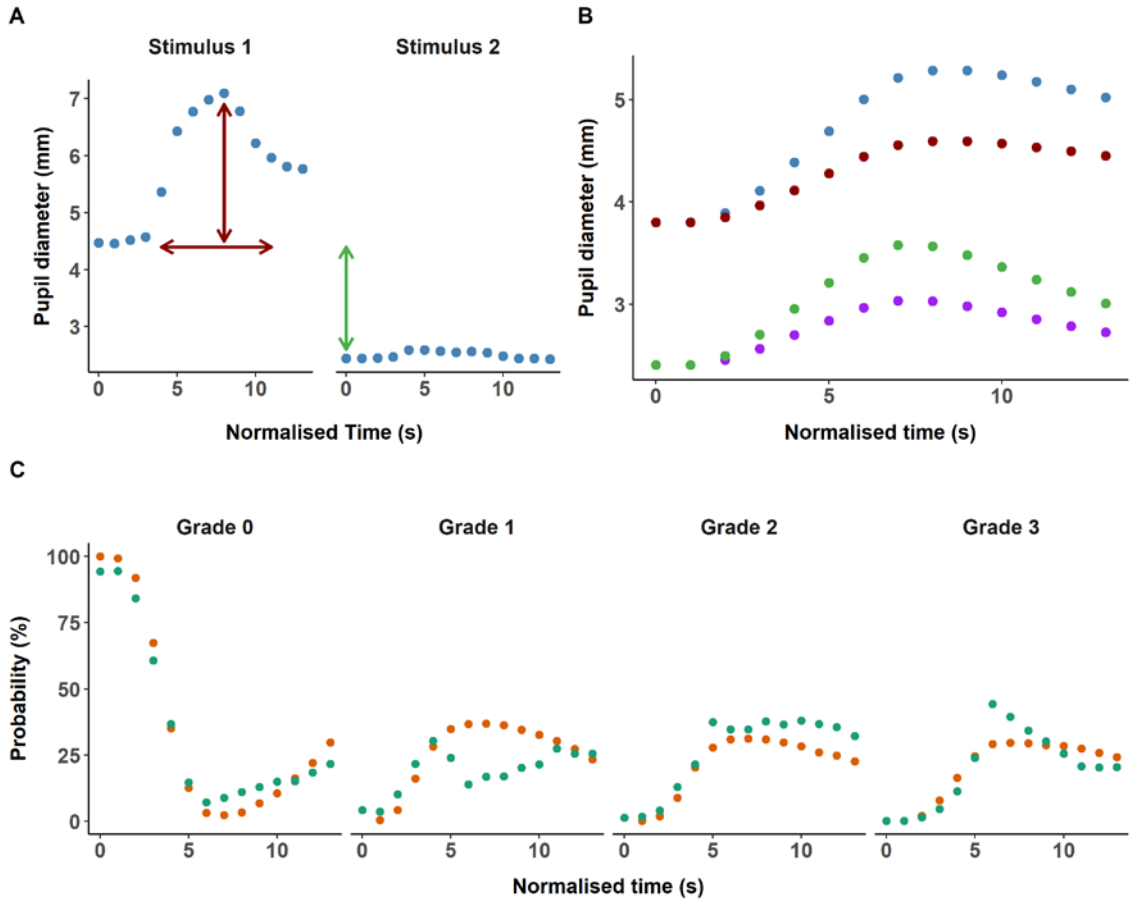

Figure 10. Exploration of key model components. A. Pupil response to tetanic stimulation before and after the administration of remifentanil for one of the study subjects. A reduction in the response to the nociceptive stimulation (***red arrows***) and a decrease in pupil diameter pre-stimulus (***green arrow***) could be observed after the administration of remifentanil. **B.** Typical pupil response to the stimulus in the absence of remifentanil (***blue***) or at a steady-state concentration of remifentanil of 1 ng/ml (***purple***), ignoring the effect of remifentanil on the (i) degradation of the activated nociceptors (***red***), or (ii) stimulus attenuation (***green***). **C.** Comparison of the probability of movement during the first stimulus for each grade maintaining (orange) or excluding (green) the Markov components of the model. Calculated from 1000 simulations.

Table 4 also lists the model parameter estimates corresponding to the movement response. All parameters were estimated precisely as confirmed by the low RSE and 95% confidence intervals. The estimate of K_D corresponds to a value of half-life of 1.58 s, and C_{50} is estimated as 0.617 ng/mL. In absence of stimulus, the probability of transitioning to movement is negligible (<0.8%). Once a certain grade is reached, the probability of maintaining the movement intensity is 85, 87 and 92% for grades 1, 2 and 3 and returning probabilities to baseline are 15, 13 and 8% respectively.

Results shown in Figure 11, corresponding to the goodness of fit (left panel) and visual predictive checks pooling all data together (right panel), indicate that the model described the data properly. SM 2 shows the NMTRAN code corresponding to the selected model incorporating the Markov elements.

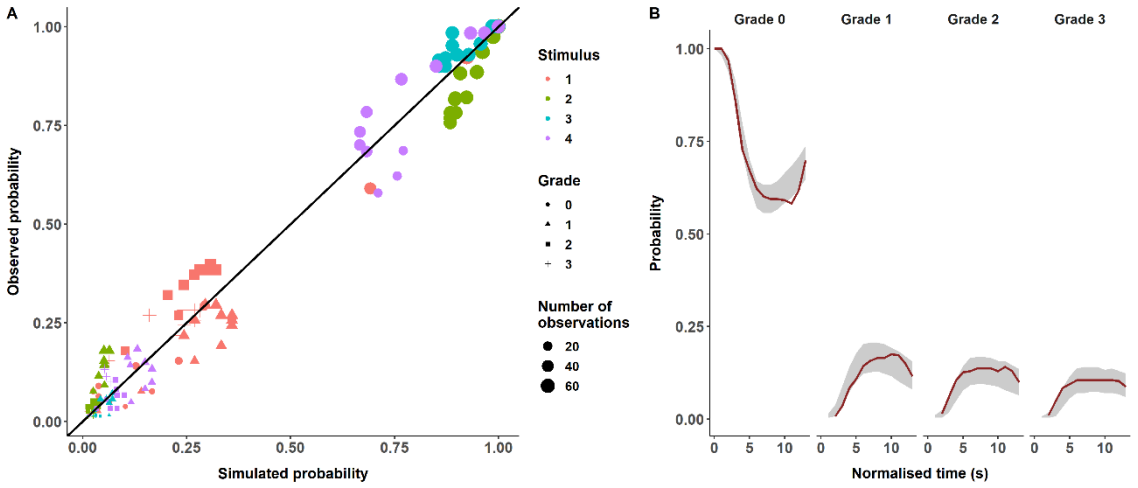

Figure 11. Movement response model evaluation. A. Observed versus predicted probability of movement for each grade and number of stimulus calculated from 500 simulations. Solid line is the identity representing a perfect fit. **B.** Visual Predictive Checks stratified by grade. Solid line corresponds to the median probability calculated from raw data, and the shaded areas represented the 95% prediction intervals computed from 1000 simulations.

Figure 12 splits the visual predictive check per stimulus and shows, in addition, good model performance for the movement responses gathered in stimulus 5 which were used for internal validation purposes. Our model was also able to capture the number of transitions between

movement grades observed in the study: 261 for the raw data and a median of 272 for the model predictions (248 to 297, 95% confidence interval).

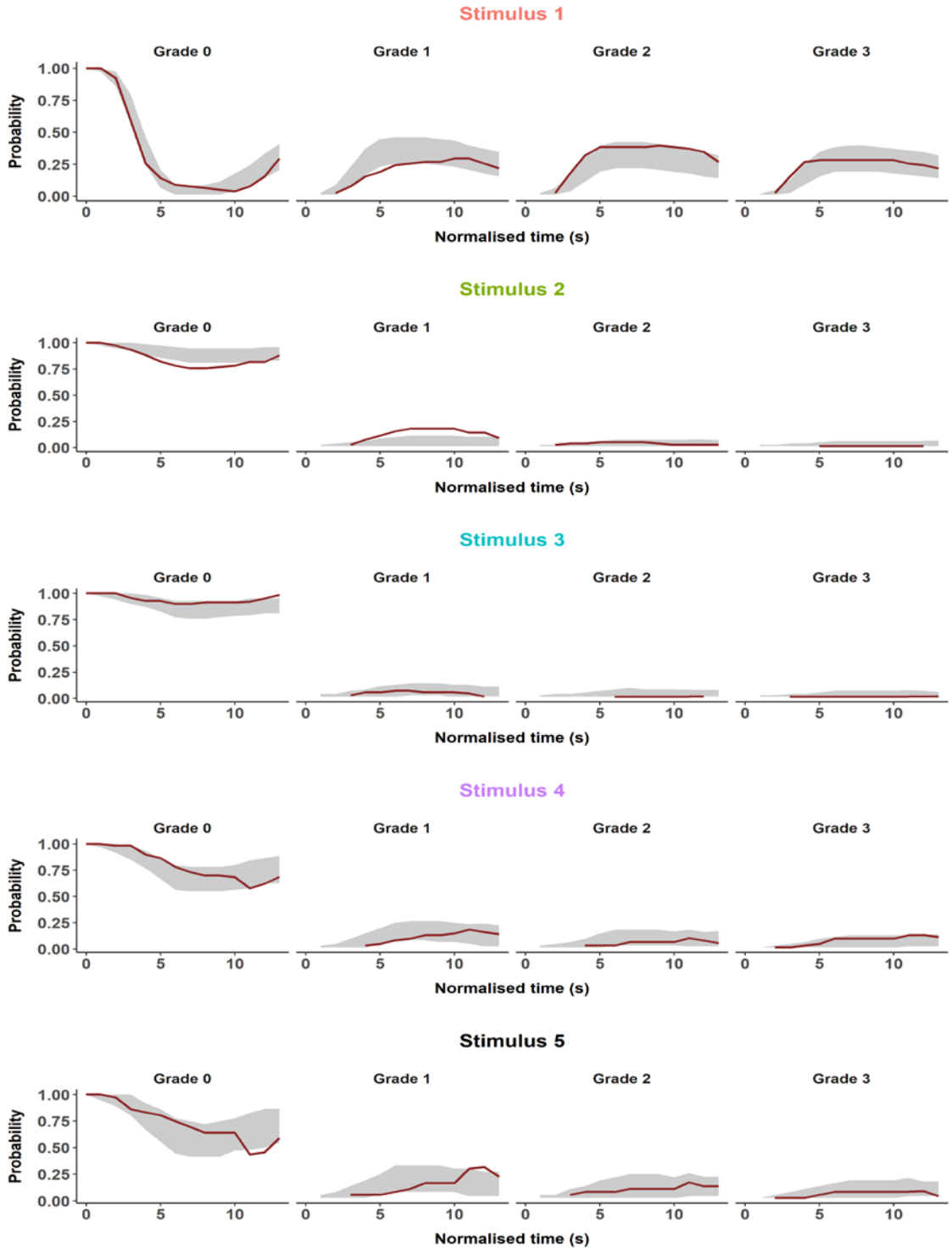

Figure 12. Visual Predictive Checks (VPCs) for the movement model stratified by grade and stimulus. Solid line corresponds to the median probability calculated from raw data, and the shaded areas represented the 95% prediction intervals computed from 1000 simulations. Note that stimulus 5 was not used for model building and was part of the internal model evaluation.

Model exploration

Figure 10 explores the impact of some of the key components of the selected models on the measured responses. Panels A and B show the changes in pupil response after the administration of remifentanil and graphically explore the individual contribution of the model effects to these changes. Figure 13A shows the time course of the predicted degree of nociceptor activation for movement and PRD, and despite similar trends, movement appears associated with a faster turnover. The relationship between the amplitude in the pupil response profile and the probability of movement vs steady-state remifentanil concentrations are shown in Figure 13B and 13C. Similar patterns between the two variables can be observed again, with the degree of steepness higher for movement.

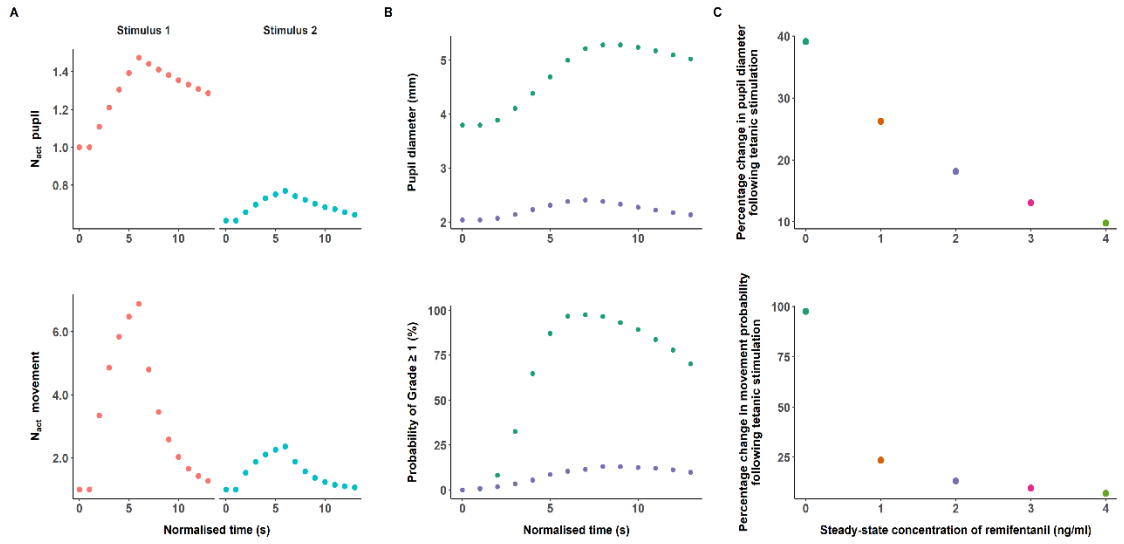

Figure 13. Models exploration. A. Dynamics of nociceptor activation. **B.** Pupil diameter and probability of movement in response to tetanic stimulation in absence (blue) or presence of remifentanil at 2 ng/ml steady-state concentration (purple). **C.** Percentage change in pupil diameter and probability of movement after tetanic stimulation at different steady-state concentrations of remifentanil.

Clinical applicability

Model-based simulations were performed to identify the concentration of remifentanil at which 80% of patients would not experience movement after the delivery of a tetanic current ranging from 1.2 to 0.8 times the one used in the experimental procedure. The simulation assumed an intensity of 1.2 for laryngoscopy and intubation while an intensity of 0.8 was assumed to represent a less painful surgical wound closure. For this purpose, we simulated one thousand individuals receiving electric stimulus of varying intensity at steady-state concentrations of remifentanil from 0 to 4 ng/ml and computed the percentage of individuals not experiencing movement. A SS concentration of 2 ng/ml was found to inhibit movement in 81% percent of the individuals with the experimental stimulus intensity and 77.8 and 83.1% of the individuals with a 20% increase and reduction in the stimulus intensity respectively.

This concentration (2 ng/ml SS) was subsequently used to simulate the PDiam of one thousand individuals from baseline to the end of a PRD. PDiam before electric stimulation for 80% of the individuals ranged from 1.69 to 2.61mm (10 and 90 percentiles) and were distinctly different from the PDiam at baseline (2.71 and 5.25 mm, 10 and 90 percentiles respectively) due to the pharmacologic effects of remifentanil. However, no correlation could be established between PRD and the pre-stimulus or basal ($PDiam_0$) pupil thus preventing recommendations on treatment individualization based on pre-stimulus pupil size.

Clinical study 2: PTC model

Pharmacokinetic models

In the absence of measured concentrations, the PK models developed by Saldien et al.[101] and De Haes et al.[102] were used to predict rocuronium concentrations over time. Saldien[101] conducted a PK/PD analysis of rocuronium in infants, children, and adults, while De Haes[102] described the time course of action of rocuronium in myasthenic patients and matched controls, comparing the results with the Sheiner model[13]. The reported parameters for adults and controls from these three-compartment models were used in our PK analysis (Table 5).

Table 5. Saldien and De Haes pharmacokinetic models' parameters for rocuronium.

	Saldien model	**De Haes model**
V_1 (mL kg^{-1})	35.6	42.0
k_{10} (min^{-1})	0.126	0.0762
k_{12} (min^{-1})	0.209	0.124
k_{13} (min^{-1})	0.0500	0.0214
k_{21} (min^{-1})	0.163	0.130
k_{31} (min^{-1})	0.0150	0.0130
k_{e0} (min^{-1})	0.168	0.150

k_{e0} - rate constant between central and effect compartment; k<u>ij</u> - rate constant for equilibration between compartments i and j; V1 - distribution volume of central compartment.

Pharmacodynamic model

The response variable analysed in the current evaluation is discrete. PTC were treated as an ordered categorical variable and divided in four *m* categories representing the increase in NMB: *m* = 0 [moderate (PTC ≥ 6)], *m* =1 [deep (PTC = 4 & 5)], *m* = 2 [profound (PTC = 2 & 3)], and *m* = 3 [very profound (PTC = 0 & 1)].

Results

In the absence of rocuronium, the model assumes a moderate NMB. For deeper levels of blockage, the cumulative conditional probability of observing NMB ≥ than a certain m category is denoted by $P(Y_{i,j} \geq m|\eta_i)$ and it is represented by the following expression:

$$P(Y_{i,j} \geq m|\eta_i) = \frac{Ce_{ij}^{\gamma}}{Ce_{ij}^{\gamma} + Ce_{50,m,i}^{\gamma}} \quad (eq.13)$$

Where $Ce_{ij,}$ is the predicted concentration of rocuronium at the effect site for the i^{th} subject at the j^{th} time, $Ce_{50,m}$ is the effect site concentration associated with 50% of probability for the m category, and γ is the Hill coefficient governing the steepness of the curve.

The probability of observing an *m* score $P(Y_{ij} = m|\eta_i)$ is calculated following equation 14:

$$P(Y_{i,j} = m|\eta_i) = P(Y_{i,j} \geq m|\eta_i) - P(Y_{i,j} \geq (m+1)|\eta_i) \quad (eq.14)$$

For the particular cases of m = 0 and m = 3, equations 15 and 16 are used respectively:

$$P(Y_{i,j} = m|\eta_i) = 1 - P(Y_{i,j} \geq (m+1)|\eta_i) \quad (eq.15)$$

$$P(Y_{i,j} = m|\eta_i) = P(Y_{i,j} \geq m|\eta_i) \quad (eq.16)$$

The time course of C_e was predicted based on the effect compartment model (also called Link model[13]) and according to equation 17:

$$\frac{dC_e}{dt} = k_{e0} \times (C_P - C_e) \quad (eq.17)$$

C_p corresponds to the plasma concentrations of rocuronium, which were generated using the current individual patient dosing and the model's parameters adjusted by the covariates (body weight) reported by Saldien and De Haes in their respective publications, and k_{e0} is the first-order rate constant that governs the equilibrium delay between the central and effect-site compartments. With respect to effect site kinetics, two approaches were followed: (i) k_{e0} was

fixed to the typical estimates reported by Saldien and De Haes, and (ii) k_{e0} was estimated as an additional parameter in the model.

During the process of model building, it was found that the fits were significantly improved when the distribution equilibrium delay between the central and effect site compartments was estimated, with respect to the use of the k_{e0} parameters reported by Saldien and De Haes ($p<0.001$). The estimated half-lives associated with k_{e0} ($t_{1/2\_ke0}$) were 7.22 and 5.25 min for the Saldien and De Haes models, respectively (as opposed to the 4.13 and 4.62 min reported in their original models). Figure 14 shows the raw PTC response and the predicted effect-site concentrations with the Saldien and De Haes models for two patients. Noteworthy, within the same individual, different PTCs are observed for similar effect-site concentrations, which might be artefacts inherent to the method of recording and/or the use of predicted concentrations.

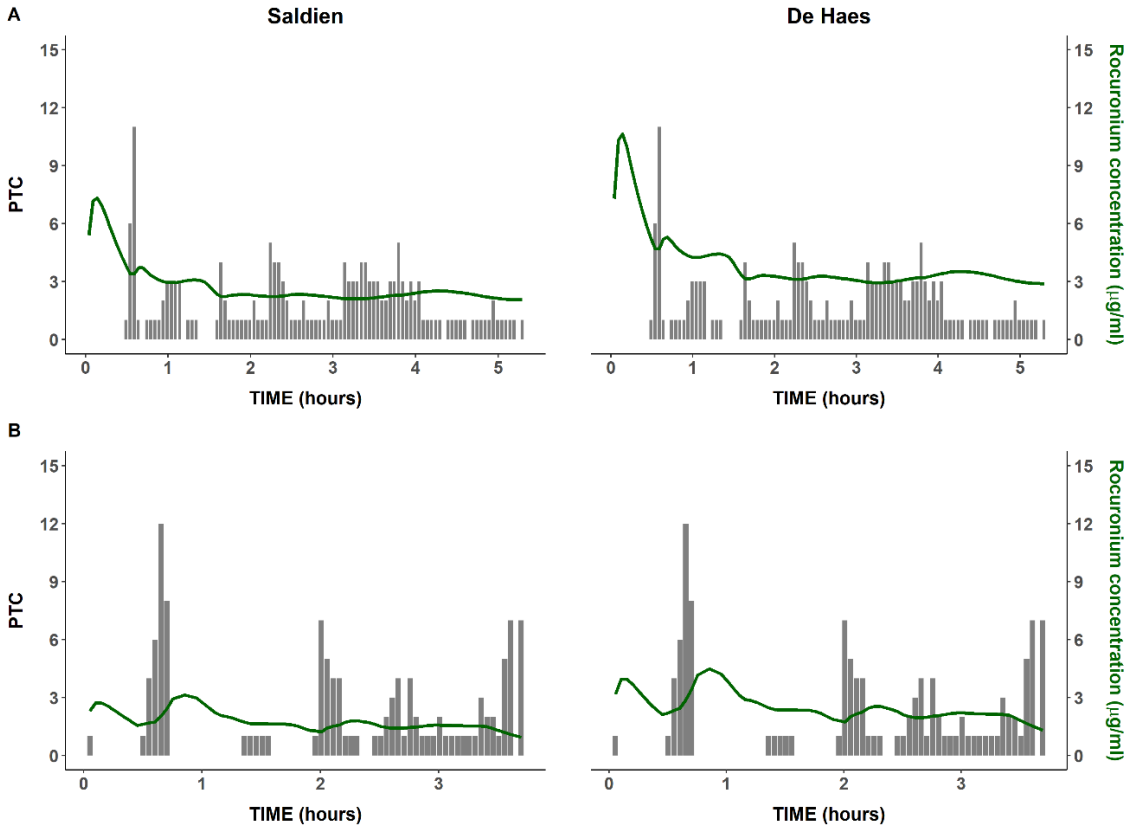

Figure 14. Overview of the raw data. Individual observed (bars) PTC response vs time profiles corresponding to two patients included in the study. For each patient, the predicted effect site concentration (C_e) profiles is presented as solid lines in green.

Results

Estimates of γ, the Hill coefficient, were very similar for both models (4.05 for Saldien and 4.15 for De Haes models). Higher discrepancies were found for the Ce_{50}, with approximately a 30% difference between models. Rocuronium C_e was found to decrease the probability of movement with Ce_{50} of 0.765, 1.05 and 1.55 μg ml^{-1} for the *m* categories 1, 2, and 3, respectively (Saldien model). For the case of the De Haes model, the corresponding values were, and 1.1, 1.5 and 2.2 μg ml^{-1}, respectively. A model incorporating the knowledge that high receptor occupancy is required to achieve 50% of neuromuscular was also considered[103] without improving the description of the data ($p>0.05$).

Table 6 lists the model parameters for the two PK/PD models. Estimates were obtained with reasonable precision since the values of RSE were lower than 30% for both, fixed and random effects parameters. With respect to random effects, IIV resulted significant in Ce_{50} for the categories m = 1 and m = 3 ($p<0.001$). The degree of IIV (expressed as coefficient of variation) was large ranging from 57 to 63% approximately and showed consistency across the two models.

Figures 15 and 16 present the results of the model evaluation exercise using simulation model-based diagnostics corresponding to the Saldien model. Figure 15 shows the visual predictive checks stratified by the degree of blockade. In general, the model captures well the time profiles of the response regardless of the observed magnitude of the NMB. Figure 16 evaluates whether the model captures the observed frequencies for each category. Results indicate that the model is able to describe the observed raw data, although with a moderate overestimation of the category m = 0. The performance of the model selected using PK profiles derived from the De Haes model was indistinguishable from the Saldien model as it is shown in Figure 17. SM 3 shows the NMTRAN code corresponding to the selected models.

Table 6. Model parameter estimates

Parameter	Estimate	RSE (%)	Bootstrap analysis 5^{th} – 95^{th}	Shrinkage (%)
Saldien pharmacokinetic model				
$Ce_{50,\ m=1}$ (μg ml^{-1})	0.765	19.2	0.537 – 1.03	-
$\Delta Ce_{50,\ m=2}$ (μg ml^{-1})	0.285	10.4	0.231 – 0.332	-
$Ce_{50,\ PTC\ m=2}$ (μg ml^{-1})	1.05	-	-	-
$\Delta Ce_{50,\ m=3}$ (μg ml^{-1})	0.501	15.2	0.378 – 0.624	-
$Ce_{50,\ m=3}$ (μg ml^{-1})	1.55	-	-	-
γ	4.05	19.0	3.13 – 5.67	-
k_{e0} (min^{-1})	0.0948	14.2	0.075 – 0.117	-
IIV $Ce_{50,\ m=1}$ (%)	57.0	22.4	34.2– 85.9	9
IIV $\Delta Ce_{50,\ m=3}$ (%)	62.9	15.0	44.4 – 84.0	5
De Haes pharmacokinetic model				
$Ce_{50,\ m=1}$ (μg ml^{-1})	1.10	18.1	0.797 – 1.47	-
$\Delta Ce_{50,\ m=2}$ (μg ml^{-1})	0.40	10.3	0.327 – 0.463	-
$Ce_{50,\ PTC\ m=2}$ (μg ml^{-1})	1.5	-	-	-
$\Delta Ce_{50,\ m=3}$ (μg ml^{-1})	0.70	14.6	0.531 – 0.867	-
$Ce_{50,\ m=3}$ (μg ml^{-1})	2.2	-	-	-
γ	4.15	17.9	3.21 – 5.69	-
k_{e0} (min^{-1})	0.134	9.7	0.114 – 0.156	-
IIV $Ce_{50,\ m=1}$ (%)	57.0	22.6	34.4 – 86.2	9
IIV $\Delta Ce_{50,\ m=3}$ (%)	61.7	15.1	42.8 – 82.9	5

Inter-individual variability (IIV) is expressed as coefficient of variation (%) calculated as $\sqrt{e^{\omega^2} - 1} \times 100$, where ω^2 corresponds to the variance of the random effects. Ce_{50} is the effect site concentration of rocuronium associated with 50% of probability for the m PTC category calculated for m=2, and m=3 categories from the corresponding parameters estimates as: $C_{50,m=i} = C_{50,m=1} + \sum_{i=2}^{3} \Delta Ce_{50,m=i}$. ΔCe_{50} is the increment in the Ce_{50} with respect to the Ce_{50} of the m-1 category. γ is the Hill coefficient governing the steepness of the concentration-response curve. k_{e0} is the first-order rate constant that governs the equilibrium delay between the central and effect-site compartments.

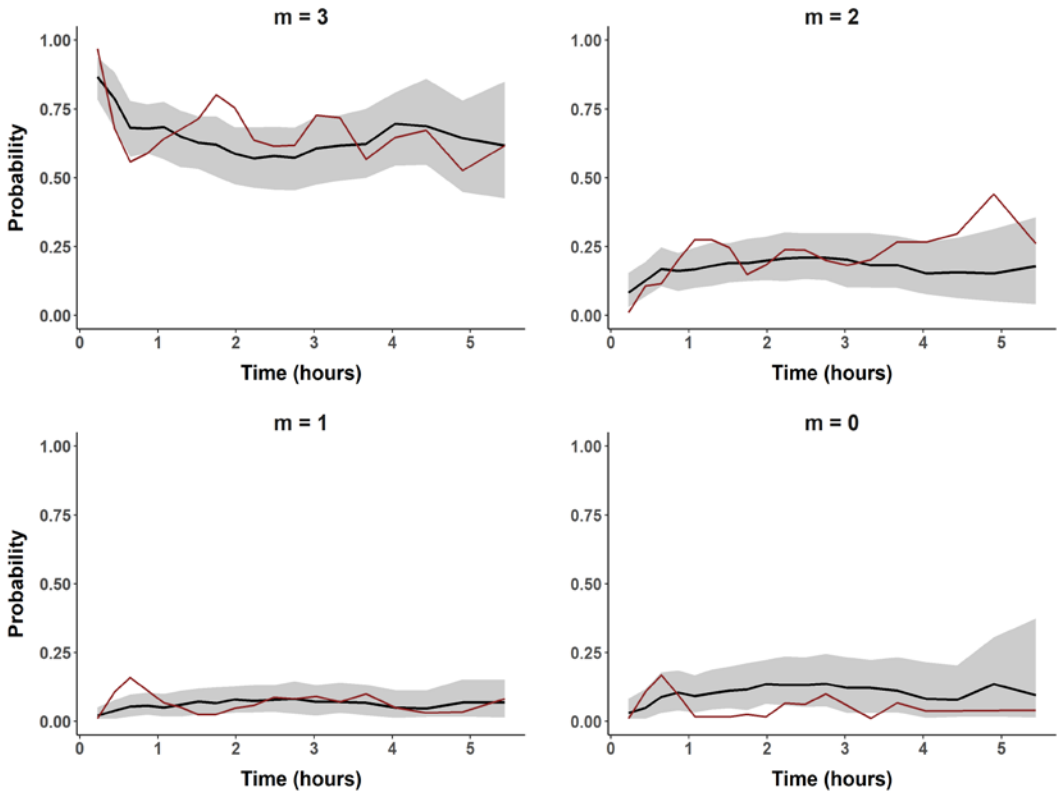

Figure 15. Visual predictive checks corresponding to the Saldien pharmacokinetic model stratified by the degree of neuromuscular blockade. Solid lines correspond to the median probability calculated from (i) raw data (red) and simulations (black). Shaded areas represent the 95% prediction intervals computed from 500 simulations.

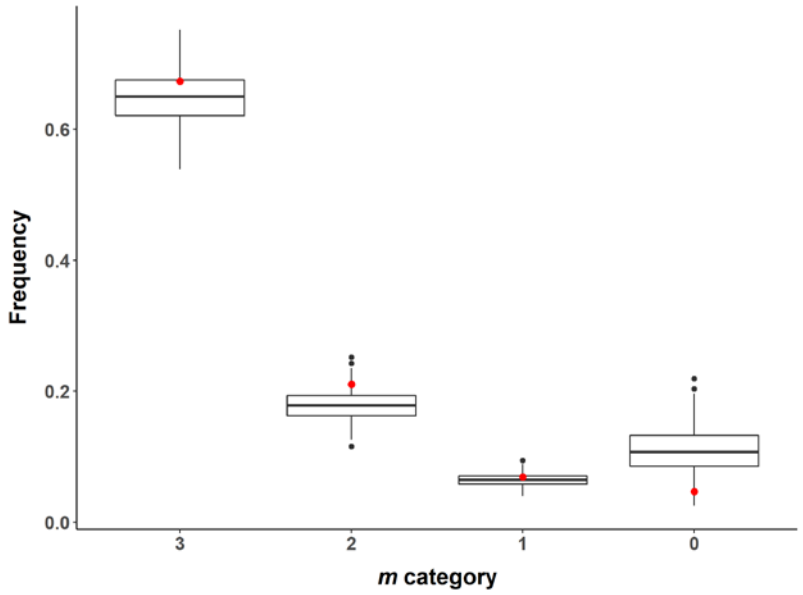

Figure 16. Predicted versus observed frequencies for the Saldien pharmacokinetic model. Observed (red circles) versus predicted frequencies (boxplot) for each *m* category calculated from 500 simulations.

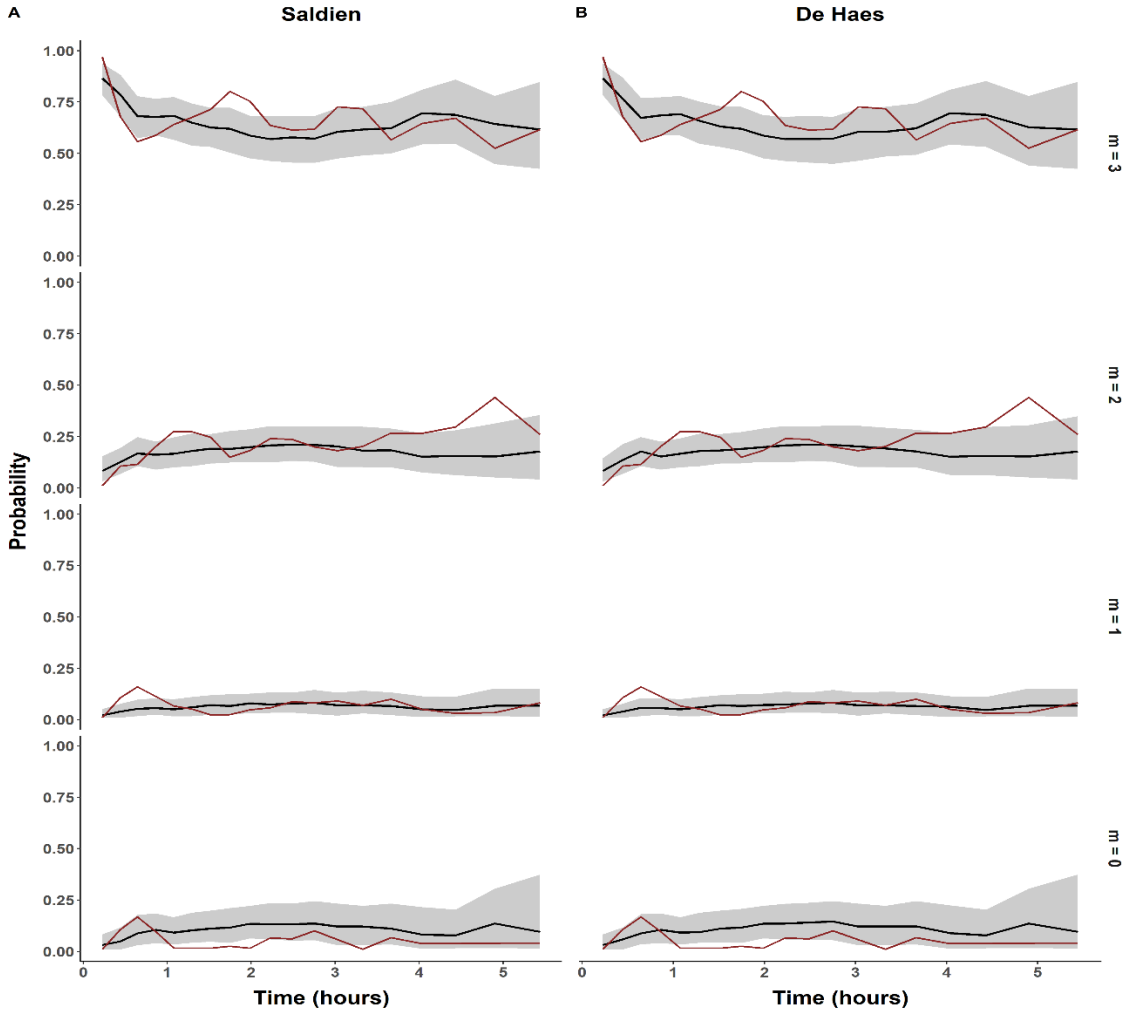

Figure 17. Visual predictive checks corresponding to the Saldien and De Haes models stratified by the degree of neuromuscular blockade. Solid lines correspond to the median probability calculated from (i) raw data (red) and simulations (black). Shaded areas represent the 95% prediction intervals computed from 500 simulations.

Clinical study 3: Haemoglobin and fluid models

Our modelling approach focused on predicting and characterizing the Hb during the first four perioperative days, as it was considered the crucial period regarding transfusion-related decisions. The model was developed using a semi-mechanistic approach, which included a mechanistic framework related to the main underlying processes that govern perioperative Hb, and a mathematical fitting using NLME models. As clinical prediction was the main aim of the model only fundamental processes were considered, and the leading efforts in modelling were focused on the parsimony of the model.

Pharmacodynamic model

Haemoglobin is a protein located, under normal conditions, only within the intravascular compartment. As other authors have stated, its concentration in blood (Hb) results from the total amount of haemoglobin suspended in the intravascular compartment and therefore[104–107], can be expressed as the ratio of its circulating mass to the volume containing it. Taking into account the observable period of this study, circulating haemoglobin mass was considered to remain steady with negligible synthesis and degradation rates, but only altered by haemoglobin mass loss (from surgical blood loss).

Therefore, in order to model Hb perioperative variations, changes in circulating haemoglobin mass due to bleeding and intravascular volume were taken into account. Equation 18 describes Hb at time *t* ($Hb_{(t)}$):

$$Hb_{(t)} = \frac{A_0 - A_{loss}}{V_{B\,(t)}} \quad (eq.\,18)$$

Where A_0 and A_{loss} are the preoperative circulating haemoglobin mass and haemoglobin mass loss, respectively, and $V_{B(t)}$ is the perioperative intravascular volume. Preoperative intravascular volume ($V_{B(0)}$) was calculated using the ICSH formula (*International Council for Standardization in Hematology Radionuclide Expert Panel*[108]), as a good agreement has been observed between

the estimates and direct measurements of preoperative intravascular volume (reported as 106 ±10% when comparing estimates with direct measurements)[109]. A_0 was calculated by multiplying the preoperative value of Hb by the estimated intravascular volume ($V_{B(0)}$). A_{loss}, which was assumed to be 0 prior to the operation, was measured directly from the blood loss during surgery as described in the *Methods* section. The remaining unknown variable, $V_{B(t)}$, was described using a model for fluid kinetics.

Pharmacokinetic model

Hb variations that occurred in the absence of changes in circulating haemoglobin mass were considered as a result of variations in $V_{B(t)}$. In turn, variations in $V_{B(t)}$ were deemed a consequence of an imbalance between fluid input and output processes. To characterize the impact of these processes over time two different structural models were proposed and evaluated. The one-compartment model assumed a single expandable volume (equation 19):

$$\frac{dV_B}{dt} = Fluid_{Rate} - B_{Rate} - k_{10} \times V_B \ (eq. 19)$$

Where infusion fluid is administered into the intravascular compartment following a zero-order infusion rate ($Fluid_{Rate}$) and eliminated via a first-order process governed by the constant k_{10}, which can be parametrized as the quotient of the elimination clearance (CL) and $V_{B(0)}$. The $Fluid_{Rate}$ for each type of infusion fluid (glucose and crystalloid) was calculated by dividing the administered volumes by the time between Hb measurements. The volume of blood lost during surgery was expressed as a constant zero-order rate (B_{Rate}), calculated as the measured volume of blood lost divided by the length of the surgery. B_{Rate} was set to 0 before and after the surgical procedure. At baseline, V_B equals $V_{B(0)}$.

The two-compartment model extended this model to include a peripheral expandable compartment (equations 20 and 21):

$$\frac{dV_B}{dt} = Fluid_{Rate} - B_{Rate} - k_{10} \times V_B - \frac{Q}{V_{B(0)}} \times V_B + \frac{Q}{V_{P(0)}} \times V_P \quad (eq.20)$$

$$\frac{dV_P}{dt} = \frac{Q}{V_{B(0)}} \times V_B - \frac{Q}{V_{P(0)}} \times V_P \quad (eq.21)$$

Where V_P is the volume of the peripheral compartment. Fluid distribution kinetics between the intravascular and peripheral compartment –and vice versa– were characterized by the intercompartmental clearance (*Q*). At baseline, V_B equals $V_{B(0)}$, while $V_{P(0)}$ was estimated in the model.

A two-compartment model described Hb significantly better than the one-compartment model ($p < 0.01$); thus, subsequent modelling was based on the two-compartment model.

Urinary elimination of fluid for both models was initially described by equation 22, assuming urinary elimination is the unique source of fluid output from the intravascular compartment after surgery:

$$\frac{dV_{UR}}{dt} = k_{10} \times V_B \quad (eq.22)$$

Where V_{UR} is the volume of urine between each Hb measurement.

However, visual exploration of the GOFs revealed that, whereas Hb was accurately described, urine volume was overpredicted, suggesting the presence of an extra fluid elimination mechanism. To account for this mechanism, a new parameter (*RF*) was added, which quantified the fraction of total fluid elimination (k_{10}) that corresponded to urinary elimination (equation 23):

$$\frac{dV_{UR}}{dt} = k_{10} \times RF \times V_B \quad (eq.23)$$

The addition of the *RF* parameter resulted in estimation issues for V_P. To improve parameter identifiability, the estimate and RSE obtained for V_P before the inclusion of *RF* were used in the model as Bayesian priors using the NWPRI subroutine available in NOMEM.

During data exploration, it was observed that urine output (volume/hour) was reduced postoperatively. Two hypotheses were considered: (1) urine volume (V_{UR}) is affected by surgery, and (2) total fluid elimination (k_{10}) is affected by surgery. The later hypothesis resulted in a significant improvement (p <0.01) in model fit, and an inhibitory model was implemented to characterize the changes of total fluid elimination after surgery (equation 24):

$$k_{10} = \frac{CL}{V_{B(0)}} \times \left(1 - Imax \times \frac{Time^{\gamma}}{Time^{\gamma} + T_{50}^{\gamma}}\right) \quad (eq. 24)$$

Where *CL* is the fluid clearance, *Imax* is the maximum inhibition of the clearance, *Time* is the perioperative time in hours (considering the beginning of the surgery as time zero), and T_{50} is the time to produce 50% inhibition of the fluid clearance. Gamma (γ) was set to a value of 9 to represent the fast clearance inhibition that could not be estimated otherwise. The final model representation and equations are presented in Figure 18.

Additionally, although alternative parametrizations for glucose and crystalloids solutions were evaluated, no differences in the elimination or distribution between them were found (p >0.05).

Covariate model

The following covariates were included in the SCM analysis: blood volume loss, age, type of surgery and monocyte count on *CL* and *RF*, and blood volume loss on *Q*. Two of these covariates, age on *CL* and type of surgery on *RF*, were selected for the final model. For the latter, types of surgeries with similar estimates of *RF* were grouped into four categories without resulting in worsening of the objective function (p >0.05): (1) robotic prostatectomy, partial nephrectomy and myomectomy (reference category); (2) radical nephrectomy and nephroureterectomy; (3) hysterectomy and hysterectomy with adnexectomy; (4) endometriosis.

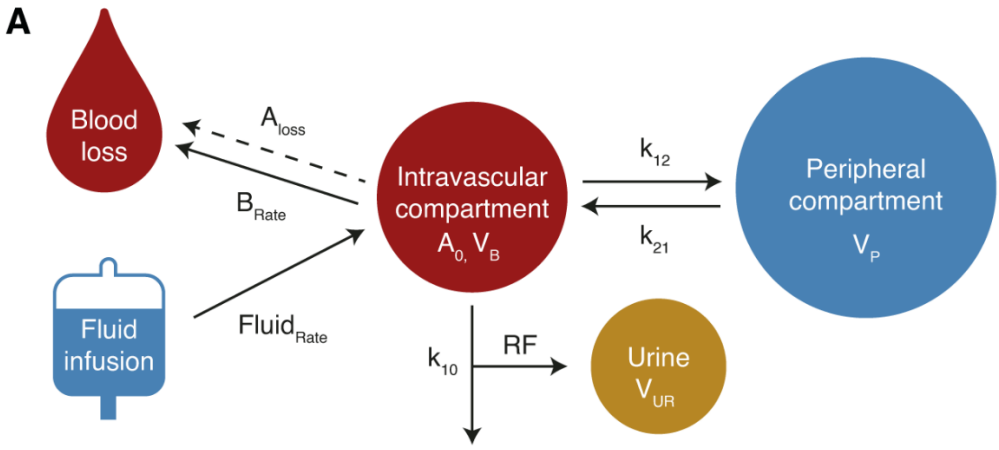

B

$$Hb(t) = \frac{A_0 - A_{loss}}{V_B(t)}$$

$$\frac{dV_B}{dt} = Fluid_{Rate} - B_{Rate} - k_{10} \times V_B - k_{12} \times V_B + k_{21} \times V_P$$

$$\frac{dV_P}{dt} = k_{12} \times V_B - k_{21} \times V_P$$

$$\frac{dV_{UR}}{dt} = k_{10} \times RF \times V_B$$

$$k_{10} = \frac{CL}{V_{B(0)}} \times \left(1 - Imax \times \frac{Time^{\gamma}}{Time^{\gamma} + T_{50}^{\gamma}}\right)$$

Initial conditions:

$$V_B = V_{B(0)}$$

$$V_P = V_{P(0)}$$

$$V_{UR} = 0$$

Derived parameters:

$$k_{12} = Q / V_{B(0)}$$

$$k_{21} = Q / V_{P(0)}$$

Figure 18. (A) Schematic and (B) mathematical representation of the model. Solid arrows represent fluid kinetics, while the dashed arrow indicates haemoglobin mass loss. All parameters are described in the main text.

Model validation

Figure 19 shows the results of the model validation performed using the validation cohort of patients, where an adequate predictive capacity is observed. For measures after surgery, 95% of the predicted errors are within -4.4 and +5.5 g/L and 100% within ±9.2 g/L. Particularly, the predicted errors for Hb values <100 g/L (a usual threshold for considering RBC transfusion in patients with cardiovascular disease) were in the same range of magnitude (-3.7 and +5.4 g/L for quantiles 2.5 and 97.5, respectively), reinforcing the consistency of the model.

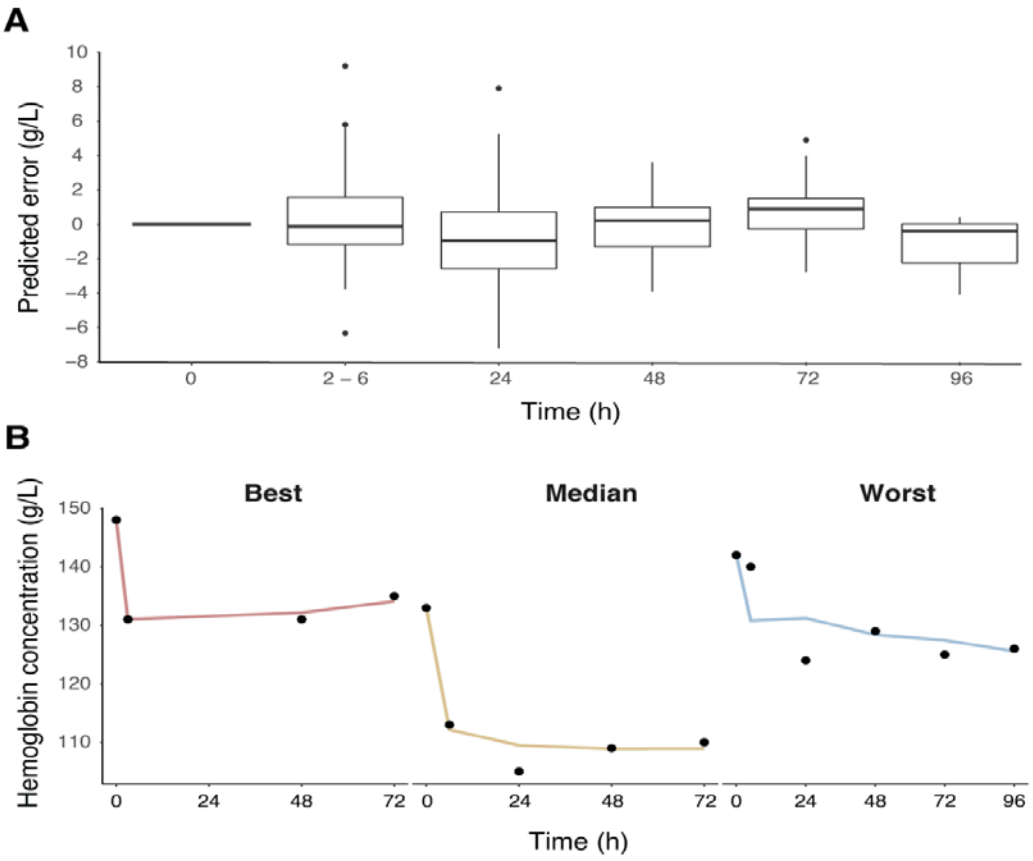

Figure 19. Model validation. (A) Predicted errors (PE) for the validation group. As in Fig. 1, the first postoperative time points are gathered into a single time point (PO). (B) Best, median and worst individual predictions of Hb for the patients in the validation group. Lines and points represent Hb predictions and measures, respectively.

Final model evaluation

Once the predictive capacity of the model had been evaluated, the estimation and validation datasets were combined and analyzed simultaneously to provide final estimates for the model (Table 7). All parameters were estimated with precision (RSE <30%) and were consistent with the results obtained in the estimation dataset. Data supported the inclusion of IIV on CL, *Q* and *RF* ranging from 21% to 73% coefficient of variation. Model evaluation showed an adequate model performance and absence of misspecifications (Figure 20). SM 4 shows the NMTRAN code corresponding to the selected model.

Table 7. Model parameter estimates

Parameter	Estimate	RSE (%)	95% CI from bootstrap analysis	Shrinkage (%)
CL (L/h)	0.253	2.8	0.240 – 0.267	-
IIV CL (%)	20.6	6.6	17.2 – 23.9	7
RF (unitless)	0.240	3.8	0.220 – 0.260	-
IIV RF (%)	47.2	7.0	36.9 – 55.3	10
Q (L/h)	4.47	7.7	3.77 – 5.19	-
IIV Q (%)	72.8	14.0	40.5 – 103	35
$V_{p(0)}$ (L)	48.1†	0.3†	48.1 – 48.1	-
Imax (unitless)	0.420	3.3	0.388 – 0.451	-
T_{50} (hours)	9.10	11.2	5.42 – 9.60	-
Gamma (unitless)	9*	-	-	-
CL ~ Age	0.00872	16.5	0.00606 – 0.0111	-
RF ~ RN, NU	-0.365	19.1	-0.454 – -0.252	-
RF ~ HT, HTA	0.307	29.6	0.150 – 0.477	-
RF ~ Endometriosis	0.846	21.9	0.579 – 1.13	-
Residual error Hb (ln g/L)	0.0208	3.2	0.0189 – 0.0230	12
Residual error urine (ln L)	0.286	3.1	0.239 – 0.339	

†Priors. *Not estimated. Inter-individual variation (IIV) is expressed as coefficient of variation (%) calculated as $\sqrt{e^{\omega^2}-1}\times 100$, where ω^2 corresponds to the variance of the random effects. Covariate effects are expressed as the fractional change with respect to the estimate of the reference category (categorical) or the fractional change of the estimate per unit of covariate from the median of the covariate (continuous). CI: confidence intervals, RN: Radical Nephrectomy, NU: Nephroureterectomy, HT: Hysterectomy, HTA: Hysterectomy with adnexectomy. The rest of the terms are defined in the main text.

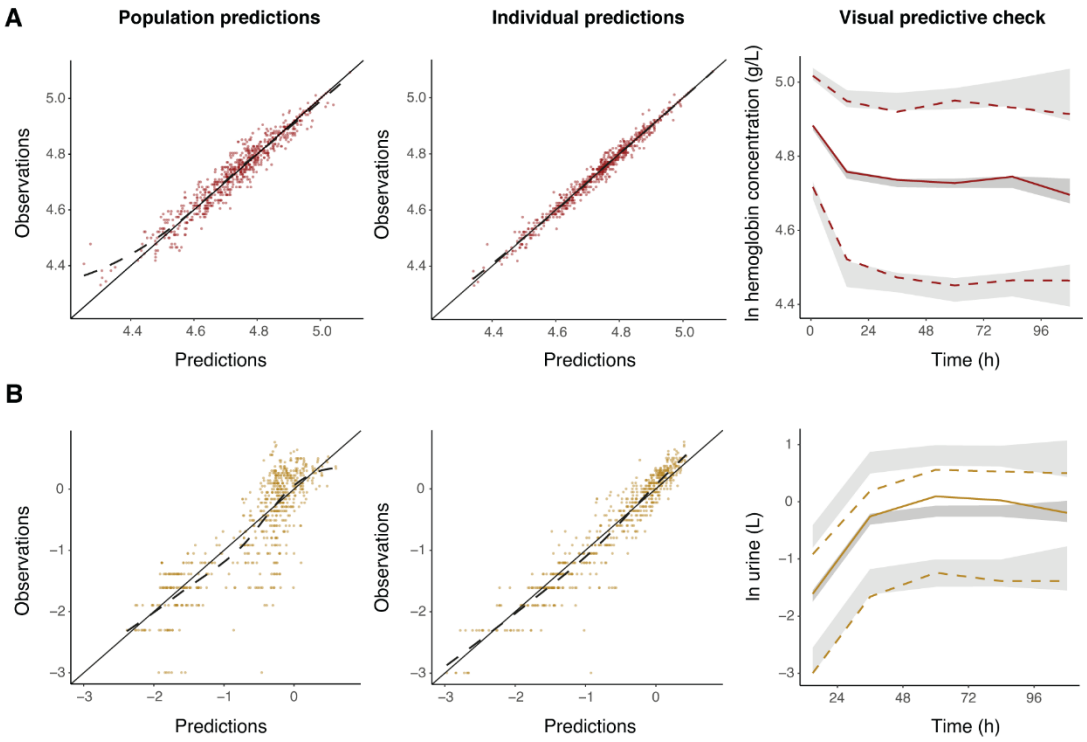

Figure 20. Final model evaluation. Goodness of fit plots for Hb (A, red) and urine data (B, yellow). Black dashed lines represent the loess smoothing curve. The last panel of each row shows the Visual Predictive Checks for Hb (A) and urine (B). Median (solid colour lines), 2.5th and 97.5th percentiles (dashed colour lines) of observed data compared to 95% prediction intervals (shaded areas) for the median, 2.5th and 97.5th percentiles based on 1000 simulations.

The effect of covariates on model parameters are displayed in a forest plot (Figure 21), and can be summarized as follows: category (2) was associated with a 36% reduction in *RF*; category (3) was associated with a 31% increase in *RF*; category (4) was associated with an 85% increase in *RF*; and a median change of −17% and 23% for *CL* was observed for the low and high extreme values of age (35 and 81 years, respectively).

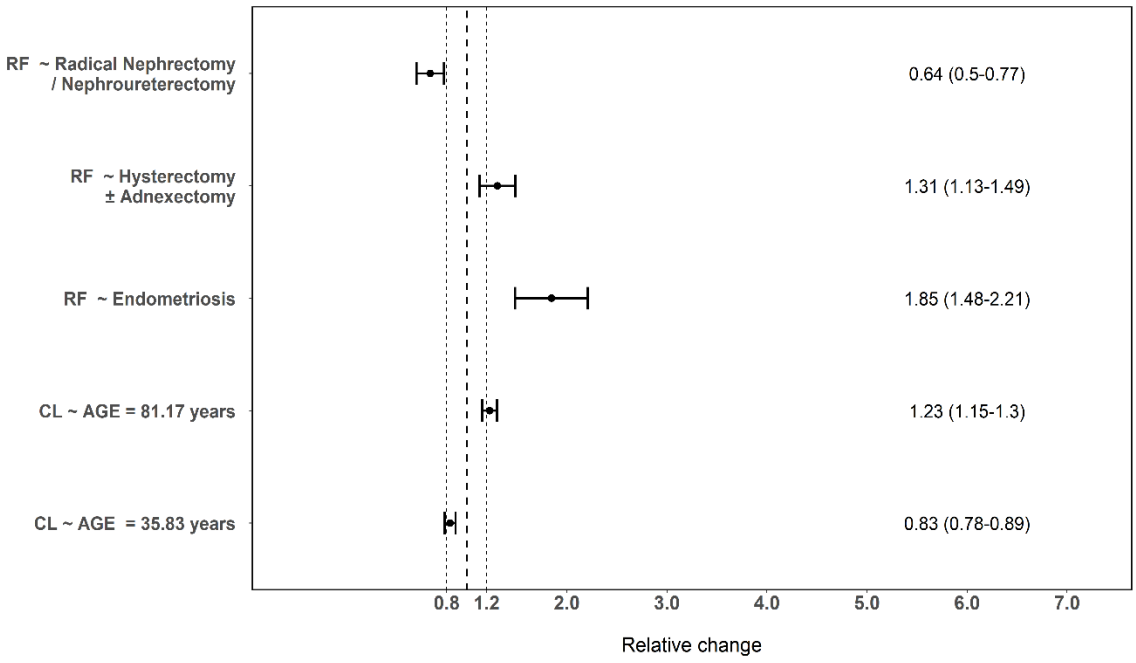

Figure 21. Covariate evaluation. Forest plot evaluating the impact of the selected covariates on model parameters. The solid line represents the normalized parameter value, while the dashed lines show a 20% interval around the reference group. Solid points represent the relative change in the parameter value caused by the covariate effect and whiskers, the 95% confidence interval around it. As a continuous covariate, the impact of Age was explored for the 2.5th and 97.5th percentiles. Abbreviations are defined in the main text.

Simulation

Model-based simulations were performed to explore the risk of reaching a Hb threshold of 70 g/L as a function of the basal Hb concentrations ($Hb_{(0)}$) of the patient and haemoglobin mass loss during surgery (A_{loss}). We simulated 1000 individuals for the combination of $Hb_{(0)}$ values ranging from 150 to 90 g/L with values of A_{loss} from 25 to 250 g and computed the percentage of individuals not reaching the Hb threshold. Two different sets of simulations were performed, one replicating the sparse sampling times used in this study and another reconstructing the full temporal profile (from surgery until 96 hours postoperatively). These simulations assumed a typical patient of 56 years and 77 kg and a 3-hours surgical procedure of the reference category. Following a standard strategy for fluid therapy[110], patients received 1.5 mL of fluid infusion per mL of blood lost, additional 2 mL/kg/h during the intraoperative period, and 25 mL/kg/24h

during the postoperative period. Results are presented in Figure 22. The volume of blood lost during surgery (necessary to estimate B_{Rate}) was extrapolated for each A_{loss} using a linear regression model as shown in Figure 23.

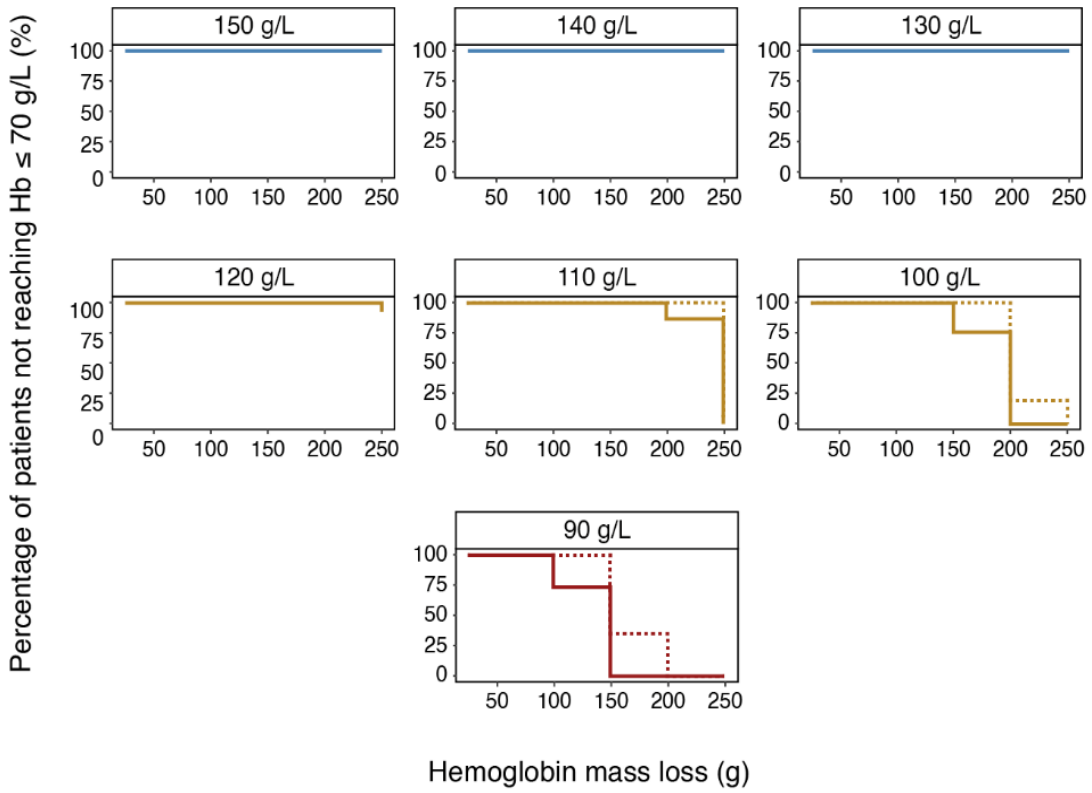

Figure 22. Model-based simulation of patients not reaching Hb ≤ 70 g/L. Each graph indicates a different preoperative Hb ($Hb_{(0)}$). The horizontal axis represents the haemoglobin mass loss (A_{loss}), while the vertical axis indicates the percentage of patients not reaching the Hb threshold. Dashed colour lines correspond to the results calculated using the sampling times used in this study, while solid colour lines represent the calculations based on a full temporal profile.

Three groups of risk could be identified. Firstly, patients with $Hb_{(0)}$ of 150, 140 and 130 g/L showed a low risk of reaching the Hb threshold independently of A_{loss}. In an intermediate case, patients with $Hb_{(0)}$ of 120, 110 and 100 g/l showed risk only at high A_{loss} (150-250 g). Finally, patients with $Hb_{(0)}$ of 90 g/l reached the Hb threshold with A_{loss} as low as 100 to 150 g. Of note, the full temporal course was able to detect a higher number of patients at risk of requiring a transfusion than the original study design.

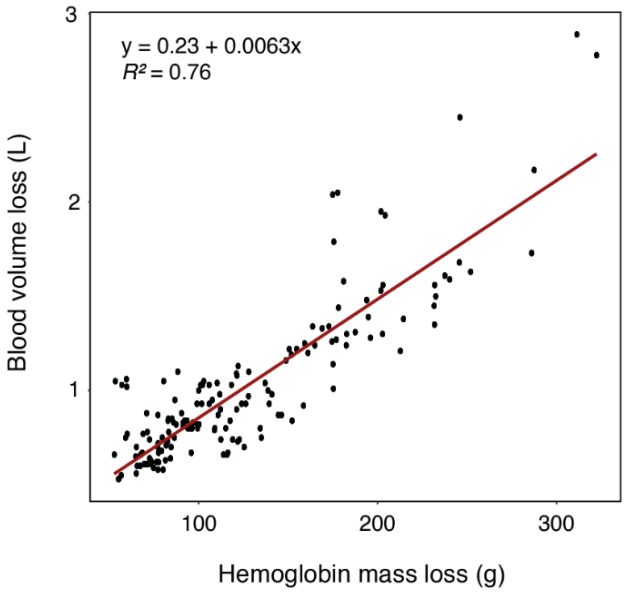

Figure 23. Extrapolation of blood volume loss. Extrapolation of the blood volume loss from the haemoglobin mass lost during surgery (A_{loss}) using a linear regression model.

Discussion

Despite that the amount of information generated every day is continuously growing since the development of new technologies, most of the decisions taken daily are not data-driven. This is evident in the field of drug development, where for example, clinical trials are becoming more complex and burdensome[111] without improving the success of development programs[112]. This apparent contradiction between data generation and data usage is a key argument for the implementation of mechanism-based quantitative methods in drug discovery.

The modelling and simulation techniques included under the umbrella of pharmacometrics offer the possibility to integrate information from multiple stages of drug development to better understand the drug-pathology interaction, which can be used to inform decision-making. This versatility has been key for the expansion and consolidation of pharmacometrics across the pharmaceutical industry. If the initial responsibilities of pharmacometricians were related to dose calculations and extrapolation, today's expectations encompass from clinical trial design to setting up Go/No-Go criteria[36], being an integral part of drug development. However, the success in drug development has put the focus of pharmacometrics on regulatory impact, to the detriment of developing synergies with other disciplines and the implementation of new technologies[113]. As a consequence, pharmacometrics is at risk of missing the boat of innovation and remaining a niche discipline limited to the area of drug development. Among the different challenges that the field will have to face in the immediate future are the integration of machine learning and artificial intelligence[114], and the transition from internal to big data coming from multiple sources such as *omics,* real-world evidence or data collection initiatives[115,116]. In this evolving context, subdisciplines such as QSP, which can integrate mechanistically data at various levels, are in advantage vs traditional popPK/PD[17]. It is likely that in the future, hybrid methodologies resulting from the combination of popPK/PD, PBPK and QSP would be the norm, and only data availability and the objective of the model would drive which modelling technique is used[117].

Discussion

Similar challenges and opportunities faces pharmacometrics in clinical practice, with the additional disadvantage that in this field, the use of pharmacometrics is much scarcer. The reasons behind the limited use of modelling and simulation techniques in clinical practice have been mentioned in the *Introduction* and are expected to continue in the near future. Aspects such as the lack of training in pharmacometrics are not easily solved as require deep changes in the already saturated curricula of medical specialities. For this reason, user-friendly tools represent a clear opportunity to facilitate the applicability of MIPD. Similarly, natural language processing tools could automatically organise clinical records into structured data, increasing the quality and quantity of the information available for analysis. Although the increase of MIPD is a positive step toward personalised medicine, not all therapies are expected to benefit from it. Drugs with narrow therapeutic windows and complex PK properties are likely the ones that will benefit the most from the application of MIPD[45].

In this thesis, we present the case of one of these drugs, remifentanil, for which the available tools are not sufficient to efficiently guide drug administration during surgical procedures. For many years, the administration of remifentanil has depended on non-specific autonomic responses such as arterial hypertension, tachycardia, involuntary movements, sweating or the presence of tears, and there is a need for more specific biomarkers. Nonetheless, developing new biomarkers for pain is a complex task. Firstly, in early phase studies, there is a need to induce pain in healthy subjects, which is often associated with ethical concerns. Then, if these studies are approved, there are no objective measures to quantify pain and validate the biomarker. In this work, the later limitation was circumvented by using movement as a surrogate measure for surgical pain. This approach represents an innovation that builds on the known physiological association between surgical pain and movement.

The models developed for PRD and movement revealed a similar response to tetanic stimulation and pharmacologic action, indicating that both variables share the same mechanisms of

regulation. These results are in agreement with the research hypothesis behind this study, although the fact that both variables were not modelled simultaneously represents a limitation for the use of the model in clinical practice. Additionally, because neither basal nor pre-stimulus pupil diameter were found to correlate with the amplitude of PRD, a tetanic stimulation would be required to assess the degree of individual patient anaesthesia. Further studies evaluating serial intensities of painful stimulation would allow characterising the full relationship between stimulus intensity and movement response, and perhaps allow the use of less painful stimulus to monitor pain perception.

Our models were able to characterise PRD and movement responses across a variety of experimental conditions (absence or presence of opioids, tetanic stimulation and surgical procedure), reflecting robustness. Regarding the pharmacodynamics of remifentanil, our estimated C_{50} for both PRD and movement models are in line with reported values for other markers of central activity such as arterial pressure[118,119], spectral edge frequency of the electroencephalogram[82] and respiratory depression[120,121] (0.92 to 11.2 ng/ml). In contrast, our value of $t_{1/2\_ke0}$ for PRD is slightly larger than previously reported (0.53 to 2.48 min[82,118–121]). This may be due to the fact that predicted instead of measured concentrations were used for this analysis. Alternatively, it may indicate that the region in the central nervous system in which remifentanil elicits analgesia is, at least from a rate of distribution point of view, different from those contributing to cortical effects and respiratory depression[121]. This argumentation also applies to the effect of remifentanil on stimulus perception, where no differences were found in the equilibration between the central and the effect site compartment. In this case, the lack of movement and PRD reflexes in the absence of tetanic stimulation, and the use of SS concentrations during the measured intervals, may have also hampered the characterization of a delay in the distribution.

Discussion

Although the use of predicted concentrations could bias parameter estimation, it represents a closer approach to clinical scenarios, where concentrations are not routinely measured. In this work, we suggest that a SS concentration of 2 ng/ml of remifentanil could suppress movement response in 80% of the patients. Considering that the target concentrations of remifentanil in combination with propofol typically range from 2 to 6 ng/ml[122], our results point out a potential dose reduction. Additional studies comparing the accuracy of TCI-predicted vs measured concentrations[123] would be necessary to build confidence in the extrapolation of results using predicted concentrations and validate our findings.

Regarding PRD, our model reproduced the results from Barvais et al.[57] and Guglielminotti et al.[124], demonstrating that it is a robust and reproducible biomarker. Previous studies have used PK/PD modelling to describe the effect of opioids[125–129] and drugs modulating noradrenergic pathways[130–132] on the pupil. Only in two cases, modelling has been extended to associate PDiam with nociception. Skarke et al.[133] modelled separately pupil and pain tolerance in response to electric stimulation to show a temporal correlation between the two variables. More recently Mangas-Sanjuan et al.[134] showed that the changes in PDiam triggered by the active components of axomadol correlated linearly with the area under the curve of the cold pressor test.

In this work, we went a step beyond previous studies and developed a semi-mechanistic framework using NLME to characterise the temporal and pharmacological response of pupil and movement responses. This methodology represents an innovative approach that could be used to guide the design and evaluation of future research studies in the field of pain management.

However, financing and executing clinical trials of new analgesics is challenging. In *Appendix 1* we propose an overview of the Innovative Medicines Initiative (IMI)-PAINCARE, a public-private collaboration aiming to improve the management of patients suffering from acute or chronic pain. We believe that collaborations of this type are key for improving the success of drug development. In first place, they represent a holistic approach to a given problem encountered

in clinical practice, as it is in this case, the lack of medicines for pain management. For example, by addressing this problem at different levels, PAINCARE is designed to provide a comprehensive toolbox of new biomarkers, outcome measures and stratifying tools, whose use spans from early preclinical to clinical practice. This broad scope is partially a consequence of the diversity of collaborators from small and medium companies, the pharmaceutical industry and academia, each of them with their own areas of interest and expertise. Despite the increased complexity in project coordination, the benefits associated with this multidisciplinary approach are evident. Putting together the expertise of pharmaceutical companies in drug development with the innovation of academia allows cross-fertilization and alignment between the different stakeholders, and optimises investment and resource allocation. The development of a strong scientific methodology for the evaluation of pain is critical to de-risk the search for new analgesics, encouraging pharmaceutical companies to invest in research programs in the field.

The subproject BioPain within the IMI-PAINCARE is intended to evaluate functional biomarkers using, among other methodologies, PK/PD modelling to improve the translation from preclinical to clinical development. The relevance of pharmacometrics was already recognised by the IMI during the grant evaluation by requesting to have a dedicated group responsible for this analysis. So far, in this project, pharmacometrics has played a central role in the selection of the drug candidates and dosing schedules that are being used in the preclinical and clinical studies[135]. As the project progresses and data is generated, pharmacometric techniques will be used for the analysis of quantitative biomarkers combining information from different areas of the nervous system. The generation of such a comprehensive amount of information for several biomarkers and drugs in multiple research centres represents a scientific and logistic challenge that would hardly have been achieved without a consortium of this nature.

This thesis also provides an example of how popPK/PK can use prior knowledge (i.e. literature data) to shed some light on an unresolved clinical problem. In this case, we used –and

evaluated– the performance of two published PK models for rocuronium to characterise the effects of this drug on profound NMB. From all the PK studies for rocuronium, Saldien[101] and De Haes models[102] were selected based on their extensive reporting of model parameters (including Ke_0), the use of covariates and a good description of the PD response. However, these studies were developed using lower levels of rocuronium —and therefore in non-profound NMB—, which contrasts with our experimental setting.

Our analysis assumed that Ce were the only driver of the effect and did not change within each recording period of a PTC (23 seconds). The same advantages and limitations associated with the use of predicted concentrations that were discussed for PRD and movement models apply to this work. Among those, the most relevant for this study is that the use of predicted concentrations can bias the estimation of the effect-site kinetics and pharmacodynamics parameters (ke_0 and Ce_{50})[136], hampering the biological interpretation of our results. However, the fact that two different PK models were evaluated represents a more neutral approach to the analysis of the data. Also, our estimates for these parameters are in line with the reported values for rocuronium[101,102].

Multiple modelling alternatives —treating data as continuous, categorical or count— were considered to analyse PTCs. Ultimately, a model for categorical data was used in order to fulfil the discrete nature and dependency between PTC twitches and, as this approach has already been used in the field of anaesthesia[123], to facilitate the interpretation of the results. This case exemplifies the versatility of the methodologies available for popPK/PD analysis and shows how data can be modelled differently depending on the purpose of the model.

During the process of data analysis, PTCs were found to follow a complex pattern with regard to rocuronium concentrations. The fact that multiple values of PTC were observed for the same concentration of rocuronium represented a challenge for building the model and could be a

limitation for the application of the model in clinical practice. This issue was partially mitigated by grouping PTCs into categories, although at the expense of model resolution.

Multiple factors could be responsible for the observed disparity between PTC counts gathered at very similar plasma concentrations of rocuronium. Some of them, such as the existence of a temporal delay between plasma concentrations and response, were accounted during model development, for example, with the use of an effect-site compartment. On the contrary, the influence of the measurement technique, the surgical procedure or the intrinsic variability in the response could not be evaluated. We hypothesise that some of these aspects may have influenced the occurrence of PTCs equal to 0 and 1, which was systematically miss-predicted despite the multiple modelling approaches used. Interestingly, Hoshino et al.[137] used a physiological receptor occupancy model[138] to model PTCs and showed a similar pattern of response to effect-site concentrations. However, because this work lacks a quantitative evaluation of model performance, it is not possible to conclude whether a more mechanistic approach would be able to provide a better description of the PTC response. Despite these mixed results, profound NMB has been shown to correlate with lower postoperative pain and better recovery[139], reinforcing the need to refine the understanding of PTCs. Further studies should be conducted to optimise the PK/PD description of rocuronium and PTCs, aiming to develop a TCI system for profound NMB.

Our last model is another example of the application of popPK/PD to perioperative management. In this work, we developed a semi-mechanistic model to characterise the time course of Hb concentrations in the early perioperative period. This model is the result of the low reliability of the individual measurements of Hb after surgery –as a consequence of the so-called haemoglobin drift– to guide transfusion decisions. We believe that a predictive tool reproducing the full profile of Hb concentrations represents a more comprehensive approach to support decision criteria in this scenario.

Discussion

In the pursuit of a model that could be reproducible, only variables routinely collected in surgical procedures or easily measured were used to develop our model. Other parameters such as the individual blood volumes were derived from the patient's characteristics using standard formulas. Although these approaches may complicate the physiological interpretation of our results, we prioritised model applicability over obtaining a deeper understanding of the biological processes involved. This is not to say that biology was disregarded during model building. We ensured that all processes and derived parameters were coherent with the known physiology of fluid dynamics. For example, we confirmed that the blood volumes predicted by the ICSH formula were similar to those estimated by the model, allowing us to reduce the number of parameters to be estimated. Similarly, some assumptions were made to simplify the modelling process. In the first place, because cumulative volumes and not infusion rates are recoded in daily clinical practice, we assumed a constant rate of infusion within the measurement periods. Secondly, blood was treated as a homogenous fluid, assuming that the fraction of fluid within the RBC can directly distribute to peripheral tissue or be eliminated via urine. The haematocrit could have been used to differentiate between plasma and RBC fluid, but at the expense of adding complexity to the model, and this approach was disregarded.

Unlike traditional PK modelling, water is the main component of both fluid therapy and blood. For this reason, our modelling approach is closer to volume kinetics[140], with which we share common elements but differentiate in the objective. The novelty of our model lies in our focus to describe Hb, not use it to characterise fluid dynamics. This approach conditioned some of the characteristics of the study protocol. Firstly, only laparoscopic surgeries, which allow for reliable measurement of blood loss (especially of haemoglobin mass loss)[89], were included in the study. The extrapolation of our model to non-laparoscopic surgeries would require the use of validated methods to quantify haemoglobin mass loss[141,142]. Secondly, due to the clinical and not experimental setup, our study was not likely to replicate the perturbations in fluid dynamics of experimental studies[143]. For example, fluid infusion was not guided by protocol and was based

on the clinician's criteria. Although a significant range of fluid volumes was expected, the relatively low infusion rates are not likely to expand the peripheral volume[144], which could not be appropriately estimated without the use of Bayesian priors. Similarly, the sparse sampling in our study is probably linked to the fact that we did not find differences in the kinetics of dextrose and crystalloid solutions. We hypothesize that differences in the experimental design and the simultaneous characterization of both fluid infusions are the reasons why our estimate for the peripheral volume is larger than total body water and the 6.9 L reported for 0.9% saline and 5.4 L for 5% dextrose[143,144] —although peripheral volumes do not necessarily represent an actual physiological volume and could be the result of an assortment of processes, such as cell uptake.

Covariate evaluation showed a significant effect of age and the type of surgical procedure on total fluid elimination and the fraction of fluid eliminated via urine, respectively. In the case of age, despite the statistical significance, a limited clinical impact was found. An association between the type of surgical procedure and haemoglobin drift has been described, being of greater magnitude in those surgeries with high intravenous fluid and blood transfusion requirements[145]. In this study, we incorporated these elements into the model, and additionally found a significant inhibition of total fluid elimination after surgery.

Part of this inhibition could be attributed to the reduced diuresis caused by the anaesthesia, hypotension, haemorrhage, and hypovolemia[146], which has been described to last from 4 hours to at least 24 hours after the surgical procedure ended[147,148]. The inhibition of urinary fluid elimination has been shown to correlate with the degree of hypovolemia in healthy volunteers[149] and animal models[150]. In our study, blood loss did not correlate with fluid elimination parameters. However, it must be taken into account that in sheep, a loss of 15% of the blood volume already inhibits urinary output by a half[150], a percentage that was clearly exceeded in our study (10% to 55% of total blood volume assuming a standard blood volume of 5 L). Interestingly, in both the sheep model from Norberg et al.[150] and our clinical study, the

impairment of urinary fluid elimination persisted even if fluid balance was restored, suggesting that mechanisms other than the decrease in blood pressure and hypovolemia play a role in this phenomenon. Unfortunately, the inhibition of the urinary output exceeded the length of our study and therefore, the recovery of renal elimination could not be characterized. This fact represents a limitation for the application of our model outside the study period.

To our knowledge, the inhibition of non-urinary fluid elimination after surgery has not been previously described. We hypothesize that this finding could be a consequence of increased fluid losses during surgery (e.g. sweating, mechanical ventilation), and/or accumulation of fluid in areas of the body not equilibrating with plasma (the so-called third space)[151], which would result in an apparent inhibition of fluid elimination after the surgical procedure. As a result, large differences between pre- and post-surgery non-urinary elimination would be associated with the formation of oedema, although this data was not available to corroborate our hypothesis. The observed increase in fluid elimination with age could also point out a higher risk of fluid accumulation in older patients. Dedicated studies in which the system is perturbed in multiple ways (fluid administration and blood losses) would be required to evaluate the individual contribution of each of these processes.

In our study, urine does not represent the main route of fluid elimination, a situation that has already been described in surgical patients during general anaesthesia[151] and that together with the aforementioned inhibition of the diuretic response, reinforces the conclusion that monitoring urine is an ineffective method to guide fluid management during surgery[140]. Our covariate analysis suggests that surgeries significantly affecting the renal system involve a larger reduction of diuresis, while gynaecological surgeries are associated with the opposite effect. The fact that the type of surgical procedure only affected the proportion of fluid eliminated via urine implies that certain surgeries (those showing a lower proportion of urinary elimination, *RF* in our model) are associated with larger non-urinary fluid elimination. This finding could be a

consequence of the stress response driven by the surgical procedure, which could cause pathologic fluid distribution and subsequent tissue edema[152,153]. In our study, an increase in inflammatory markers (C-reactive protein, monocytes and neutrophils) was observed after surgery. However, no correlation between these markers and model parameters could be established, likely due to the sparse data, and thus further investigation is required.

This work integrates a semi-mechanistic model with routine clinical data to predict Hb in the perioperative settings. Predictive models represent an opportunity to support decision-making in clinical scenarios and individualize treatment administration[154]. In the case of RBC transfusions, our model can be used to identify patients at risk of postoperative anaemia, guide fluid administration by detecting haemoconcentration and haemodilution states, and define the preoperative Hb target to avoid an RBC transfusion (assuming a predictable amount of bleeding). Extrapolation to surgical procedures not included in this study would require previous validation of the model, particularly of parameters related to fluid elimination, which may change for each type of surgery. We believe that model-based approaches represent a non-invasive and cost-effective method to guide RBC transfusion, supporting the decision-making in this complicated scenario.

A wide range of models spanning from empirical to semi-mechanistic has been developed in this thesis. In all of these models, parameters were estimated with precision, as supported by the low RSE and bootstrap results. Similarly, the developed models were extensively evaluated, and in the case of pupil, movement and Hb, validated using a set of data not used not for model development. We ensured that the maximum standards for popPK/PD analysis were applied throughout the modelling process. For this reason, and despite the complexity of clinical research, we think that these models represent a suitable framework to answer our research hypothesis and draw valid conclusions from our results.

Discussion

Either because of the lack of awareness or expertise, the use of pharmacometrics is uncommon in the clinic. This thesis provides concrete examples of the potential applicability of pharmacometric techniques in a wide range of perioperative scenarios, some of them as unusual in popPK/PD as blood transfusion. The use of the population approach provides pharmacometrics with a distinct advantage to characterise the wide range of variability observed in clinical settings. This feature is a key step towards individualising dose administration and ultimately, with the integration of the "omics" data, to precision medicine.

We foresee a future where collaborations between scientists, quantitative disciplines (among those pharmacometricians) and clinicians would be the norm and not the exception, resulting in a multidisciplinary approach to disease management.

Conclusions

The primary aim of this thesis was to develop and apply pharmacometric models in the areas of pain and perioperative management, expanding the application of these techniques in clinical practice. The main findings from this work are summarised in the following conclusions:

1. Two pharmacodynamic models relating painful stimulation with pupillary and movement reflexes in the presence and absence of opioids were developed. A similar temporal as well as pharmacological response to tetanic stimulation was found for both reflexes, pointing out to a common physiological mechanism of control.

2. The developed models were used to propose dose recommendations minimising the percentage of patients that experience movement during the surgical procedures. Altogether, this work constitutes a semi-mechanistic framework to evaluate the use of pupillary reflex as a biomarker for pain during surgical procedures, providing anaesthetists with a quantitative tool to individualise drug administration.

3. A population PK/PD model to characterise the effects of rocuronium in post-tetanic counts (PTC) during profound neuromuscular blockade was built. This work evaluated the performance of two published PK models and found an adequate and equivalent performance for assessing the PTC effect, modelled as an order categorical variable.

4. This study serves as a basis for optimising rocuronium administration in surgical procedures, in particular when a deep level of neuromuscular blockade is required. Further confirmatory studies are necessary to improve the understanding of the concentration/effect relationship for low PTC counts, increasing the resolution in which deep neuromuscular blockade can be characterised.

5. Clinical variables collected in everyday surgical procedures were used to develop and validate a quantitative model to describe haemoglobin concentrations in the early perioperative period. This model was subsequently used to evaluate the risk of requiring a

blood transfusion in different clinical scenarios and provide recommendations on the administration of blood and fluid therapy.

6. In these patients, urinary fluid elimination represented only a quarter of the total fluid elimination and was found to be inhibited after surgery in a time dependent-manner, indicating that monitoring urine is an ineffective method to guide fluid administration in perioperative settings.

7. In summary, this thesis used pharmacometrics techniques to develop a toolbox of quantitative methods in the fields of pain and perioperative management. We expect that this work constitutes a step towards the use of model-informed precision dosing in clinical practice.

Conclusiones

El objetivo principal de la presente tesis doctoral ha sido desarrollar modelos de farmacometría en las áreas del dolor y el manejo perioperatorio, expandiendo la aplicación de estas técnicas en la práctica clínica. Los principales resultados de este trabajo se pueden sintetizar en las siguientes conclusiones:

1. Se han desarrollado dos modelos de farmacodinamia que relacionan, respectivamente, la estimulación dolorosa con el reflejo pupilar y el movimiento. Así, se ha identificado una respuesta temporal y farmacológica similar entre ambas variables, sugiriendo que ambas comparten un mecanismo fisiológico de control común.

2. Dichos modelos han sido utilizados para recomendar pautas de dosificación que minimicen el porcentaje de pacientes que experimentan movimiento durante los procedimientos quirúrgicos. En su conjunto, el presente trabajo constituye una aproximación semicuantitativa para evaluar el uso del reflejo pupilar como un biomarcador del dolor durante la cirugía, proporcionando una herramienta cuantitativa para individualizar la administración de fármacos.

3. Siguiendo esta línea de investigación, se ha desarrollado un modelo de farmacocinética/farmacodinamia poblacional para caracterizar los efectos del rocuronio en el recuento postetánico. En este trabajo se evaluaron dos modelos de farmacocinética publicados en la literatura científica, demostrando que ambos modelos poseen una capacidad adecuada y muy semejante para describir el recuento postetánico, que fue modelado como una variable categórica ordenada.

4. Este estudio sirve de base para optimizar la administración de rocuronio en procedimientos quirúrgicos, especialmente para aquellos que requieran un elevado nivel de bloqueo neuromuscular. No obstante, nuevos estudios son necesarios para mejorar la comprensión de la relación contracción/efecto para bajos recuentos postetánicos, aumentando así la precisión para caracterizar el bloqueo neuromuscular profundo.

5. Se ha desarrollado y validado un modelo cuantitativo para describir las concentraciones de hemoglobina en el periodo perioperatorio usando variables recogidas de forma rutinaria durante los procedimientos quirúrgicos. Posteriormente, dicho modelo fue utilizado para evaluar la necesidad de recibir una transfusión en diferentes escenarios clínicos y proporcionar recomendaciones sobre la administración de terapia sanguínea y de fluidos.

6. En estos pacientes, la eliminación de fluido por vía urinaria solo representó un cuarto del volumen total eliminado y se constató que este último queda inhibido de forma tiempo-dependiente después de la cirugía. Estos hechos indican que la monitorización de la orina es un método ineficaz para guiar la administración de fluido en el periodo perioperatorio.

7. Finalmente, cabe destacar que en la presente tesis doctoral se ha utilizado la farmacometría para desarrollar un conjunto de herramientas cuantitativas en los campos del dolor y el manejo perioperatorio. De acuerdo con lo anterior, creemos que este trabajo representa una importante contribución al desarrollo de la dosificación de precisión guiada por modelos en la práctica clínica.

Bibliography

1. Marco-Ariño N, Vide S, Agustí M, et al. Semimechanistic models to relate noxious stimulation, movement, and pupillary dilation responses in the presence of opioids. *CPT Pharmacometrics Syst Pharmacol*. November 2021. doi:10.1002/psp4.12729

2. Couto M, Vide S, Marco-Ariño N, et al. Comparison of two pharmacokinetic–pharmacodynamic models of rocuronium bromide during profound neuromuscular block: analysis of estimated and measured post-tetanic count effect. *Br J Anaesth*. February 2022. doi:10.1016/j.bja.2021.12.010

3. Petrovska BB. Historical review of medicinal plants' usage. *Pharmacogn Rev*. 2012;6(11):1-5. doi:10.4103/0973-7847.95849

4. Jones AW. Early drug discovery and the rise of pharmaceutical chemistry. *Drug Test Anal*. 2011;3(6):337-344. doi:10.1002/dta.301

5. Hay M, Thomas DW, Craighead JL, Economides C, Rosenthal J. Clinical development success rates for investigational drugs. *Nat Biotechnol*. 2014;32(1):40-51. doi:10.1038/nbt.2786

6. DiMasi JA, Grabowski HG, Hansen RW. Innovation in the pharmaceutical industry: New estimates of R&D costs. *J Health Econ*. 2016;47:20-33. doi:10.1016/j.jhealeco.2016.01.012

7. Wouters OJ, McKee M, Luyten J. Estimated Research and Development Investment Needed to Bring a New Medicine to Market, 2009-2018. *JAMA - J Am Med Assoc*. 2020;323(9):844-853. doi:10.1001/jama.2020.1166

8. Department of Health and Human Services Food and Drug Administration. *Innovation or Stagnation: Challenge and Opportunity on the Critical Path to New Medical Products. Technical Report*.; 2004.

9. Morgan P, Brown DG, Lennard S, et al. Impact of a five-dimensional framework on R&D productivity at AstraZeneca. *Nat Rev Drug Discov*. 2018;17(3):167-181. doi:10.1038/nrd.2017.244

10. Ette EI, Williams PJ. *Pharmacometrics: The Science of Quantitative Pharmacology*.; 2006. doi:10.1002/9780470087978

11. Sheiner LB, Rosenberg B, Melmon KL. Modelling of individual pharmacokinetics for computer-aided drug dosage. *Comput Biomed Res*. 1972;5(5):441-459. doi:10.1016/0010-4809(72)90051-1

12. Lee C, Barnes A, Katz RL. Neuromuscular sensitivity to tubocurarine a comparison of 10 parameters. *Br J Anaesth*. 1976;48(11):1045-1051. doi:10.1093/bja/48.11.1045

13. Sheiner LB, Stanski DR, Vozeh S, Miller RD, Ham J. Simultaneous modeling of pharmacokinetics and pharmacodynamics: Application to d-tubocurarine. *Clin Pharmacol Ther*. 1979;25(3):358-371. doi:10.1002/cpt1979253358

14. Barrett JS, Fossler MJ, Cadieu KD, Gastonguay MR. Pharmacometrics: A multidisciplinary field to facilitate critical thinking in drug development and translational research settings. *J Clin Pharmacol*. 2008;48(5):632-649. doi:10.1177/0091270008315318

15. Gobburu JVS. Pharmacometrics 2020. *J Clin Pharmacol*. 2010;50(9):151S-157S. doi:10.1177/0091270010376977

16. Bradshaw EL, Spilker ME, Zang R, et al. Applications of Quantitative Systems Pharmacology in Model-Informed Drug Discovery: Perspective on Impact and Opportunities. *CPT Pharmacometrics Syst Pharmacol*. 2019;8(11):777-791. doi:10.1002/psp4.12463

17. Azer K, Kaddi CD, Barrett JS, et al. History and Future Perspectives on the Discipline of Quantitative Systems Pharmacology Modeling and Its Applications. *Front Physiol*. 2021;12:637999. doi:10.3389/fphys.2021.637999

18. Rowland M, Peck C, Tucker G. Physiologically-based pharmacokinetics in drug development and regulatory science. *Annu Rev Pharmacol Toxicol*. 2011;51:45-73. doi:10.1146/annurev-pharmtox-010510-100540

19. Gillespie WR. Noncompartmental Versus Compartmental Modelling in Clinical Pharmacokinetics. *Clin Pharmacokinet*. 1991;20(4):253-262. doi:10.2165/00003088-199120040-00001

20. Foster DM. Noncompartmental Versus Compartmental Approaches to Pharmacokinetic Analysis. In: *Principles of Clinical Pharmacology*. Elsevier Inc.; 2007:89-105. doi:10.1016/B978-012369417-1/50048-1

21. Derendorf H, Lesko LJ, Chaikin P, et al. Pharmacokinetic/pharmacodynamic modeling in drug research and development. *J Clin Pharmacol*. 2000;40(12 Pt 2):1399-1418.

22. Holford NHG, Sheiner LB. Kinetics of pharmacologic response. *Pharmacol Ther*. 1982;16(2):143-166. doi:10.1016/0163-7258(82)90051-1

23. Dayneka NL, Garg V, Jusko WJ. Comparison of four basic models of indirect pharmacodynamic responses. *J Pharmacokinet Biopharm*. 1993;21(4):457-478. doi:10.1007/BF01061691

24. Felmlee MA, Morris ME, Mager DE. Mechanism-Based Pharmacodynamic Modeling. In: *Methods in Molecular Biology (Clifton, N.J.)*. Vol 929. NIH Public Access; 2012:583-600. doi:10.1007/978-1-62703-050-2_21

25. Holford N. Clinical pharmacology = disease progression + drug action. *Br J Clin Pharmacol*. 2015;79(1):18-27. doi:10.1111/bcp.12170

26. Agresti A. Modelling ordered categorical data: recent advances and future challenges. *Stat Med*. 1999;18(17-18):2191-2207. doi:10.1002/(SICI)1097-0258(19990915/30)18:17/18<2191::AID-SIM249>3.0.CO;2-M

27. Plan E. Modeling and Simulation of Count Data. *CPT Pharmacometrics Syst Pharmacol*. 2014;3(8):129. doi:10.1038/psp.2014.27

28. Holford N. A time to event tutorial for pharmacometricians. *CPT Pharmacometrics Syst Pharmacol*. 2013;2(5):e43. doi:10.1038/psp.2013.18

29. Ette EI, Williams PJ. Population pharmacokinetics II: Estimation methods. *Ann Pharmacother*. 2004;38(11):1907-1915. doi:10.1345/aph.1E259

30. Sheiner LB, Beal SL. Evaluation of methods for estimating population pharmacokinetic parameters II. Biexponential model and experimental pharmacokinetic data. *J Pharmacokinet Biopharm*. 1981;9(5):635-651. doi:10.1007/BF01061030

31. Sheiner LB. The population approach to pharmacokinetic data analysis: Rationale and standard data analysis methods. *Drug Metab Rev*. 1984;15(1-2):153-171. doi:10.3109/03602538409015063

32. Duffull SB, Wright DFB, Winter HR. Interpreting population pharmacokinetic-pharmacodynamic analyses - a clinical viewpoint. *Br J Clin Pharmacol*. 2011;71(6):807-814. doi:10.1111/j.1365-2125.2010.03891.x

33. Bonate PL. *Pharmacokinetic-Pharmacodynamic Modeling and Simulation*. Springer US; 2011. doi:10.1007/978-1-4419-9485-1

34. Karlsson MO, Sheiner LB. The importance of modeling interoccasion variability in population pharmacokinetic analyses. *J Pharmacokinet Biopharm*. 1993;21(6):735-750.

doi:10.1007/BF01113502

35. Sheiner LB. Learning versus confirming in clinical drug development. In: *Clinical Pharmacology and Therapeutics*. Vol 61. John Wiley & Sons, Ltd; 1997:275-291. doi:10.1016/S0009-9236(97)90160-0

36. Lalonde RL, Kowalski KG, Hutmacher MM, et al. Model-based drug development. *Clin Pharmacol Ther*. 2007;82(1):21-32. doi:10.1038/sj.clpt.6100235

37. EFPIA MID3 Workgroup EM, Marshall SF, Burghaus R, et al. Good Practices in Model-Informed Drug Discovery and Development: Practice, Application, and Documentation. *CPT pharmacometrics Syst Pharmacol*. 2016;5(3):93-122. doi:10.1002/psp4.12049

38. Marshall S, Madabushi R, Manolis E, et al. Model-Informed Drug Discovery and Development: Current Industry Good Practice and Regulatory Expectations and Future Perspectives. *CPT Pharmacometrics Syst Pharmacol*. 2019;8(2):87-96. doi:10.1002/psp4.12372

39. Lee JY, Garnett CE, Gobburu JVS, et al. Impact of Pharmacometric Analyses on New Drug Approval and Labelling Decisions. *Clin Pharmacokinet*. 2011;50(10):627-635. doi:10.2165/11593210-000000000-00000

40. Lee JY, Garnett CE, Gobburu JVS, et al. Impact of pharmacometric analyses on new drug approval and labelling decisions: A review of 198 submissions between 2000 and 2008. *Clin Pharmacokinet*. 2011;50(10):627-635. doi:10.2165/11593210-000000000-00000

41. Huang SM, Abernethy DR, Wang Y, Zhao P, Zineh I. The utility of modeling and simulation in drug development and regulatory review. *J Pharm Sci*. 2013;102(9):2912-2923. doi:10.1002/jps.23570

42. Wang Y, Zhu H, Madabushi R, Liu Q, Huang SM, Zineh I. Model-Informed Drug Development: Current US Regulatory Practice and Future Considerations. *Clin Pharmacol Ther*. 2019;105(4):899-911. doi:10.1002/cpt.1363

43. Jain L, Mehrotra N, Wenning L, Sinha V. PDUFA VI: It Is Time to Unleash the Full Potential of Model-Informed Drug Development. *CPT Pharmacometrics Syst Pharmacol*. 2019;8(1):5-8. doi:10.1002/psp4.12365

44. Madabushi R, Wang Y, Zineh I. A Holistic and Integrative Approach for Advancing Model-Informed Drug Development. *CPT Pharmacometrics Syst Pharmacol*. 2019;8(1):9-11. doi:10.1002/psp4.12379

45. Wright DFB, Martin JH, Cremers S. Spotlight Commentary: Model-informed precision dosing must demonstrate improved patient outcomes. *Br J Clin Pharmacol*. 2019;85(10):2238-2240. doi:10.1111/bcp.14050

46. Minto CF, Schnider TW. Contributions of PK/PD modeling to intravenous anesthesia. *Clin Pharmacol Ther*. 2008;84(1):27-38. doi:10.1038/clpt.2008.100

47. Buclin T, Thoma Y, Widmer N, et al. The Steps to Therapeutic Drug Monitoring: A Structured Approach Illustrated With Imatinib. *Front Pharmacol*. 2020;11. doi:10.3389/fphar.2020.00177

48. Bonate PL. What happened to the modeling and simulation revolution? *Clin Pharmacol Ther*. 2014;96(4):416-417. doi:10.1038/clpt.2014.123

49. Buil-Bruna N, López-Picazo J, Martín-Algarra S, Trocóniz IF. Bringing Model-Based Prediction to Oncology Clinical Practice: A Review of Pharmacometrics Principles and Applications. *Oncologist*. 2016;21(2):220-232. doi:10.1634/theoncologist.2015-0322

50. Standing JF. Understanding and applying pharmacometric modelling and simulation in clinical practice and research. *Br J Clin Pharmacol*. 2017;83(2):247-254. doi:10.1111/bcp.13119

51. Liu Q, Ramamoorthy A, Huang SM. Real-World Data and Clinical Pharmacology: A Regulatory Science Perspective. *Clin Pharmacol Ther*. 2019;106(1):67-71. doi:10.1002/cpt.1413

52. Joerger M, von Pawel J, Kraff S, et al. Open-label, randomized study of individualized, pharmacokinetically (PK)-guided dosing of paclitaxel combined with carboplatin or cisplatin in patients with advanced non-small-cell lung cancer (NSCLC). *Ann Oncol*. 2016;27(10):1895-1902. doi:10.1093/ANNONC/MDW290

53. Zhang J, Zhou F, Qi H, et al. Randomized study of individualized pharmacokinetically-guided dosing of paclitaxel compared with body-surface area dosing in Chinese patients with advanced non-small cell lung cancer. *Br J Clin Pharmacol*. 2019;85(10):2292-2301. doi:10.1111/bcp.13982

54. Neely MN, Kato L, Youn G, et al. Prospective trial on the use of trough concentration versus area under the curve to determine therapeutic vancomycin dosing. *Antimicrob Agents Chemother*. 2018;62(2). doi:10.1128/AAC.02042-17

55. Larson MD, Behrends M. Portable Infrared Pupillometry. *Anesth Analg*.

2015;120(6):1242-1253. doi:10.1213/ANE.0000000000000314

56. Larson MD, Sessler DI. Pupillometry to guide postoperative analgesia. *Anesthesiology*. 2012;116(5):980-982. doi:10.1097/ALN.0b013e318251d21b

57. Barvais L, Engelman E, Eba JM, Coussaert E, Cantraine F, Kenny GN. Effect site concentrations of remifentanil and pupil response to noxious stimulation. *Br J Anaesth*. 2003;91(3):347-352. doi:10.1093/bja/aeg178

58. Funcke S, Sauerlaender S, Pinnschmidt HO, et al. Validation of innovative techniques for monitoring nociception during general anesthesia: A clinical study using tetanic and intracutaneous electrical stimulation. *Anesthesiology*. 2017;127(2):272-283. doi:10.1097/ALN.0000000000001670

59. Leslie K, Sessler DI, Smith WD, et al. Prediction of movement during propofol/nitrous oxide anesthesia: Performance of concentration, electroencephalographic, pupillary, and hemodynamic indicators. *Anesthesiology*. 1996;84(1):52-63. doi:10.1097/00000542-199601000-00006

60. Nitahara K, Sugi Y, Higa K. Neuromuscular monitoring. *Japanese J Anesthesiol*. 2008;57(7):824-830. doi:10.1213/ane.0b013e3181cdb093

61. Fuchs-Buder T. *Neuromuscular Monitoring in Clinical Practice and Research*. Berlin, Heidelberg: Springer Berlin Heidelberg; 2010. doi:10.1007/978-3-642-13477-7

62. Wierda JM, Kleef UW, Lambalk LM, Kloppenburg WD, Agoston S. The pharmacodynamics and pharmacokinetics of Org 9426, a new non-depolarizing neuromuscular blocking agent, in patients anaesthetized with nitrous oxide, halothane and fentanyl. *Can J Anaesth*. 1991;38(4):430-435. doi:10.1007/BF03007578

63. Szenohradszky J, Fisher DM, Segredo V, et al. Pharmacokinetics of rocuronium bromide (ORG 9426) in patients with normal renal function or patients undergoing cadaver renal transplantation. *Anesthesiology*. 1992;77(5):899-904. doi:10.1097/00000542-199211000-00010

64. Alvarez-Gomez JA, Estelles ME, Fabregat J, Perez F, Brugger AJ. Pharmacokinetics and pharmacodynamics of rocuronium bromide in adult patients. In: *European Journal of Anaesthesiology, Supplement*. Vol 11. ; 1994:53-56.

65. Magorian T, Wood P, Caldwell J, et al. The pharmacokinetics and neuromuscular effects of rocuronium bromide in patients with liver disease. *Anesth Analg*. 1995;80(4):754-759.

doi:10.1097/00000539-199504000-00018

66. Kleijn HJ, Zollinger DP, van den Heuvel MW, Kerbusch T. Population pharmacokinetic-pharmacodynamic analysis for sugammadex-mediated reversal of rocuronium-induced neuromuscular blockade. *Br J Clin Pharmacol*. 2011;72(3):415-433. doi:10.1111/j.1365-2125.2011.04000.x

67. Cooper RA, Maddineni VR, Mirakhur RK, Wierda JMKH, Brady M, Fitzpatrick KTJ. Time course of neuromuscular effects and pharmacokinetics of rocuronium bromide (org 9426) during isoflurane anaesthesia in patients with and without renal failure. *Br J Anaesth*. 1993;71(2):222-226. doi:10.1093/bja/71.2.222

68. Goodnough LT, Levy JH, Murphy MF. Concepts of blood transfusion in adults. *Lancet*. 2013;381(9880):1845-1854. doi:10.1016/S0140-6736(13)60650-9

69. Carson JL, Guyatt G, Heddle NM, et al. Clinical Practice Guidelines From the AABB. *JAMA*. 2016;316(19):2025. doi:10.1001/jama.2016.9185

70. American Society of Anesthesiologists Task Force on Perioperative Blood Management. Practice Guidelines for Perioperative Blood Management. *Anesthesiology*. 2015;122(2):241-275. doi:10.1097/ALN.0000000000000463

71. Grant MC, Whitman GJ, Savage WJ, Ness PM, Frank SM. Clinical predictors of postoperative hemoglobin drift. *Transfusion*. 2014;54(6):1460-1468. doi:10.1111/trf.12491

72. Scott DA, Tung HMA, Slater R. Perioperative hemoglobin trajectory in adult cardiac surgical patients. *J Extra Corpor Technol*. 2015;47(3):167-173.

73. Tezuka K, Kimura W, Hirai I, Moriya T, Watanabe T, Yano M. Postoperative hematological changes after spleen-preserving distal pancreatectomy with preservation of the splenic artery and vein. *Dig Surg*. 2012;29(2):157-164. doi:10.1159/000337312

74. George TJ, Beaty CA, Kilic A, et al. Hemoglobin Drift after Cardiac Surgery. *Ann Thorac Surg*. 2012;94(3):703. doi:10.1016/J.ATHORACSUR.2012.03.038

75. Shander A, Javidroozi M, Ozawa S, Hare GMT. What is really dangerous: anaemia or transfusion? *Br J Anaesth*. 2011;107(SUPPL. 1):i41-i59. doi:10.1093/bja/aer350

76. Dunne JR, Malone D, Tracy JK, Gannon C, Napolitano LM. Perioperative Anemia: An Independent Risk Factor for Infection, Mortality, and Resource Utilization in Surgery. *J*

Surg Res. 2002;102(2):237-244. doi:10.1006/jsre.2001.6330

77. Turan A, Rivas E, Devereaux PJ, et al. Association between postoperative haemoglobin concentrations and composite of non-fatal myocardial infarction and all-cause mortality in noncardiac surgical patients: post hoc analysis of the POISE-2 trial. *Br J Anaesth*. 2021;126(1):87-93. doi:10.1016/j.bja.2020.08.054

78. Glance LG, Dick AW, Mukamel DB, et al. Association between Intraoperative Blood Transfusion and Mortality and Morbidity in Patients Undergoing Noncardiac Surgery. *Anesthesiology*. 2011;114(2):283-292. doi:10.1097/ALN.0b013e3182054d06

79. Carson JL. Perioperative Blood Transfusion and Postoperative Mortality. *JAMA*. 1998;279(3):199. doi:10.1001/jama.279.3.199

80. Schnider TW, Minto CF, Shafer SL, et al. The influence of age on propofol pharmacodynamics. *Anesthesiology*. 1999;90(6):1502-1516. doi:10.1097/00000542-199906000-00003

81. Schnider TW, Minto CF, Gambus PL, et al. The influence of method of administration and covariates on the pharmacokinetics of propofol in adult volunteers. *Anesthesiology*. 1998;88(5):1170-1182. doi:10.1097/00000542-199805000-00006

82. Minto CF, Schnider TW, Egan TD, et al. Influence of age and gender on the pharmacokinetics and pharmacodynamics of remifentanil I. Model development. *Anesthesiology*. 1997;86(1):10-23. doi:10.1097/00000542-199701000-00004

83. SMART Servier Medical Art. https://smart.servier.com/. Accessed July 26, 2021.

84. Freepik. https://www.freepik.com/. Accessed May 31, 2021.

85. Fuchs-Buder T, Claudius C, Skovgaard LT, et al. Good clinical research practice in pharmacodynamic studies of neuromuscular blocking agents II: The Stockholm revision. *Acta Anaesthesiol Scand*. 2007;51(7):789-808. doi:10.1111/j.1399-6576.2007.01352.x

86. Janmahasatian S, Duffull SB, Ash S, Ward LC, Byrne NM, Green B. Quantification of lean bodyweight. *Clin Pharmacokinet*. 2005;44(10):1051-1065. doi:10.2165/00003088-200544100-00004

87. De Hert S, Imberger G, Carlisle J, et al. Preoperative evaluation of the adult patient undergoing non-cardiac surgery. *Eur J Anaesthesiol*. 2011;28(10):684-722. doi:10.1097/EJA.0b013e3283499e3b

88. Kristensen SD, Knuuti J, Saraste A, et al. 2014 ESC/ESA Guidelines on non-cardiac surgery: cardiovascular assessment and management. *Eur Heart J*. 2014;35(35):2383-2431. doi:10.1093/eurheartj/ehu282

89. Jaramillo S, Montane-Muntane M, Capitan D, et al. Agreement of surgical blood loss estimation methods. *Transfusion*. 2019;59(2):508-515. doi:10.1111/trf.15052

90. Jaramillo S, Montane-Muntane M, Gambus PL, Capitan D, Navarro-Ripoll R, Blasi A. Perioperative blood loss: Estimation of blood volume loss or haemoglobin mass loss? *Blood Transfus*. 2020;18(1):20-29. doi:10.2450/2019.0204-19

91. Beal SL, Sheiner LB, Boeckmann AJ, Bauer RJ. NONMEM 7.4. 3 Users Guides.(1989-2018). *Hanover, MD, USA ICON Dev Solut*. 2018.

92. Karlsson MO, Beal SL, Sheiner LB. Three new residual error models for population PK/PD analyses. *J Pharmacokinet Biopharm*. 1995;23(6):651-672. doi:10.1007/BF02353466

93. Ludden TM, Beal SL, Sheiner LB. Comparison of the Akaike Information Criterion, the Schwarz criterion and the F test as guides to model selection. *J Pharmacokinet Biopharm*. 1994;22(5):431-445. doi:10.1007/BF02353864

94. Jonsson EN, Karlsson MO. Automated covariate model building within NONMEM. *Pharm Res*. 1998;15(9):1463-1468. doi:10.1023/a:1011970125687

95. Holford N. The visual predictive check—superiority to standard diagnostic (Rorschach) plots. PAGE 14 (2005) Abstr 738 [www.page-meeting.org/?abstract=738].

96. RStudio Team (2019). RStudio: Integrated Development for R. RStudio, Inc., Boston, MA URL http://www.rstudio.com/.

97. Jonsson EN, Karlsson MO. Xpose - An S-PLUS based population pharmacokinetic/pharmacodynamic model building aid for NONMEM. *Comput Methods Programs Biomed*. 1998;58(1):51-64. doi:10.1016/S0169-2607(98)00067-4

98. Wickham H. *Ggplot2: Elegant Graphics for Data Analysis*. Springer-Verlag New York; 2016.

99. Lindbom L, Ribbing J, Jonsson EN. Perl-speaks-NONMEM (PsN) - A Perl module for NONMEM related programming. *Comput Methods Programs Biomed*. 2004;75(2):85-94. doi:10.1016/j.cmpb.2003.11.003

100. Lindbom L, Pihlgren P, Jonsson N. PsN-Toolkit - A collection of computer intensive

statistical methods for non-linear mixed effect modeling using NONMEM. *Comput Methods Programs Biomed*. 2005;79(3):241-257. doi:10.1016/j.cmpb.2005.04.005

101. Saldien V, Vermeyen KM, Wuyts FL. Target-controlled infusion of rocuronium in infants, children, and adults: A comparison of the pharmacokinetic and pharmacodynamic relationship. *Anesth Analg*. 2003;97(1):44-49. doi:10.1213/01.ANE.0000066262.32103.60

102. De Haes A, Proost JH, Kuks JBM, van den Tol DC, Wierda JMKH. Pharmacokinetic/Pharmacodynamic Modeling of Rocuronium in Myasthenic Patients Is Improved by Taking into Account the Number of Unbound Acetylcholine Receptors. *Anesth Analg*. 2002;95(3):588-596. doi:10.1097/00000539-200209000-00018

103. De Haes A, Proost JH, De Baets MH, Stassen MHW, Houwertjes MC, Wierda JMKH. Pharmacokinetic-pharmacodynamic modeling of rocuronium in case of a decreased number of acetylcholine receptors: A study in myasthenic pigs. *Anesthesiology*. 2003;98(1):133-142. doi:10.1097/00000542-200301000-00022

104. Hahn RG. Body volumes and fluid kinetics. In: Hahn RG, ed. *Clinical Fluid Therapy in the Perioperative Setting*. Cambridge: Cambridge University Press; 2016:41-51. doi:10.1017/CBO9781316401972.009

105. Otto JM, Montgomery HE, Richards T. Haemoglobin concentration and mass as determinants of exercise performance and of surgical outcome. *Extrem Physiol Med*. 2013;2(1):33. doi:10.1186/2046-7648-2-33

106. Otto JM, Plumb JOM, Clissold E, et al. Hemoglobin concentration, total hemoglobin mass and plasma volume in patients: implications for anemia. *Haematologica*. 2017;102(9):1477-1485. doi:10.3324/haematol.2017.169680

107. Dill DB, Costill DL. Calculation of percentage changes in volumes of blood, plasma, and red cells in dehydration. *J Appl Physiol*. 1974;37(2):247-248. doi:10.1152/jappl.1974.37.2.247

108. Pearson TC, Guthrie DL, Simpson J, et al. Interpretation of measured red cell mass and plasma volume in adults: Expert Panel on Radionuclides of the International Council for Standardization in Haematology. *Br J Haematol*. 1995;89(4):748-756. doi:10.1111/j.1365-2141.1995.tb08411.x

109. JACOB M, CHAPPELL D, CONZEN P, FINSTERER U, REHM M. Blood volume is normal after

pre-operative overnight fasting. *Acta Anaesthesiol Scand*. 2008;52(4):522-529. doi:10.1111/j.1399-6576.2008.01587.x

110. Joshi GP, O'Connor MF, Nussmeier NA. Intraoperative fluid management, 2020. In: *UpToDate*. Waltham, MA. https://www.uptodate.com/contents/intraoperative-fluid-management (Accessed on May 14, 2021).

111. Getz KA, Campo RA, Kaitin KI. Variability in Protocol Design Complexity by Phase and Therapeutic Area. *Ther Innov Regul Sci*. 2011;45(4):413-420. doi:10.1177/009286151104500403

112. Hay M, Thomas DW, Craighead JL, Economides C, Rosenthal J. Clinical development success rates for investigational drugs. *Nat Biotechnol*. 2014;32(1):40-51. doi:10.1038/nbt.2786

113. Barrett JS. Time to Expect More From Pharmacometrics. *Clin Pharmacol Ther*. 2020;108(6):1129-1131. doi:10.1002/cpt.1914

114. Ekins S, Puhl AC, Zorn KM, et al. Exploiting machine learning for end-to-end drug discovery and development. *Nat Mater*. 2019;18(5):435-441. doi:10.1038/s41563-019-0338-z

115. Brown N, Cambruzzi J, Cox PJ, et al. Big Data in Drug Discovery. In: *Progress in Medicinal Chemistry*. Vol 57. ; 2018:277-356. doi:10.1016/bs.pmch.2017.12.003

116. Qian T, Zhu S, Hoshida Y. Use of big data in drug development for precision medicine: anupdate. *Expert Rev Precis Med drug Dev*. 2019;4(3):189. doi:10.1080/23808993.2019.1617632

117. Benson N. Quantitative Systems Pharmacology and Empirical Models: Friends or Foes? *CPT Pharmacometrics Syst Pharmacol*. 2019;8(3):135-137. doi:10.1002/psp4.12375

118. Glass PSA, Hardman D, Kamiyama Y, et al. Preliminary pharmacokinetics and pharmacodynamics of an ultra-short- acting opioid: Remifentanil (GI87084B). *Anesth Analg*. 1993;77(5):1031-1040. doi:10.1213/00000539-199311000-00028

119. Hannam JA, Borrat X, Trocóniz IF, et al. Modeling respiratory depression induced by remifentanil and propofol during sedation and analgesia using a continuous noninvasive measurement of pCO2. *J Pharmacol Exp Ther*. 2016;356(3):563-573. doi:10.1124/jpet.115.226977

120. Bouillon T, Bruhn J, Radu-Radulescu L, Andresen C, Cohane C, Shafer SL. A model of the ventilatory depressant potency of remifentanil in the non-steady state. *Anesthesiology*. 2003;99(4):779-787. doi:10.1097/00000542-200310000-00007

121. Olofsen E, Boom M, Nieuwenhuijs D, et al. Modeling the non-steady state respiratory effects of remifentanil in awake and propofol-sedated healthy volunteers. *Anesthesiology*. 2010;112(6):1382-1395. doi:10.1097/ALN.0b013e3181d69087

122. Nimmo AF, Absalom AR, Bagshaw O, et al. Guidelines for the safe practice of total intravenous anaesthesia (TIVA). *Anaesthesia*. 2019;74(2):211-224. doi:10.1111/ANAE.14428

123. Fábregas N, Rapado J, Gambús PL, et al. Modeling of the sedative and airway obstruction effects of propofol in patients with Parkinson disease undergoing stereotactic surgery. *Anesthesiology*. 2002;97(6):1378-1386. doi:10.1097/00000542-200212000-00008

124. Guglielminotti J, Grillot N, Paule M, et al. Prediction of Movement to Surgical Stimulation by the Pupillary Dilatation Reflex Amplitude Evoked by a Standardized Noxious Test. *Anesthesiology*. 2015;122(5):985-993. doi:10.1097/ALN.0000000000000624

125. Westerling D, Persson C, Hoglund P. Plasma concentrations of morphine, morphine-3-glucuronide, and morphine-6-glucuronide after intravenous and oral administration to healthy volunteers: Relationship to nonanalgesic actions. *Ther Drug Monit*. 1995;17(3):287-301. doi:10.1097/00007691-199506000-00013

126. Dershwitz M, Walsh JL, Morishige RJ, et al. Pharmacokinetics and pharmacodynamics of inhaled versus intravenous morphine in healthy volunteers. *Anesthesiology*. 2000;93(3):619-628. doi:10.1097/00000542-200009000-00009

127. Lötsch J, Skarke C, Schmidt H, Grösch S, Geisslinger G. The transfer half-life of morphine-6-glucuronide from plasma to effect site assessed by pupil size measurement in healthy volunteers. *Anesthesiology*. 2001;95(6):1329-1338. doi:10.1097/00000542-200112000-00009

128. Schmidt H, Lötsch J. Pharmacokinetic-pharmacodynamic modeling of the miotic effects of dihydrocodeine in humans. *Eur J Clin Pharmacol*. 2007;63(11):1045-1054. doi:10.1007/s00228-007-0363-8

129. Ladebo L, Foster DJR, Abuhelwa AY, et al. Population pharmacokinetic-pharmacodynamic modelling of liquid and controlled-release formulations of oxycodone in healthy

volunteers. *Basic Clin Pharmacol Toxicol*. 2020;126(3):263-276. doi:10.1111/bcpt.13330

130. VALLES J, OBACH R, MENARGUES A, PRUÑONOSA J, JANE F. A Pharmacokinetic-pharmacodynamic Linking Model for the α2-Adrenergic Antagonism of Idazoxan on Clonidine-induced Mydriasis in the Rat. *J Pharm Pharmacol*. 1995;47(2):157-161. doi:10.1111/j.2042-7158.1995.tb05770.x

131. Lindauer A, Siepmann T, Oertel R, et al. Pharmacokinetic/pharmacodynamic modelling of venlafaxine: Pupillary light reflex as a test system for noradrenergic effects. *Clin Pharmacokinet*. 2008;47(11):721-731. doi:10.2165/00003088-200847110-00003

132. Liem-Moolenaar M, de Boer P, Timmers M, et al. Pharmacokinetic-pharmacodynamic relationships of central nervous system effects of scopolamine in healthy subjects. *Br J Clin Pharmacol*. 2011;71(6):886-898. doi:10.1111/j.1365-2125.2011.03936.x

133. Skarke C, Darimont J, Schmidt H, Geisslinger G, Lötsch J. Analgesic effects of morphine and morphine-6-glucuronide in a transcutaneous electrical pain model in healthy volunteers. *Clin Pharmacol Ther*. 2003;73(1):107-121. doi:10.1067/mcp.2003.5

134. Mangas-Sanjuan V, Pastor JM, Rengelshausen J, Bursi R, Troconiz IF. Population pharmacokinetic/pharmacodynamic modelling of the effects of axomadol and its O-demethyl metabolite on pupil diameter and nociception in healthy subjects. *Br J Clin Pharmacol*. 2016;82(1):92-107.

135. Mouraux A, Bloms-Funke P, Boesl I, et al. IMI2-PainCare-BioPain-RCT3: a randomized, double-blind, placebo-controlled, crossover, multi-center trial in healthy subjects to investigate the effects of lacosamide, pregabalin, and tapentadol on biomarkers of pain processing observed by electroencephalography (EEG). *Trials 2021 221*. 2021;22(1):1-31. doi:10.1186/S13063-021-05272-Y

136. Coppens MJ, Eleveld DJ, Proost JH, et al. An evaluation of using population pharmacokinetic models to estimate pharmacodynamic parameters for propofol and bispectral index in children. *Anesthesiology*. 2011;115(1):83-93. doi:10.1097/ALN.0b013e31821a8d80

137. Hoshino H, Furutani E, Sugawara T, Takeda T, Sawanobori Y, Shirakami G. Physiological Modeling of Concentration-Effect Relationship for Nondepolarizing Neuromuscular Blocking Drugs. In: *Proceedings of the Annual International Conference of the IEEE Engineering in Medicine and Biology Society, EMBS*. Vol 2020-July. ; 2020:5202-5207.

doi:10.1109/EMBC44109.2020.9175229

138. Nigrovic V, Amann A. Competition between acetylcholine and a nondepolarizing muscle relaxant for binding to the postsynaptic receptors at the motor end plate: Simulation of twitch strength and neuromuscular block. *J Pharmacokinet Pharmacodyn*. 2003;30(1):23-51. doi:10.1023/A:1023245409315

139. Bruintjes MHD, Krijtenburg P, Martini CH, et al. Efficacy of profound versus moderate neuromuscular blockade in enhancing postoperative recovery after laparoscopic donor nephrectomy: A randomised controlled trial. *Eur J Anaesthesiol*. 2019;36(7):494-501. doi:10.1097/EJA.0000000000000992

140. Hahn RG. Volume kinetics for infusion fluids. *Anesthesiology*. 2010;113(2):470-481. doi:10.1097/ALN.0b013e3181dcd88f

141. Holmes AA, Konig G, Ting V, et al. Clinical Evaluation of a Novel System for Monitoring Surgical Hemoglobin Loss. *Anesth Analg*. 2014;119(3):588-594. doi:10.1213/ANE.0000000000000181

142. Konig G, Waters JH, Javidroozi M, et al. Real-time evaluation of an image analysis system for monitoring surgical hemoglobin loss. *J Clin Monit Comput*. 2018;32(2):303-310. doi:10.1007/s10877-017-0016-0

143. Yi JM, Bang JY, Choi B, et al. Population-based volume kinetics of crystalloids and colloids in healthy volunteers. *Sci Rep*. 2019;9(1). doi:10.1038/s41598-019-55171-1

144. Drobin D, Hahn RG. Kinetics of isotonic and hypertonic plasma volume expanders. *Anesthesiology*. 2002;96(6):1371-1380. doi:10.1097/00000542-200206000-00016

145. Grant MC, Whitman GJ, Savage WJ, Ness PM, Frank SM. Clinical predictors of postoperative hemoglobin drift. *Transfusion*. 2014;54(6):1460-1468. doi:10.1111/trf.12491

146. Sear JW. Kidney dysfunction in the postoperative period. *Br J Anaesth*. 2005;95(1):20-32. doi:10.1093/bja/aei018

147. Holte K, Hahn RG, Ravn L, Bertelsen KG, Hansen S, Kehlet H. Influence of “liberal” versus “restrictive” intraoperative fluid administration on elimination of a postoperative fluid load. *Anesthesiology*. 2007;106(1):75-79. doi:10.1097/00000542-200701000-00014

148. Svensén C, Ponzer S, Hahn RG. Volume kinetics of Ringer solution after surgery for hip

fracture. *Can J Anaesth*. 1999;46(2):133-141. doi:10.1007/BF03012547

149. Dan Drobin MD, Hahn RG. Volume kinetics of Ringer's solution in hypovolemic volunteers. *Anesthesiology*. 1999;90(1):81-91. doi:10.1097/00000542-199901000-00013

150. Norberg Å, Brauer KI, Prough DS, et al. Volume turnover kinetics of fluid shifts after hemorrhage, fluid infusion, and the combination of hemorrhage and fluid infusion in sheep. *Anesthesiology*. 2005;102(5):985-994. doi:10.1097/00000542-200505000-00018

151. Hahn RG, Nemme J. Volume kinetic analysis of fluid retention after induction of general anesthesia. *BMC Anesthesiol*. 2020;20(1). doi:10.1186/s12871-020-01001-1

152. Holte K, Sharrock NE, Kehlet H. Pathophysiology and clinical implications of perioperative fluid excess. *Br J Anaesth*. 2002;89(4):622-632. doi:10.1093/bja/aef220

153. Doherty M, Buggy DJ. Intraoperative fluids: how much is too much? *Br J Anaesth*. 2012;109(1):69-79. doi:10.1093/bja/aes171

154. McGeechan K, Macaskill P, Irwig L, Liew G, Wong TY. Assessing New Biomarkers and Predictive Models for Use in Clinical Practice. *Arch Intern Med*. 2008;168(21):2304. doi:10.1001/archinte.168.21.2304

Supplementary material

Supplementary material 1

```
;; 1. Based on:
;; 2. Description: PRD model
;; x1. Author: user

$PROB Pupil

$INPUT ID Time FLAG DVN DV MDV STIM CpREMI CpPROPO EVID NOcc_REMI NOcc_Stimul NT
Post_surgery PSDV

$DATA Example_NM_dataset.csv IGNORE=@ IGNORE=(FLAG.GT.1) IGNORE=(NOcc_REMI.GT.3)
; FLAG=1: Pupil diameter
; FLAG=2: Movement

$SUBROUTINES ADVAN13  TOL=9

$MODEL
COMP= (BP) ;Biophase comparment
COMP= (SP) ;Nact comparment
COMP= (DP) ;Pupil diameter

$PK
SLOPE   = THETA(2) * EXP(ETA(2))
C50     = THETA(3) * EXP(ETA(3))
Limit   = THETA(4) * EXP(ETA(4))
KE0     = THETA(5) * EXP(ETA(5))
KS      = THETA(6) * EXP(ETA(6))
KPD     = THETA(7) * EXP(ETA(7))
PDiam0 = THETA(8) * EXP(ETA(8))
KPS     = PDiam0*KPD
ES      = THETA(9) * EXP(ETA(9))
```

```
A_0(1)=0
A_0(2)=1
A_0(3)=PDiam0

$DES
LM=0
DELTA=A(3)-Limit
IF (DELTA.GT.0) LM=((A(3)-Limit)/A(3))

DADT(1)=KE0*(CpREMI-A(1))
DADT(2)=KS*(1+((ES*STIM)/(1+(CpREMI/C50))))-KS*A(2)*(1+(LM*A(1)*SLOPE))
DADT(3)=KPS*A(2)-KPD*A(3)

$ERROR
BP=A(1)
NACT=A(2)
DiamPupil=A(3)
IPRED= LOG(DiamPupil)
W = THETA(1)* EXP(ETA(1))
Y = IPRED + W*EPS(1)
IRES = DV-IPRED
IWRES = IRES/W

$THETA
(0, 0.09)      ; Add.RE   -Additive error (log data)
(0, 1.35)      ; SLOPE    -Remifentanil SLOPE
(0, 0.9)       ; C50      -Remifentanil C50
(0, 1.6)       ; Limit    -Pupil diameter at which remifentanil effects on KS cease
(0, 0.0025)    ; KE0      -Equilibration constant effect site
(0, 0.06)      ; KS       -Nact synthesis constant
(0, 0.48)      ; KDP      -Pupil degradation constant
(0, 3.6)       ; PDiam0   -Baseline pupil
(0, 1.4)       ; ES       -Electric stimulus perception
```

```
$OMEGA
0 FIX        ; IIV RE
0.35         ; IIV SLOPE
0 FIX        ; IIV C50
0 FIX        ; IIV Limit
0 FIX        ; IIV Ke0
0 FIX        ; IIV KS
0.15         ; IIV KDP

$OMEGA BLOCK(2)
0.1              ; IIV PDiam0
-0.07  0.25      ; IIV ES

$SIGMA
1 FIX            ; ERROR

$ESTIMATION MAXEVAL=9999 NOABORT METHOD=COND INTERACTION MSFO=msfb5 PRINT=5
SIGL=9
$COV PRINT=E
$TABLE ID TIME NT IPRED CPRED STIM IWRES CWRES CpPROPO CpREMI BP NACT EVID
NOcc_REMI NOcc_Stimul Post_surgery ONEHEADER NOPRINT FILE=sdtab_SM _1
$TABLE ID ETAS(1:LAST) KS PDiam0 KPS KPD C50 SLOPE ES Limit Ke0 NOAPPEND ONEHEADER
NOPRINT FILE=patab_SM_1
```

Supplementary material 2

```
;; 1. Based on:
;; 2. Description: Movement model
;; x1. Author: user

$PROB Movement

$INPUT ID Time FLAG DVN DV MDV STIM CpREMI CpPROPO EVID NOcc_REMI NOcc_Stimul NT
Post_surgery PDV

$DATA Example_NM_dataset.csv IGNORE=@ IGNORE=(FLAG.EQ.1) IGNORE=(NOcc_REMI.GT.3)

; FLAG=1: Pupil diameter
; FLAG=2: Movement

$SUBROUTINES ADVAN13  TOL=9

$MODEL
COMP= (SP)  ;Nact comparment

$PK
KS = THETA(7)
ES = THETA(8)
NOCIP0=1
A_0(1)=NOCIP0
C50 = THETA(9)

$DES
DADT(1)=KS*(1+((ES*STIM)/(1+(CpREMI/C50))))-KS*A(1)

$ERROR
NACT=A(1)
```

```
NOCIP=A(1)-NOCIP0

B01=THETA(1)
B02=B01+THETA(2)
B03=B02+THETA(3)

LGT01=B01 + NOCIP + ETA(1)
LGT02=B02 + NOCIP + ETA(1)
LGT03=B03 + NOCIP + ETA(1)

PLGT01 = EXP(LGT01)/(1+EXP(LGT01))
PLGT02 = EXP(LGT02)/(1+EXP(LGT02))
PLGT03 = EXP(LGT03)/(1+EXP(LGT03))

P00 = 1-PLGT01
P01 = PLGT01-PLGT02
P02 = PLGT02-PLGT03
P03 = PLGT03

B11=THETA(4)
LGT11=B11 + NOCIP + ETA(1)
PLGT11 = EXP(LGT11)/(1+EXP(LGT11))

P10 = 1-PLGT11
P11 = PLGT11

B22=THETA(5)
LGT22=B22 + NOCIP + ETA(1)
PLGT22 = EXP(LGT22)/(1+EXP(LGT22))

P20 = 1-PLGT22
P22 = PLGT22
```

```
B33=THETA(6)

LGT33=B33 + NOCIP + ETA(1)

PLGT33 = EXP(LGT33)/(1+EXP(LGT33))

P30 = 1-PLGT33
P33 = PLGT33

;====================================

IF(PDV.EQ.0.AND.DV.EQ.0) Y=P00
IF(PDV.EQ.0.AND.DV.EQ.1) Y=P01
IF(PDV.EQ.0.AND.DV.EQ.2) Y=P02
IF(PDV.EQ.0.AND.DV.EQ.3) Y=P03

IF(PDV.EQ.1.AND.DV.EQ.0) Y=P10
IF(PDV.EQ.1.AND.DV.EQ.1) Y=P11

IF(PDV.EQ.2.AND.DV.EQ.0) Y=P20
IF(PDV.EQ.2.AND.DV.EQ.2) Y=P22

IF(PDV.EQ.3.AND.DV.EQ.0) Y=P30
IF(PDV.EQ.3.AND.DV.EQ.3) Y=P33

IPRED=Y

$THETA
(-INF,-5.0)          ; P01
(-INF,-0.7,0)        ; P02
(-INF,-1.0,0)        ; P03

(-INF,2.0)           ; P11
```

```
(-INF,2.2)          ; P22
(-INF,-2.3)         ; P33

$THETA
(0, 0.45)           ; KS  -Nact synthesis constant
(0, 6.15)           ; ES  -Electric stimulus perception
(0, 0.65)           ; C50 -Remifentanil C50

$OMEGA
0 FIX               ; IIV Logit

$ESTIMATION MAXEVAL=9999 NOABORT METHOD=1 LAPLACIAN LIKE NUMERICAL SLOW
MSFO=msfb5 PRINT=5 SIGL=9
$COV PRINT=E
$TABLE ID TIME NT FLAG IPRED CPRED STIM CpPROPO CpREMI NACT NOCIP EVID NOcc_REMI
NOcc_Stimul Post_surgery ONEHEADER NOPRINT FILE=sdtab_SM_2
$TABLE ID ETAS(1:LAST) KS ES C50 P01 P02 P03 P11 P22 P33 NOAPPEND ONEHEADER NOPRINT
FILE=patab_SM _2
```

Supplementary material 3

```
;; 1. Based on:
;; 2. Description:  Saldien and De Haes PK models, PTC model
;; x1. Author: user
$PROBLEM PTC
$INPUT ID TIME PTC DV AMT RATE CMT EVID MDV VOL AVOL NN AAVOL CE_SW CE_HW AGE
WEIGHT HEIGHT GENDER=DROP BMI FFM
$DATA rocuroniumPTCdataset.csv  IGNORE=@
$SUBROUTINE ADVAN13 TOL=9

; CMT=1: Central
; CMT=2: Peripheral Shallow
; CMT=3: Peripheral Deep
; CMT=4: PTC
; CMT=5: Effect compartment

$MODEL
COMP=(CENTR)
COMP=(PERIPHERAL_S)
COMP=(PERIPHERAL_D)
COMP=(PTC DEFOBS)
COMP=(CE)

$PK
V1  = 35.6  * WEIGHT    ;Saldien PK Model
V2  = 72    * WEIGHT
V3  = 122   * WEIGHT
K10 = 0.126 /60
K12 = 0.209 /60
K13 = 0.050 /60
K21 = 0.163 /60
K31 = 0.015 /60
```

```
;KE0 = 0.168 /60

; V1  = 42   * WEIGHT    ;De Haes PK Model
; V2  = 40   * WEIGHT
; V3  = 69   * WEIGHT
; K10 = 0.076 /60
; K12 = 0.124 /60
; K13 = 0.021 /60
; K21 = 0.130 /60
; K31 = 0.013 /60

KE0=THETA(1) * EXP(ETA(1))

 A_0(1)=0
 A_0(2)=0
 A_0(3)=0
 A_0(4)=0
 A_0(5)=0

$DES
DADT(1)= -K10*A(1) -K12*A(1) +K21*A(2) -K13*A(1) +K31*A(3)    ;CC en mg/ml
DADT(2)=          K12*A(1) -K21*A(2)
DADT(3)=                        K13*A(1) -K31*A(3)
DADT(4)= 0
DADT(5)= KE0*((A(1)/V1)-A(5))

$ERROR
CC   = A(1)/V1
CP_S = A(2)/V2
CP_D = A(3)/V3
CE   = A(5)*1000            ; CC en ug/ml
```

Supplementary material

```
;----------------------PD model--------------------------
CE50_1= THETA(2)         * EXP(ETA(2))
CE50_2= CE50_1 + THETA(3) * EXP(ETA(3))
CE50_3= CE50_2 + THETA(4) * EXP(ETA(4))

GAM=THETA(5)* EXP(ETA(5))

P1=CE**GAM/(CE50_1**GAM+CE**GAM) ; P(Y) >= 1
P2=CE**GAM/(CE50_2**GAM+CE**GAM) ; P(Y) >= 2
P3=CE**GAM/(CE50_3**GAM+CE**GAM) ; P(Y) >= 3

 ;----------------------Probability--------------------------

 PA=1-P1       ; P(m=0 == PTC>=6)
 PB=P1-P2      ; P(m=1 == PTC =4 or 5)
 PC=P2-P3      ; P(m=2 == PTC =2 or 3)
 PD=P3         ; P(m=3 == PTC =0 or 1)

;----------------------Set likelihood--------------------------

 IF(DV.EQ.0) Y=PA
 IF(DV.EQ.1) Y=PB
 IF(DV.EQ.2) Y=PC
 IF(DV.EQ.3) Y=PD

IPRED=Y

$THETA
 (0, 0.0022)   ; Ke0
 (0, 0.65)     ; IC50_1
 (0, 0.17)     ; IC50_2
 (0, 0.74)     ; IC50_3
 (0, 3.7)      ; Gamma
```

```
$OMEGA
 0 FIX          ; IIV KE0
 0.15           ; IIV m=1
 0 FIX          ; IIV m=2
 0.2            ; IIV m=3
 0 FIX          ; IIV Gamma

$ESTIMATION MAXEVAL=9999 NOABORT METHOD=1 LAPLACIAN LIKE NUMERICAL SLOW
MSFO=msfb5 PRINT=5 SIGL=9

$COV PRINT=E

$TABLE ID TIME EVID CC CP_S CP_D CE CE_SW CE_HW CE ONEHEADER NOPRINT FILE=sdtab_SM
_3

$TABLE ID ETAS(1:LAST) NOAPPEND ONEHEADER NOPRINT FILE=patab_SM _3
```

Supplementary material 4

```
;; 1. Based on:
;; 2. Description: Hb model
;; x1. Author: user

$PROBLEM

$INPUT  ID TIME DVN DV HCT DVID AMT SID SFLAG=DROP RATIOGS DINF RATE CMT EVID MDV OP VLOST TIMEOP ALOST ALOST2 BRATE VC HB0 HBPS VURIPRE VSALPRE SEX AGE WGT HGT BMI HBLOSS VLOSS PCR MON MON_C NEU NEU_C SURG REM STUDY

$DATA Haemoglobin_NM_dataset.csv  IGNORE=@;

; CMT=1: Central
; CMT=2: Peripheral
; CMT=3: Urine

$SUBROUTINE ADVAN13 TOL=9

$MODEL
COMP=(CENTR)
COMP=(PERIPHERAL)
COMP=(URINE)

$PK
;;; FRSURG-DEFINITION START
FRSURG = 1 ; robotic prostatectomy, partial nephrectomy and myomectomy (reference category)
IF(SURG.EQ.3.0000E+00) FRSURG = ( 1 + THETA(12)) ; radical nephrectomy
IF(SURG.EQ.4.0000E+00) FRSURG = ( 1 + THETA(12)) ; nephroureterectomy;
IF(SURG.EQ.5.0000E+00) FRSURG = ( 1 + THETA(13)) ; hysterectomy
IF(SURG.EQ.6.0000E+00) FRSURG = ( 1 + THETA(13)) ; hysterectomy with adnexectomy
IF(SURG.EQ.8.0000E+00) FRSURG = ( 1 + THETA(14)) ; endometriosis.
```

```
;;; FRSURG-DEFINITION END

;;; FR-RELATION START
FRCOV=FRSURG
;;; FR-RELATION END

;;; CLAGE-DEFINITION START
CLAGE = ( 1 + THETA(11)*(AGE - 56.50))
;;; CLAGE-DEFINITION END

;;; CL-RELATION START
CLCOV=CLAGE
;;; CL-RELATION END

VP    = THETA(1)
TVCL  = THETA(2)

TVCL = CLCOV*TVCL
CL    = TVCL * EXP(ETA(2))
TVQ   = THETA(5)
Q     = TVQ * EXP(ETA(5))
V0    = VC + THETA(6)* EXP(ETA(1))
TVFR  = THETA(8)

TVFR = FRCOV*TVFR
PHU   = LOG((TVFR)/(1-TVFR))
FR    = EXP(PHU+ETA(6))/(1+EXP(PHU+ETA(6)))

T50   = THETA(7)* EXP(ETA(7))
GAMMA = THETA(9)
IMAX  = THETA(10)
```

Supplementary material

```
 A_0(1)= V0
 A_0(2)= VP
 A_0(3)= 0

CLT    = CL*(1-IMAX*((TIME**GAMMA)/((TIME**GAMMA) + (T50**GAMMA))) )

K10    = CLT/V0
K12    = Q/V0
K21    = Q/VP
K13    = K10*FR

$DES
DADT(1)= -K10*A(1) -BRATE -K12*A(1) +K21*A(2)
DADT(2)=                  K12*A(1) -K21*A(2)
DADT(3)=  K13*A(1)

$ERROR
VCEN= A(1)
VPER= A(2)
VORI= A(3)

AHM = HB0*VC - ALOST
VOLUME=A(1)

IF(CMT.EQ.1) THEN
IPRED= LOG(AHM/VOLUME + 0.000001)
W = THETA(3) * EXP(ETA(3))
ENDIF

IF(CMT.EQ.3) THEN
IPRED = LOG(A(3)+ 0.000001)
W = THETA(4) * EXP(ETA(4))
ENDIF
```

```
Y = IPRED + W*EPS(1)
IRES = DV-IPRED
IWRES = IRES/W

$THETA
(0, 40.1)          ; VP
(0, 0.222)         ; CL
(0, 0.017)         ; Add.RE Hb
(0, 0.35)          ; RE Urine
(0, 4.29)          ; Q
(0) FIX            ; VC
(0, 9.5)           ; T50
(0, 0.21, 1)       ; FR
9 FIX              ; GAMMA
(0, 0.5, 1)        ; IMAX

$THETA
(-0.031,0.006,0.035) ; CLAGE1

$THETA
 (-1,-0.5,5)       ; FRSURG34 = radical nephrectomy and nephroureterectomy;
 (-1,0.35,5)       ; FRSURG56 = hysterectomy and hysterectomy with adnexectomy
 (-1,0.79,5)       ; FRSURG8   = endometriosis.

$OMEGA
 0 FIX             ; IIV VC
 0.05              ; IIV CL
 0 FIX             ; IIV RE Hb
 0 FIX             ; IIV RE Urine
 0.2               ; IIV Q
 0.1               ; IIV FR
 0 FIX             ; IIV T50
```

```
$SIGMA
 1 FIX              ; Residual Error

$PRIOR  NWPRI
$THETAP
48.1   FIX         ; VP

$THETAPV
0.0225 FIX         ; VP

$ESTIMATION MAXEVAL=9999 NOABORT METHOD=COND INTERACTION PRINT=5 SIGL=9
$COV PRINT=E MATRIX=R

$TABLE ID TIME IPRED CWRES IWRES CMT DVID SID EVID MDV OP VCEN VPER VORI AHM VLOST
ALOST RATIOGS MON ONEHEADER NOPRINT FILE=sdtab_SM _4
$TABLE ID ETAS(1:LAST) K13 NOAPPEND ONEHEADER NOPRINT FILE=patab_SM _4
$TABLE ID TIMEOP HBPS VURIPRE VSALPRE AGE WGT HGT BMI HBLOSS VLOSS MON NEU
NOAPPEND ONEHEADER NOPRINT FILE=cotab_SM _4
$TABLE ID SEX SURG TIMEOP NOAPPEND ONEHEADER NOPRINT FILE=catab_SM _4
```

Appendix

Appendix 1

Perspectives on Public-Private-Partnership in Pain Research: Concepts, Methods and Findings of the IMI-PainCare Consortium

Manuscript in preparation

Petra Bloms-Funke[1,2,*], Nicolás Marco-Ariño[3,4], Judy Birch[5], Tony Blockeel[6], Ombretta Caspani[7], Marcel Froehlich[1], Lone Hummelshoj[8], Hiltrud Liedgens[1], Marcus Komann[9], Jane Meijlink[10], Winfried Meissner[9], Jens Nagel[11], Paulina Nunez-Badinez[12], Keith Phillips[13], Esther Pogatzki-Zahn[14,15], Daniel Schubart[16], Iñaki F. Trocóniz[3,4], Katy Vincent[17], Claudia Weinmann[9], Rolf-Detlef Treede[7]

[1]Grünenthal GmbH, Zieglerstrasse 6, 52078 Aachen, Germany.

[2]Present address: IMI-PainCare consultant, Gerhart-Hauptmann-Strasse 36, 52146 Würselen, Germany.

[3]Pharmacometrics & Systems Pharmacology Research Unit, Department of Pharmaceutical Technology and Chemistry, School of Pharmacy and Nutrition, University of Navarra, Pamplona, Spain.

[4]IdiSNA, Navarra Institute for Health Research, Pamplona, Spain.

[5]Pelvic Pain Support Network, 21 Stourpaine Road, Poole BH17 9AT, United Kingdom.

[6]School of Physiology, Pharmacology & Neuroscience, University of Bristol, Bristol BS8 1TD, United Kingdom.

[7]Department of Neurophysiology, Mannheim Center for Translational Neuroscience (MCTN), Ruprecht-Karls-University Heidelberg, Ludolf-Krehl-Str. 13-17, 68167 Mannheim, Germany.

[8]Endometriosis.org Ltd, Southgate Road 89, London N1 3JS, United Kingdom.

[9]Klinik für Anästhesiologie und Intensivmedizin, Universitätsklinikum Jena, Am Klinikum 1, 07747 Jena, Germany.

[10]International Painful Bladder Foundation, Mahlerlaan 4, 1411 HW Naarden, The Netherlands.

[11]Bayer Aktiengesellschaft, Research & Development, Pharmaceuticals. Aprather Weg 18a 42096 Wuppertal, Germany.

[12]Bayer Aktiengesellschaft, Research & Development, Pharmaceuticals. Müllerstr. 178, 13342 Berlin, Germany.

[13]Eli Lilly and Company, Neuroscience Next Generation Therapeutics, Lilly Innovation Center, Cambridge, MA 02142 U.S.A.

[14]Department of Anaesthesiology, Intensive Care and Pain Medicine, University Hospital Münster, Münster, Germany.

[15]Westfälische Wilhelms-Universität Münster, Schlossplatz 2, 48149 Münster, Germany.

[16]ConsulTech GmbH, Morgensternstrasse 24, 12207 Berlin, Germany.

[17]Nuffield Department of Women's & Reproductive Health, University of Oxford, John Radcliffe Hospital, Oxford, OX3 9DU, United Kingdom.

[*]Corresponding author:

Petra Bloms-Funke, PhD. Gerhart-Hauptmann-Strasse 36, 52146 Würselen, Germany. Tel: +49 172 14 994 89, e-mail: Petra.Blomsfunke@gmail.com.

Appendix 2

Population Pharmacokinetics of Piperacillin in critically ill children including those undergoing continuous kidney replacement therapy.

Submitted

Laura Butragueño-Laiseca[1,2,3,4], Nicolás Marco-Ariño[5,6], Iñaki F. Troconiz[5,6], Santiago Grau[7], Nuria Campillo[7], Xandra García[8], Belén Padilla[9], Sarah Nicole Fernández[1,2,3,4], María Slöcker[1,2,3,4] and María José Santiago[1,2,3,4,*]

[1]Pediatric Intensive Care Unit, Hospital General Universitario Gregorio Marañón, Madrid, Spain

[2]Gregorio Marañón Health Research Institute (IISGM), Madrid, Spain

[3]Pediatrics Department, Universidad Complutense de Madrid, Spain

[4]Maternal and Child Health and Development Research Network (REDSAMID), Institute of Health Carlos III, Madrid, Spain

[5]Pharmacometrics & Systems Pharmacology Research Unit, Department of Pharmaceutical Technology and Chemistry, School of Pharmacy and Nutrition, University of Navarra, Pamplona, Spain

[6]IdiSNA, Navarra Institute for Health Research, Pamplona, Spain

[7]Pharmacy Department, Hospital del Mar, Universitat Autònoma de Barcelona Barcelona, Spain

[8]Pharmacy Department, Hospital General Universitario Gregorio Marañón

[9]Clinical Microbiology Department, Hospital General Universitario Gregorio Marañón

[*]Corresponding author:

María José Santiago, MD., PhD. Pediatric Intensive Care Unit, Hospital General Universitario Gregorio Marañón, Madrid, Spain. Postal code 28009. Tel: +91 661946672, e-mail: msanti20@ucm.es